A SUBMILLIMETER-WAVELENGTH TELESCOPE ARRAY: SCIENTIFIC, TECHNICAL, AND STRATEGIC ISSUES

J.M. Moran, M.S. Elvis, G.G. Fazio, P.T.P. Ho,
P.C. Myers, M.J. Reid, and S.P. Willner

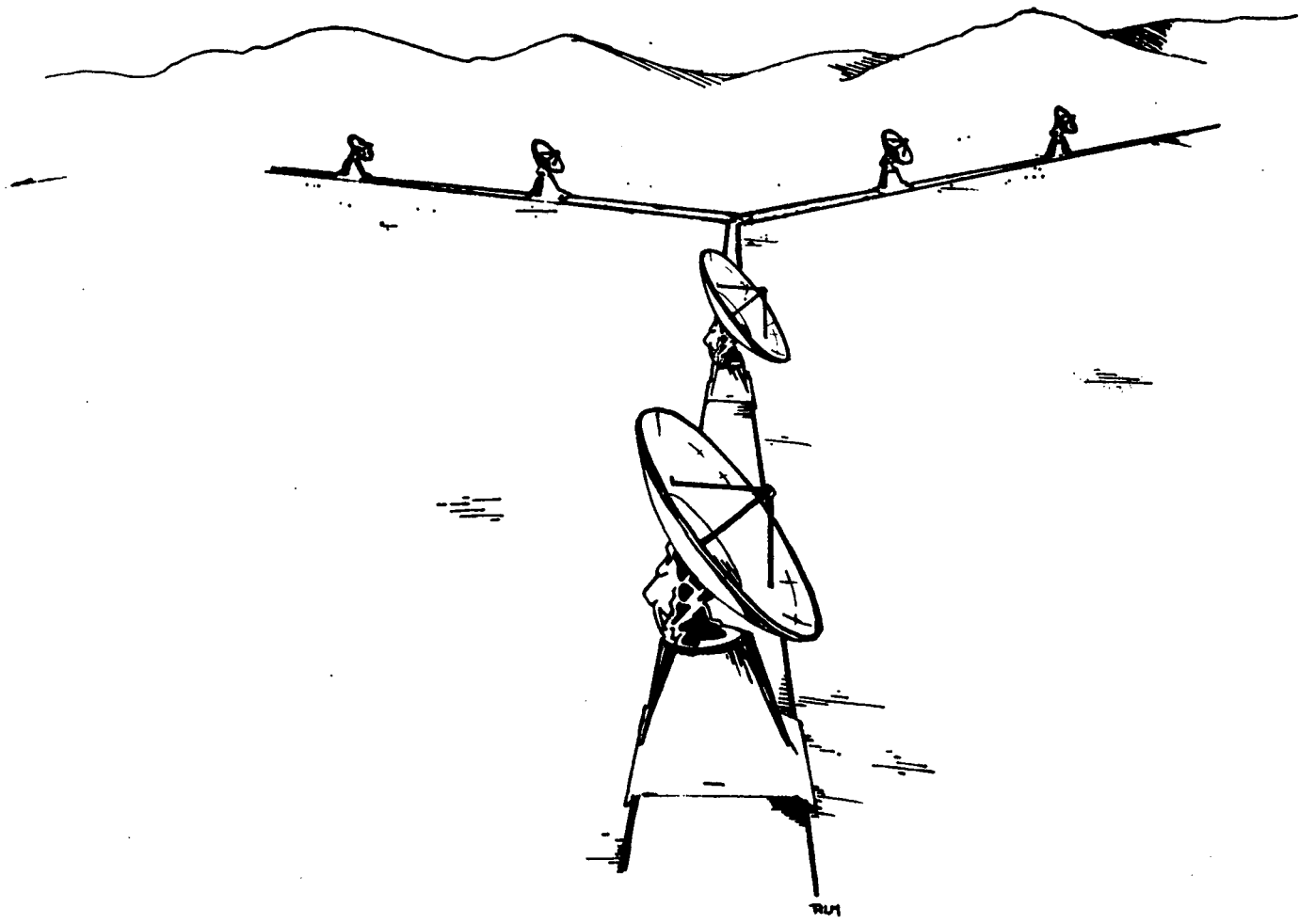

Smithsonian Astrophysical Observatory

Cover design: *Robert L. Marvin*

A SUBMILLIMETER-WAVELENGTH TELESCOPE ARRAY: SCIENTIFIC, TECHNICAL, AND STRATEGIC ISSUES

Report of the Submillimeter Telescope Committee
of the Harvard-Smithsonian Center for Astrophysics

J.M. Moran[1], Chairman
M.S. Elvis[1]
G.G. Fazio[1]
P.T.P. Ho[2]
P.C. Myers[3]
M.J. Reid[1]
S.P. Willner[1]

July 11, 1984

[1]Smithsonian Astrophysical Observatory.

[2]Harvard College Observatory.

[3]Visiting Scientist, Smithsonian Astrophysical Observatory.

TABLE OF CONTENTS

SUMMARY

There is wide recognition among astronomers that the sky at submillimeter wavelengths is virtually unexplored, and that the wavelength range ~ 1.3 to ~ 0.3 mm observable with ground-based telescopes offers potentially rich rewards to many areas of astronomy. The Astronomy Survey Committee of the National Research Council and the Astronomy Advisory Committee of the National Science Foundation have strongly recommended the development of ground-based submillimeter-wavelength telescopes, and three such single-aperture telescopes are now in the process of construction. The next logical step in the development of submillimeter astronomy is an array of telescopes operating as an interferometer. An array can achieve one arcsecond resolution, more than one order-of-magnitude improvement over single-aperture instruments. No other instrument, operating or planned, can achieve this resolution at submillimeter wavelengths. Such an array could make fundamental contributions to our understanding of star formation, galactic structure, quasars and active galactic nuclei, and planets. It would be particularly well suited to high-resolution studies of the cool (10 - 100 K) dust and gas clouds in the Milky Way and other galaxies, because submillimeter emission from dust and molecules in such regions is much stronger than at millimeter or infrared wavelengths.

Construction of a submillimeter array is a practical objective. We believe an array of six movable 6-m-diameter telescopes with a maximum separation between telescopes of 150 meters is a reasonable initial concept. It would have a field of view and a typical resolution, respectively, of 53 arcseconds and 1.2 arcseconds at 1.3 mm, and 14 arcseconds and 0.3 arcseconds at 0.35 mm. The sensitivity at 0.87 mm would be 5 mJy in a 1 GHz continuum band and 0.6 K in a 1 km s^{-1} spectral

line channel, based on current receiver performance and 10^5 sec integration time. There are at least two acceptable mountain sites for a submillimeter array, at which the water vapor overhead is low enough to allow for reasonable atmospheric transparency and stability: Mt. Graham in Arizona and Mauna Kea in Hawaii. Both offer 30 - 80 usable nights per year at 0.35 mm wavelength, and virtually every clear day and night at 1.3 mm. Each site appears to have space for an array with baselines of a few hundred meters. The total construction cost is estimated to be about 25 million 1984-dollars, including a 4-million dollar contingency. The time required for design and construction would be about five years and the annual operating cost would be about 2 million dollars.

A submillimeter array will have the greatest scientific impact if it is brought into operation within the first part of the next decade, perhaps by 1990. To meet this goal, it will be necessary to assemble the senior members of the scientific and technical team within the next year, to begin a detailed design study and to work on pacing items. The technical area most crucial to the project is the receiver development, and it is essential that receiver experts begin work with first-class facilities as soon as possible.

I. INTRODUCTION

In July 1983 a committee of astronomers at the Harvard-Smithsonian Center for Astrophysics was formed by the Director to consider the desirability and the feasibility of the development of a ground-based, submillimeter-wavelength interferometer. After many discussions, calculations, and consultations with experts in various fields, we conclude that such an instrument is of fundamental scientific importance, is technically feasible, and is of a scope and complexity appropriate for undertaking by the Smithsonian Astrophysical Observatory.

This report presents the results of the committee's evaluation of a submillimeter interferometer -- its scientific potential, its probable performance in comparison with that of other instruments, and its possible locations. Also included are a timetable of activities and an estimate of the funds needed to bring about its successful operation. This introduction provides an overview of the more detailed sections of the report. We discuss the historical context, a tentative design, and four of the main scientific applications of a submillimeter interferometer.

A. Historical Context

At this writing (mid-1984) the range of wavelengths $\lambda \sim 0.3$ to ~ 1.3 mm has been the subject of only a small number of astronomical measurements. (We refer to the range 0.3 to 1.3 mm as 'submillimeter' wavelengths even though the longer wavelengths exceed 1.0 mm slightly.) This region, perhaps the 'last frontier' for ground-based astronomical observations, has a rich scientific potential (Longair 1982). Some submillimeter observations have been made from balloon-borne or aircraft

platforms, where size and weight constraints limit telescope diameters to ~ 1 meter, and thus limit angular resolution to more than 1 arcminute. Submillimeter observations are practical for $\lambda \gtrsim 0.3$ mm from high, dry sites on the earth, but such observations from these sites have so far been made only with optical or near-infrared telescopes of a few meters diameter, giving resolution only slightly better than that of the airborne observations. It has been recognized for nearly a decade that the need for higher angular resolution and sensitivity requires ground-based telescopes designed to operate at submillimeter wavelengths.

Five efforts to build single-aperture submillimeter telescopes are now underway. Two are true submillimeter instruments, intended to operate at wavelengths as short as the atmospheric limit, 0.3 mm: the California Institute of Technology 10-m-diameter telescope now under construction on Mauna Kea in Hawaii, and the University of Arizona/Max-Planck-Institut-für-Radioastronomie (UA/MPI) 10-m-diameter telescope, to begin construction soon on Mt. Graham in Arizona. The other three are larger-diameter instruments that will probably be limited to $\gtrsim 1$ mm: the United Kingdom/Netherlands 15-m-diameter telescope, under construction on Mauna Kea; the Institut de Radio Astronomie Millimetrique (IRAM) 30-m-diameter telescope, now under test on Pico de Veleta in Spain; and the 15-m-diameter telescope of the European Space Agency and the Onsala Space Observatory, planned to be placed on a mountain site in Chile. None of these telescopes will have angular resolution better than 10 arcseconds at their shortest operating wavelengths.

A much more elaborate submillimeter telescope, the NASA Large Deployable Reflector (LDR), is currently in the planning stage. If current plans are realized, it will be a submillimeter telescope in space with a

diameter of 15 to 30 meters. Like the Infrared Astronomy Satellite (IRAS), it would be free of limits on wavelength coverage due to atmospheric absorption. It would be launched no sooner than the late 1990's. These efforts and others indicate a significant and growing interest in, and commitment to, submillimeter astronomy among astronomical institutions around the world.

None of the currently planned instruments takes advantage of the potential superiority in angular resolution allowed by interferometry. (Hereafter we will use 'aperture synthesis' to mean the operation of an 'array' of two or more antennas, forming one or more two-element interferometers, the data from which can be Fourier-transformed into a two-dimensional map of sky brightness (Ryle 1975).) At centimeter wavelengths, instruments such as the Three-Element Interferometer of the National Radio Astronomy Observatory (NRAO), various interferometers of Cambridge University in England, and the ten-element Westerbork Synthesis Radio Telescope in The Netherlands dramatically demonstrated these advantages over single-aperture telescopes of the same total collecting area. The success of these 'pioneering' instruments contributed to the development of the Very Large Array (VLA), a large-scale centimeter-wavelength synthesis instrument that has had a major impact on astronomy. Because of the increased complexity and cost of a multiple-telescope system, it is appropriate that the first submillimeter telescopes be single-aperture instruments. It is reasonable, however, to expect that the next major step in submillimeter astronomical facilities will be the construction of a 'pioneering' aperture synthesis system.

At millimeter wavelengths, two pioneering aperture synthesis instruments are now operating. They are currently capable of resolution of

just under 5 arcseconds. The University of California, Berkeley, interferometer now consists of three 6-m-diameter telescopes in Hat Creek, California, operating as an interferometer at 3 mm, and the University has requested funds from the National Science Foundation (NSF) for three more antennas. The California Institute of Technology has three 10-m-diameter telescopes in Owens Valley, California, operating as an interferometer. Looking to the future, the IRAM plans to have three 15-m-diameter telescopes on the Plateau de Bure in southern France. The University of Tokyo group is constructing five 10-m-diameter telescopes in Nobeyama, near Tokyo, Japan. Due to limitations of site altitude and surface accuracy, none of these instruments will operate for significant periods at $\lambda < 2$ mm, with the possible exception of the Caltech interferometer, which may reach 1 mm eventually. A group within the NRAO has begun planning for a millimeter-wavelength array, a major instrument analogous to the VLA. It would consist of more than 15 telescopes, each having a diameter of about 10 meters and operable at wavelengths longer than 1.2 mm. Such an instrument was the highest-priority recommendation of the 'Barrett Committee,' a subcommittee of the NSF Astronomy Advisory Committee appointed to study the future of millimeter and submillimeter astronomy instrumentation. Even if funded by the NSF, this array would probably not operate before the early to mid-1990's. Thus, extensive activity is underway now in relatively modest millimeter interferometers and arrays, and there are plans for a major instrument in the 1990's. These efforts demonstrate widespread recognition of the scientific potential of millimeter interferometry and show that aperture synthesis at short millimeter wavelengths is technically feasible.

This summary of telescope capabilities suggests that the combination of submillimeter-wavelength coverage and arcsecond resolution provided by a submillimeter array would be unmatched by any operating or planned telescope. This point is illustrated in Figure 1. The array we envision here would uniquely fill an empty area of significant size in the wavelength-resolution plane.

The desirability of observations in the submillimeter wavelength region was recognized in the ten-year plan of the Astronomy Survey Committee of the National Research Council (Field et al. 1982). Among 'small new programs' the Committee assigned highest priority to a ground-based submillimeter telescope of about 10-m-diameter. As described above, two such telescopes are now in the process of construction. Looking beyond single aperture telescopes, the Committee recommended the 'study and development of advanced spatial interferometers for the radio, infrared, and optical spectral regions.' Finally, the Committee specifically recognized the potential of a 10-m-diameter submillimeter antenna as an interferometric element when combined with another telescope at the same site. Therefore we believe that a submillimeter array represents a bold next step in keeping with the spirit of the recommendations of the Astronomy Survey Committee.

In summary, submillimeter astronomy is a rapidly growing field but the angular resolution of currently planned instruments is poorer than 10 arcseconds. Aperture synthesis techniques have steadily advanced so that the wavelength limit on currently planned interferometers is 1 to 2 mm, close to the submillimeter regime, and there is widespread recognition among astronomers that submillimeter observations of the finest possible angular resolution are highly desirable and technically feasible.

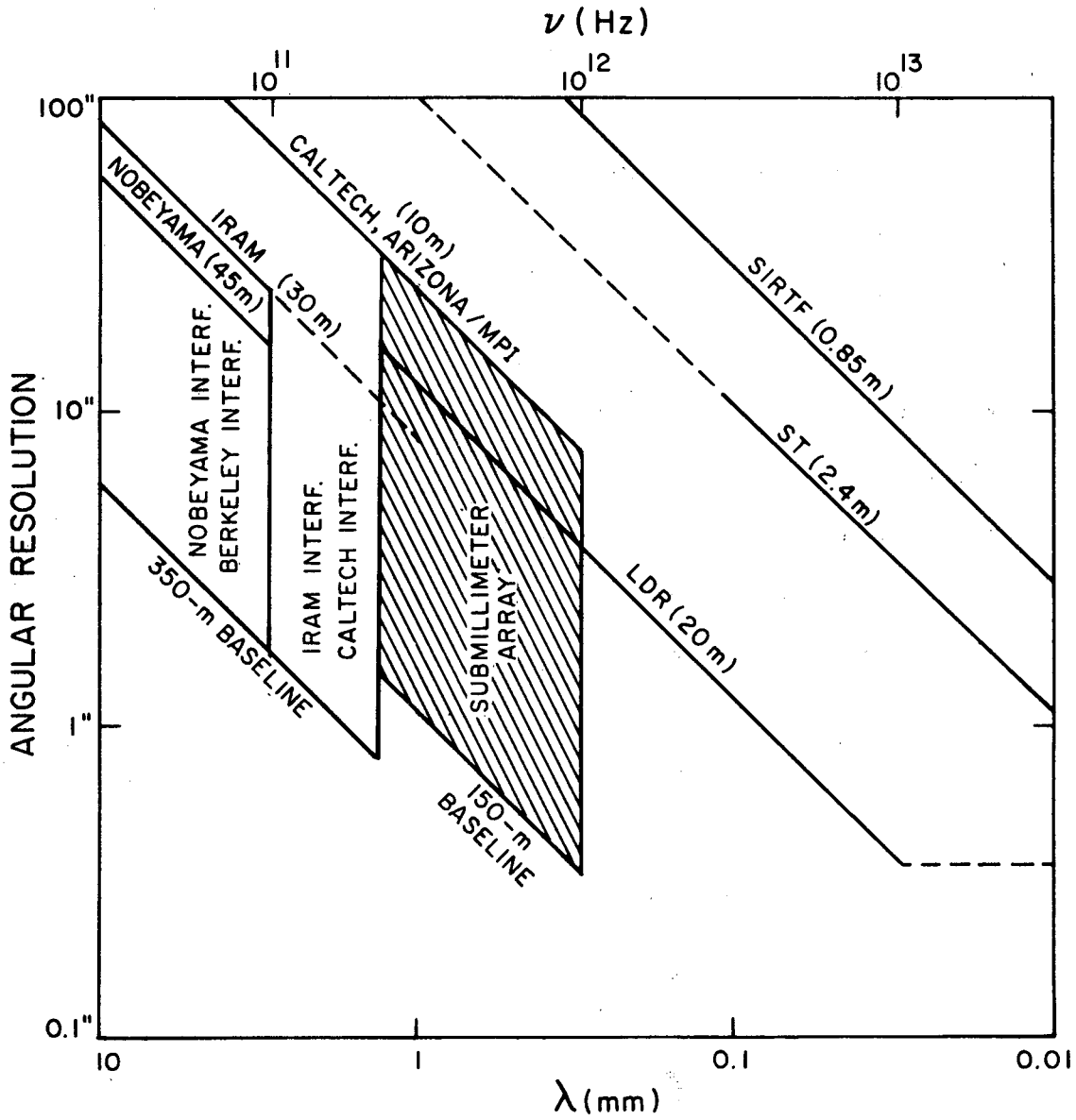

Figure 1. Angular resolution versus wavelength for various existing and proposed telescopes, and the submillimeter array (cross-hatched). Acronyms: IRAM = Institut de Radio Astronomie Millimetrique (Grenoble), MPI = Max-Planck-Institut für Radioastronomie (Bonn), LDR = NASA Large Deployable Reflector, ST = NASA Space Telescope, SIRTF = NASA Shuttle Infrared Telescope Facility.

Therefore, it is now timely to consider the scientific, technical, and strategic issues associated with building a pioneering submillimeter array.

B. Conceptual Design

In this report we adopt as a tentative design an array of six 6-m-diameter telescopes, operating with baselines from about 10 to 150 m, and at wavelengths from 1.3 to 0.3 mm. We envision the array located on a high, dry site such as Mt. Graham in Arizona or Mauna Kea in Hawaii. The array will be operable in both continuum and spectral line modes simultaneously. We consider array configuration, telescope design, telescope mobility, telescope enclosures, and other similar questions in Section III and reserve a detailed discussion to a design study. For our adopted design, the sensitivity with existing receivers in 10^5 s of integration time at 0.87 mm is 5 mJy in a 1 GHz continuum band, and 0.6 K in a 1 km s^{-1} spectral line channel (Section III). The angular resolution at 0.87 mm will range from 12 arcseconds (10 m spacing) to 0.8 arcsecond (150-m spacing).

C. Primary Scientific Applications

We believe that an array similar to the one considered here will make fundamental contributions to a wide range of astronomical disciplines, including studies of the solar system, star formation, astrochemistry, evolved stars, structure of galaxies, and energetics of quasars and active galactic nuclei. In addition, such an array will likely make unexpected discoveries, since its wavelength coverage would be equalled by only a few telescopes of very recent vintage, and since its angular resolution, one arcsecond, would be finer by at least an order of magnitude than that

of any other submillimeter telescope. Such an improvement in angular resolution can dramatically clarify our understanding of an astronomical object. For example, Figure 2 shows the effect of a 16-fold improvement in resolution on an optical image of NGC 1232. In the image with the coarse resolution (~ 25 arcseconds, typical of a single 10-m-diameter antenna), almost no structure is visible. In the image with fine resolution (~ 1.5 arcsecond, typical of an interferometer), the spiral structure is clear. The submillimeter array will be able to produce maps with this resolution of emission from dust and CO molecules in spiral galaxies. As detailed in Section I C(ii), such maps will help illuminate the mechanisms by which galaxies form stars in spiral patterns.

As explained in Section II, the submillimeter wavelengths are well matched to the emission from the cool (10 to 50 K) dust and molecules found in all molecular clouds in the Milky Way and other galaxies. We believe that high-resolution studies of such clouds, and of the stars forming in them, will be the main scientific thrust of the array. These and other applications are discussed from the viewpoint of detection in Section II. We have selected four applications, having the most fundamental scientific importance, to discuss here in greater depth. These are (i) star formation, (ii) structure of galaxies, (iii) quasars and active galactic nuclei, and (iv) solar system studies. Some of these issues are discussed in other documents about millimeter and submillimeter astronomy, including Longair (1982), Hollenbach et al. (1982), Owen (1982), and Barrett et al. (1983). Here, we emphasize how a submillimeter array would have crucial advantages over other instruments in a study of these subjects.

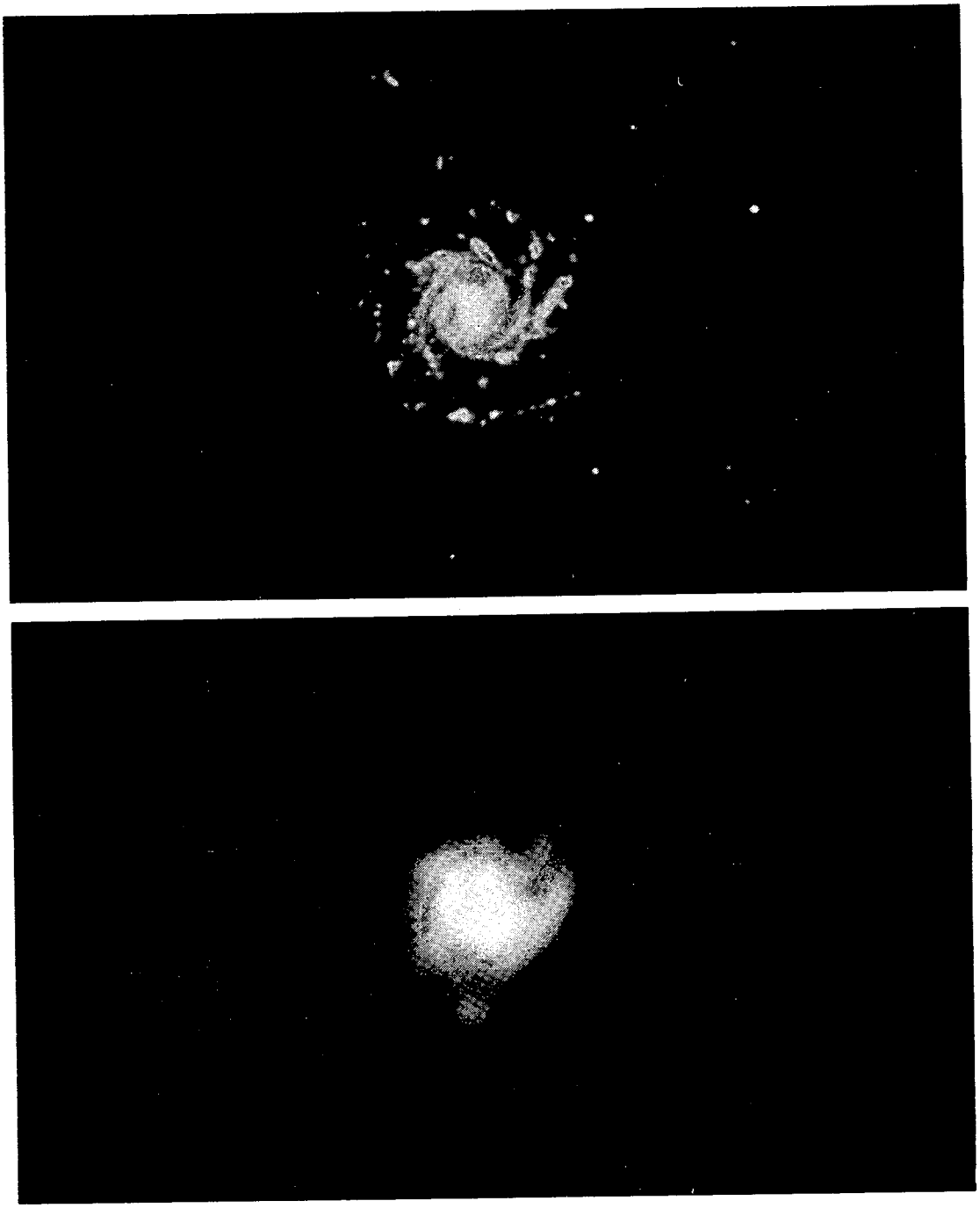

Figure 2. (Top) Optical image of the galaxy NGC 1232 seen with 1.5-arcsecond resolution, typical of the proposed submillimeter array, and (Bottom) the same image smoothed to 25-arcsecond resolution, typical of the single-antenna telescopes soon to be available in the submillimeter band. In the submillimeter band, an array could produce images of the dust and CO emission, which are well-known tracers of spiral arms, with resolution comparable to that obtained in the optical regime. These two images were obtained by digitizing and smoothing the photograph of NGC 1232 in the Hubble Atlas of Galaxies (Sandage 1961).

i. Star Formation

Despite intensive effort in the last decade, knowledge about how stars form is still rudimentary. Three questions of the most basic nature remain unanswered: (a) What motions occur during gravitational collapse? (b) How do stars acquire their main-sequence mass, or how does the collapse 'turn off'? and (c) What is the role of disk-like structures in the formation of single stars, binary stars, and planets?

The belief that stars form by gravitational collapse is widely held, but has essentially no direct supporting evidence. Such evidence has been sought for decades, but none has yet been found -- probably because suitable candidates have been lacking, and because instrumental sensitivity and angular resolution have been inadequate (e.g., Gehrz, Black, and Solomon 1984).

The arcsecond resolution of the array will allow for the first time a mapping of submillimeter line emission from the environs of young sunlike stars, on a spatial scale fine enough to resolve the motions expected from gas in gravitational infall. In the nearest star-forming complexes (in Taurus and Ophiuchus, ~ 450 light years distant), a one-arcsecond beam has a radius of 10^{15} cm, approximately the diameter of Pluto's orbit. Only with resolution of this order, or finer, is it possible to distinguish gravitational infall motions from turbulent cloud motions. A substantial fraction (one-fourth, in a simple spherical model) of the freely falling molecules within radius r will have line-of-sight velocity greater than the free-fall speed at r, $(GM/r)^{\frac{1}{2}}$, where M is the central mass. Detailed models (Larson 1972; Stahler, Shu, and Tamm 1980) validate the use of the free-fall speed at the radii considered here. At $r = 1 \times 10^{15}$ cm and

$M = 1$ solar mass, this speed is ~ 4 km s^{-1}, significantly greater than the normal turbulent broadening of ~ 1 km s^{-1}. In contrast, a 10-arcsecond beam that includes the same region will have only about one four-hundredth of its received emission with line-of-sight velocity $\gtrsim 4$ km s^{-1}, and the high-velocity emission due to gravitational infall will be much less evident. Thus, the arcsecond resolution of the array will be essential to resolve gravitational infall motions near young stars.

Arcsecond resolution is already available to imaging observations with optical telescopes and with the centimeter-wavelength VLA, and will soon be available to observations with millimeter-wavelength interferometers. But infalling gas at $\sim 10^{15}$ cm from a young star is too cold and too heavily obscured to emit detectable optical radiation; and its emission is likely to be significantly stronger at submillimeter wavelengths than at millimeter or centimeter wavelengths, as explained in Section II D. Thus the submillimeter array may offer the best foreseeable way, and possibly the only adequate way, to resolve and detect gas infall motions near young stars.

If the submillimeter array produces maps of localized line broadening, as described above, it will be necessary to distinguish further between gravitational infall and weak outflow from the star of the type described later in this section. From this early vantage point, three properties may allow this distinction. (1) Many outflows are bipolar. It has been suggested that the degree of collimation is highest early in the outflow evolution, when overlap in time between outflow and infall is most likely (Shu 1984). Then, outflow motions may be confined to polar latitudes while infall motions are confined to equatorial latitudes. (2) The infall line broadening is expected to vary with projected distance d from the star as

$d^{-\frac{3}{2}}$, whereas currently known outflows show no such dependence.
(3) Optical-depth effects can, under plausible conditions, render emission from gas in front of the star more intense than emission from gas behind the star (Hummer and Rybicki 1968). The resulting asymmetry in the line profile will have one sense if the gas is falling inward and the opposite sense if the gas is flowing outward. Thus, observations with the submillimeter array may be able to resolve and detect gravitational infall motions near young stars and distinguish them from outflow motions.

In the past, these technical problems of studying infall near young stars have been accompanied by uncertainty about the locations of the youngest stars. The youngest stars are too obscured by dust to be visible optically, and it is possible that such stars are also invisible to ground-based near-infrared observations (wavelengths ~ 0.001 to 0.02 mm). However, the all-sky far-infrared survey of the IRAS satellite has significantly increased the number of young star candidates in nearby molecular cloud complexes, from about 30 (Wynn-Williams 1982) to 10^3 - 10^4 (Rowan-Robinson *et al.* 1984). Thus, the submillimeter array may come at an especially opportune time to find and study gravitational infall near young stars.

The outflow motions near young stars, evident in sky maps of molecular line emission (Snell, Loren, and Plambeck 1980) and in Hα photographs (Mundt and Fried 1983), are currently thought to help terminate the collapse process and clear away the remnant of the parental gas clump. If so, the outflow process is extremely important in determining the final mass of a star. The velocities of the outflowing material, typically tens to hundreds of kilometers per second, are much larger than expected infall velocities during collapse. In many cases the outflow is bipolar, with two

streams of material being channeled in opposite directions. In a few cases, this channeling has been observed on scales of a few arcseconds, or linear distances of ~ 10^{16} cm (Cohen, Bieging, and Schwartz 1982; 6-cm wavelength). The outflow mechanism is unknown and requires study on scales as close to the star as possible. It is therefore crucial to measure gas velocities with spectral resolution of a few kilometers per second and angular resolution on the order of an arcsecond. Optically thin emission in the extreme high- and low-velocity parts ('wings') of the CO line profiles will be stronger in the shorter-wavelength submillimeter transitions than in the millimeter transitions, as discussed in Section II D.

The size and motions of disk-like structures around forming stars have implications for understanding the way in which a protostellar clump solves the 'angular momentum problem,' i.e., how it produces a star having far less angular momentum than the original clump. Circumstellar accretion disks are important in models of how stars form from rotating clumps. Such disks may play a role in channeling the bipolar flows described above, and they are obviously relevant to the formation of planetary systems and binaries. It is impossible to image circumstellar disks in optical emission because they are too cool to emit significantly at optical wavelengths and they are obscured by the intervening dust. Evidence supporting the presence of disks has been presented in a few cases at mid-infrared (Cohen 1983), millimeter (Plambeck et al. 1982), and centimeter wavelengths (Bally, Snell, and Predmore 1983). However, the prevalence, sizes, motions, and lifetimes of such disks are still essentially unknown. The sensitivity of the proposed array to motions of relatively cold emitting gas on the arcsecond scale makes it a potentially very valuable tool to study protostellar disks.

For each of the preceding spectral line studies, a submillimeter array can also provide simultaneously a sky map of the continuum emission due to dust. Two such maps spanning the submillimeter wavelengths (e.g., at 1.3 and 0.3 mm) can be used to determine the spatial distribution of dust temperature near the star. When combined with IRAS measurements at 0.10, 0.06, 0.03, and 0.01 mm, the maps can be used to estimate the stellar luminosity. The dust temperature distribution will help us understand how the star heats the dust; how the dust heats the gas; and how dust and gas densities are distributed near the star. The stellar luminosity will be crucial to estimating the mass and evolutionary state of the star. Since a submillimeter instrument can measure dust continuum in addition to CO line emission, it has a distinct advantage over a millimeter instrument of the same resolution and collecting area. This advantage occurs because the flux density from emission of optically thin dust increases with decreasing wavelength as λ^{-3} to λ^{-4} (Section II). Therefore, dust emission at 0.87 mm (near the CO J = 3-2 line) will be more intense than at 2.6 mm (near the CO J = 1-0 line) by a factor between 27 and 81, a highly significant increase, even after one allows for a relative disadvantage in submillimeter receiver noise temperature and atmospheric attenuation. This disadvantage is now typically a factor ~ 5, and it may be much reduced by 1990.

ii. Structure of Galaxies

A number of important and fundamental problems in galactic structure can be studied with the submillimeter array through observations in the CO lines and dust continuum. We first discuss CO observations. The density-wave theory (Lindblad 1963; Lin and Shu 1964) offered the first plausible model for the persistence of spiral structure of galaxies.

Confirmation or refutation of this theory, or of competing theories, has been difficult: for our own galaxy, identification and interpretation of possible spiral structure have been controversial because of our poor perspective and inadequate measurements of line-of-sight distance. For external galaxies, the coarse angular resolution allowed by existing instruments operable at millimeter and submillimeter wavelengths has made detailed quantitative studies practically impossible. For example, in the CO line, only one galaxy has been resolved so far (Lo et al. 1984). Some high resolution studies have been made of 21-cm emission from atomic hydrogen, but this emission is a poor tracer of the mass because in many regions most of the mass is in H_2 molecules, not H atoms, and the two types of region do not always coincide. In molecular clouds, the low temperature and high ultraviolet extinction that protect H_2 molecules from collisional or radiative dissociation also inhibit the destruction of CO molecules. Hence, observations of CO molecules offer the hope of tracing more of the mass than observations of H atoms, and array observations with one arcsecond resolution will allow detailed study of the structure of galaxies in our local group of galaxies.

Arcsecond-resolution maps of the CO lines can have important implications for the lifetime and formation of giant molecular clouds. For example, if many molecular clouds are seen outside of the spiral arms defined by the light from hot young stars, then these clouds probably live longer than the period of the spiral density wave; and the clouds probably form independent of spiral structures. On the other hand, if most molecular clouds appear confined to spiral arms, then the clouds and their stars may form only after compression due to passage of a spiral density wave, and the clouds may be younger than the period of the density wave (Scoville and Hersh 1979; Cohen et al. 1980).

The study of galactic nuclei will also be aided by CO observations at arcsecond resolution. The predominance of molecular over atomic gas, discussed earlier, is enhanced in many nuclei (Morris and Rickard 1982). There, CO molecules will be a better tracer of mass than H atoms, as discussed earlier in this section. There is evidence (Ho, Martin, and Ruf 1982) that gas in the nuclear regions may be hotter than elsewhere. This warm ($\gtrsim$ 30K) gas is especially well-matched to studies at submillimeter wavelengths, as explained in Section II A. In addition to revealing the mass and distribution of molecular gas in galactic nuclei, CO observations will trace the patterns of gas velocity, while comparison of submillimeter and millimeter lines will determine the excitation of the gas. Our sensitivity calculations in Section II B below indicate that the array will be able to map easily the spatial and velocity distribution of giant molecular clouds in the 10 nearest spirals, even with present receiver sensitivity.

The investigation of velocity fields in the nuclei of galaxies is particularly important. These velocity fields have been mapped with one-arcsecond resolution by means of optical emission lines (Hα, H II, etc.) by Rubin and Ford (1971) and by Rubin, Ford, and Kumar (1973). These investigations revealed unexpectedly strong deviations from circular motions that are not understood within present theories. There are many dark clouds of arcsecond angular size in the nuclear regions of M31 and other nearby galaxies. The measurement of the velocities of these clouds from their molecular line emission can be used to study kinematic phenomena on the same scale size as from optical studies. Hence, a submillimeter array would enable the study of molecular gas kinematics that is complementary to optical studies of ionized gas but does not depend on the presence of hot stars that ionize the gas.

Array observations of dust emission from spiral galaxies will give high-resolution maps of the total luminosity and spatial distribution of very young stars. Knowledge of the total luminosity of young stars is important to the problem of estimating the rate of star formation in the galaxy. The spatial distribution of obscured young stars is valuable for comparison with the distribution of optically visible stars and of molecular clouds, particularly for analysis of spiral galaxies. The spectra of several nearby spiral galaxies, shown in Figure 3, suggest that dust is the primary source of emission in the submillimeter range. The distribution of dust emission in galaxies will give information that is not available by any other means. At optical and near-infrared wavelengths, dust absorption of starlight is significant, and only the less-obscured stars are directly visible. Grains that obscure the youngest stars reemit most of the energy they absorb from stellar photons, but at much longer wavelengths, because the grains are cooler than the stars. Therefore, the youngest stars that are optically obscured are indirectly observable by long-wavelength (infrared and submillimeter) emission from obscuring circumstellar dust. A grain heated to 30K by stellar photons will have maximum emission intensity at $\lambda \sim 0.1$ mm, and its intensity will decline with increasing wavelength as λ^{-3} to λ^{-4} (Section II A). At 0.1 mm, ground-based observations are excluded by atmospheric absorption; and airborne or satellite observations with arcsecond resolution will probably remain impossible for at least several decades. Thus a ground-based submillimeter array offers the best way to study the total luminosity and spatial distribution of the youngest stars in galaxies -- better than at optical, near-infrared, or millimeter wavelengths because of the properties of interstellar dust; and better than at mid-infrared wavelengths because of superior angular resolution.

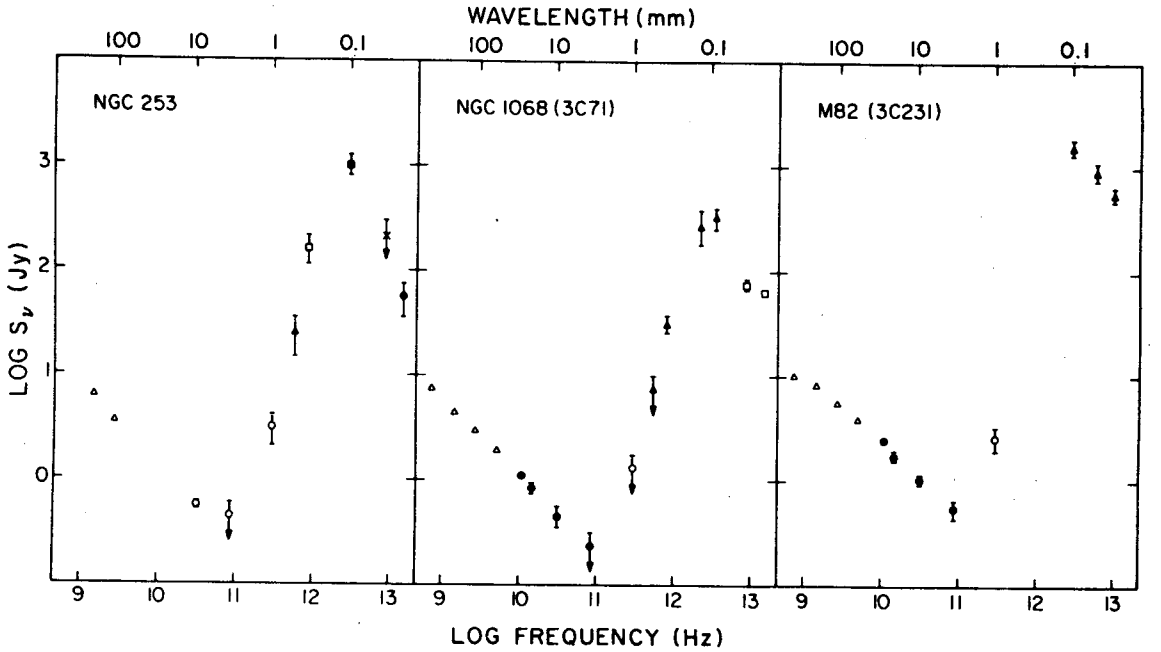

Figure 3. Spectra of three nearby galaxies. Note the prominent peak near 0.10 mm in each case. The excess submillimeter and far-infrared emission are believed to be due to thermal emission from dust. (From Elias et al. 1978.)

Submillimeter-wavelength dust emission will be detectable from many spiral galaxies. Observations with the IRAS satellite show that there are about 10,000 galaxies with emission stronger than ~ 0.5 Jy at 0.06 mm; nearly all these are probably spirals (Soifer et al. 1984). Most of these galaxies have not been optically identified and are 3 - 10 times brighter at 0.06 and 0.10 mm than typical identified galaxies. As outlined in Section I C(i) for individual stars, submillimeter observations will help measure the shape of the emission spectrum, the range of dust temperature, and the total luminosity. If, as in NGC 253 (see Figure 3 and Elias et al. 1978), flux density, S_ν, from 1 to 0.06 mm varies approximately as λ^{-2}, then there should be about 40 galaxies in this sample with $S_\nu(0.87\ mm) > 0.5$ Jy that are observable from the northern hemisphere (declination greater than -30^o). Hence ~ 40 galaxies should be detectable with signal-to-noise ratio > 100 (see Section II) with the proposed submillimeter array, even with the sensitivity of present-day receivers. These galaxies would be prime candidates for detailed mapping studies and comparison with the nearby spirals. Since the number of objects with flux density greater than S_o is proportional to $S_o^{-\frac{3}{2}}$, more than 1,000 should be detectable with signal-to-noise ratio greater than 10.

Applications of maps of galaxies in the CO lines and in the dust continuum were discussed above as separate subjects. We can expect further scientific benefits when such maps are analyzed together. When maps of dust emission are combined with CO maps of molecular clouds and optical photographs of more evolved stars, we will have matched-resolution 'snapshots' of spiral structure at distinctly different stages in the evolution of young stars. In addition, the dust emission gives a good estimate of the total stellar luminosity in a cloud, and the CO line

emission gives a good estimate of the total mass of the cloud. Thus, a comparison of continuum and spectral line maps will tell us the efficiency of star formation in molecular clouds as a function of position in the galaxy. This information will allow us to identify and study those galaxies with significant differences in star-formation activity between the nucleus and outlying regions; and between spiral arms and interarm regions.

iii. Quasars and Active Galactic Nuclei

One of the greatest challenges in extragalactic astrophysics is to learn the mechanism of the enormous energy production in compact objects, including quasars, nuclei of giant elliptical galaxies, BL Lac objects, and cores of radio galaxies. The most active of these sources are 'radio-loud' with nearly flat spectra, as measured from ~ 10 cm to 3 mm. They are rapidly variable (timescales of days or less) and have strong (> 3%) polarization in their optical and infrared emission, and occasionally in their radio emission. These 'blazars' (Angel and Stockman 1980) have been interpreted as relativistic jets beamed toward us, each perhaps powered by accretion onto a black hole (Rees 1978 a,b). The strongest constraints on models of these sources come from combining radio maps with data on flux density, polarization, and variability across the radio, infrared, and optical spectrum. However, present-day spectral coverage has a large gap: the properties of most compact objects in the spectral region from 3 to 0.02 mm, a span of more than two orders of magnitude in wavelength, are largely unknown.

The submillimeter array would be valuable for three related types of observation: (1) The flux densities, variability, and polarization of the

emission from radio-loud objects can be measured with high signal-to-noise ratio, as estimated in Section II B(i). The wavelength at which the flat radio spectrum turns down (i.e., becomes optically thin), is an important parameter in several synchrotron emission models of active galactic nuclei (e.g., Blumenthal and Gould 1970). In combination with measurements from other wavelengths (especially x-ray and longer radio wavelengths), an estimate can be made of the size and magnetic field strength of the continuum emitting region. Various models that fit existing spectral measurements are shown in Figure 4; it is clear that submillimeter-wavelength measurements provide a powerful discriminant. Pioneering measurements of this type have been reported by Roellig et al. (1984). We expect that the submillimeter array will have greater sensitivity for long integration times than a single-aperture telescope of the same total area and receiver noise temperature, because the sum of receiver and atmospheric noise is uncorrelated from one array element to the next (see Section II B). Therefore, the submillimeter array is well suited to study radio-loud quasars. (2) Many quasars are 'radio-quiet,' that is, their emission cannot be detected at centimeter wavelengths, but they have strong emission (~ 1 Jy) at 0.1 mm. The emission from such objects probably peaks in the submillimeter band and could be measured with the array. The importance of these measurements is discussed below. Finally, (3) the environments of some of the compact objects can be mapped on arcsecond scales, thereby matching the resolution available at centimeter wavelengths with the VLA, and at optical wavelengths. Such maps might reveal the presence of the dust in an underlying galaxy, thus helping to provide an understanding of the relation between compact objects and their environment.

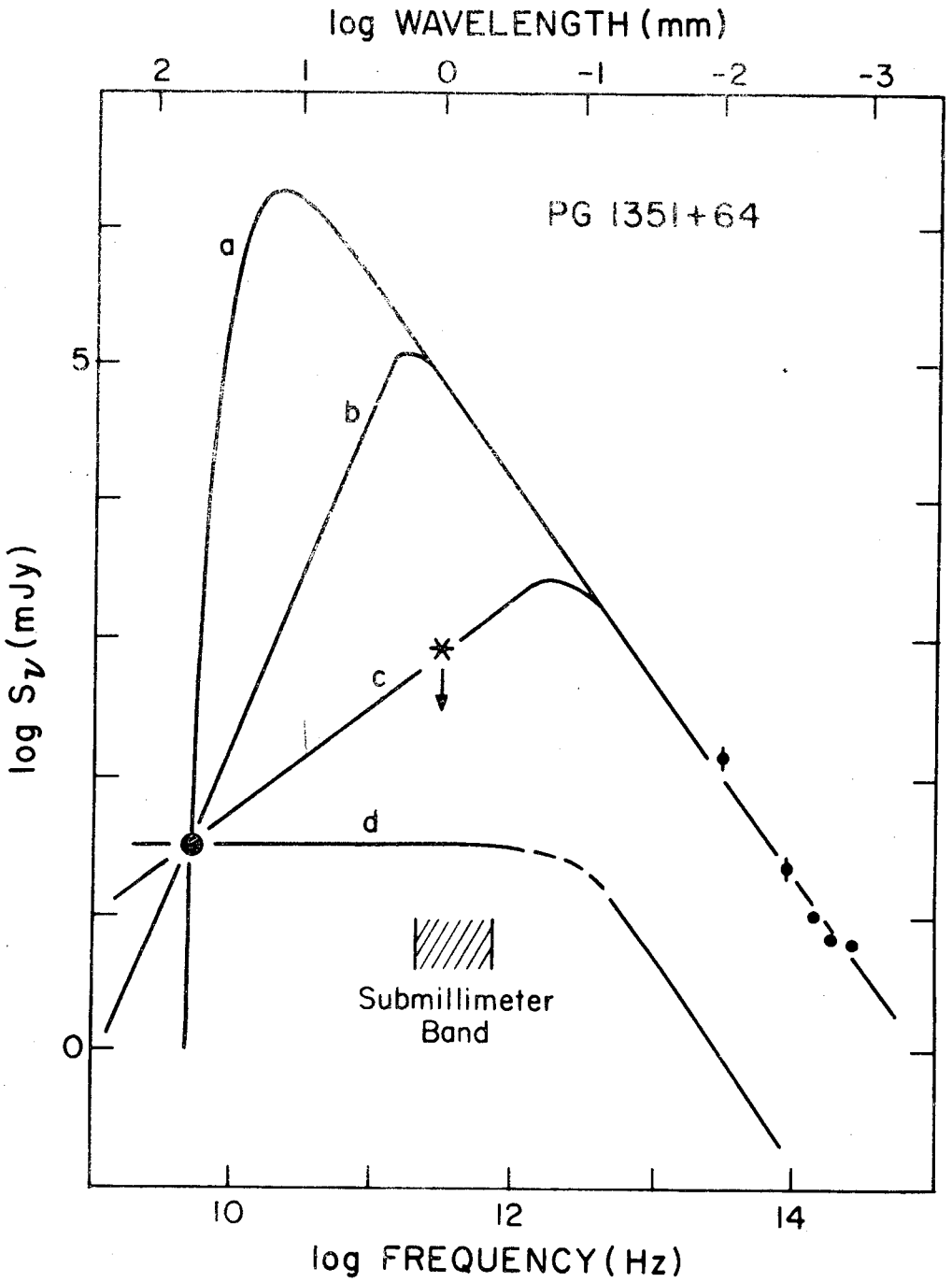

Figure 4. The flux density measurements on the radio-quiet quasar PG 1351 + 64. Even an upper limit (*) in the submillimeter band can be of crucial importance in distinguishing between the various models that fit optical, infrared, and radio data: (a) synchrotron source and external absorbing plasma, (b) homogeneous synchrotron, (c) inhomogeneous synchrotron, and (d) relativistic jet. (Adapted from Ennis, Neugebauer, and Werner 1982.)

The distinction between radio-loud and radio-quiet quasars seems to be basic to understanding the nature of quasars and active galactic nuclei, and the relationship between them. Only a minority of quasars are radio-loud. Most quasars have luminosity a thousand times weaker at radio wavelengths than at optical or x-ray wavelengths. There is currently no accepted explanation for this fundamental dichotomy in the quasar phenomenon. There is some evidence that radio-loud quasars reside preferentially in elliptical galaxies and radio-quiet quasars in spirals, but this relationship is not well established (e.g., Balick and Heckman 1982). Alternatively, if the radiation from quasars is highly beamed, then the difference between radio-loud and radio-quiet quasars may not be an intrinsic property but only an accident of viewing direction (Scheuer and Readhead 1979). The spectra of both the radio-loud and the radio-quiet quasars appear similar in the infrared, up to wavelengths as long as 0.1 mm. However, the radio limits at 6 cm are quite stringent in the radio-quiet cases (Figure 5). Therefore, the wavelength at which the spectrum 'turns over' must lie in the submillimeter region, as noted above. As can be seen in Figure 5, this region is precisely where measurements are lacking. An important possible outcome of such measurements is an excess above the power law deduced from the intensities at mid- and far-infrared wavelengths. This result would imply emission from dust, either in an underlying galaxy or in the outer parts of the quasar nucleus itself. Either of these implications would significantly strengthen our understanding of quasars.

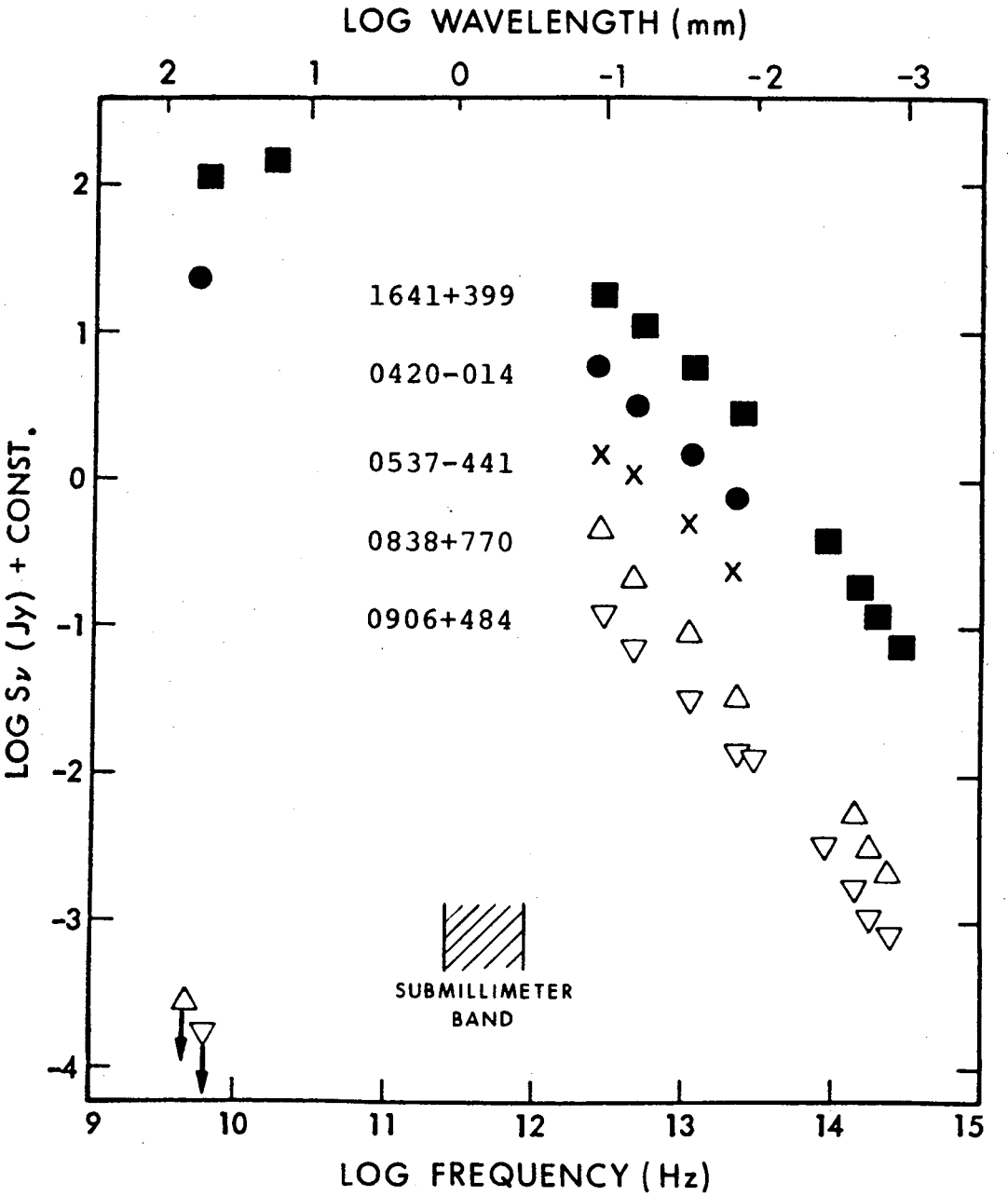

Figure 5. The spectra of several radio-quiet and radio-loud quasars. Filled symbols are radio-loud quasars, and open symbols are radio-quiet quasars. Note that the infrared spectra are similar. The presence of cold dust, detectable as an excess in the submillimeter range, would indicate the presence of an underlying galaxy. From Neugebauer et al. (1984).

iv. Solar System Studies

The array can be expected to make major contributions to the study of planetary surfaces and atmospheres. Radio observations provide important information on the properties of the solid surfaces of planets, moons, and asteroids. These properties are revealed through measurements of brightness temperature as a function of wavelength and insolation. For solar system bodies with atmospheres, high-resolution submillimeter-wavelength observations of spectral lines can be used to determine the molecular content versus the time of day.

The brightness temperature of a body depends on the physical temperature of the material and its electrical properties. In particular, the thermal radiation from the surface of a body is equal to the physical temperature of each layer weighted by the emissivity and the absorption coefficient. The temperature profile in the surface layer is controlled by solar radiation and any internal heat sources, and depends on the thermal properties of the material, such as thermal conductivity and specific heat, as well as on density. The brightness temperature of a portion of the surface will vary with time as the solar flux on it varies; generally temperatures are lower further away from the subsolar point. The radiation will be polarized towards the limbs, with the amount depending on the dielectric constant and surface roughness. The effective depth from which the radiation emerges is given by $\lambda/(2\pi\sqrt{\varepsilon}\tan\delta)$, where ε is the real part of the dielectric constant and $\tan\delta$ is the loss tangent, which generally decreases with increasing wavelength. Typical effective depths are between a few wavelengths and a few hundred wavelengths. The array would be very sensitive (5 mJy or 0.05K standard error with 1-arcsecond resolution at 0.87 mm in 10^5 s) to thermal radiation, more sensitive in terms of

brightness temperature than the VLA because of the λ^{-2} dependence of blackbody radiation. The surfaces of Mercury, Mars, Pluto, at least 10 asteroids, most of the Jovian moons, and the rings of Saturn could be studied effectively. Consider, for example, observations that could be made of Io, the innermost Galilean satellite of Jupiter. It has been detected, but not mapped, by the VLA, and barely detected by planetary radar. At 2 cm the brightness temperature is about 100 K and the mean depth from which the radiation can emerge may be several meters. Measurements are needed in the millimeter and submillimeter ranges to probe the properties closer to the surface. De Pater, Brown, and Dickel (1984) stress the importance of such measurements. Knowledge of the subsurface properties is important to the understanding of the contraction history of the satellite and its bombardment history (Morrison and Cruikshank 1974). Submillimeter observations can only be made with an interferometer since the signals from Jupiter, less than 2 arcminutes away, are 2000 times greater than those of Io, and are not easily rejected in single telescopes because of their extended sidelobe response. Io subtends an angle of 1 arcsecond and has a flux density of about 7 Jy (~ 100 K) at a wavelength of 0.87 mm, so that it can be easily detected. It should even be possible to make maps of Io with a modest number of pixels at the shorter submillimeter wavelengths.

Mercury subtends an angle of about 6 arcseconds and at 0.5-arcsecond resolution can be mapped with the array in about 30 pixels. Each pixel in such a map would have a signal-to-noise ratio of ~ 100 given 300 seconds of integration. The surface temperature varies between 600 K on the sunlit side to less than 150 K on the dark side. The variation in the radio emission that originates below the surface will show less excursion (Ulich,

Cogdell, and Davis 1973). From the variation in submillimeter emission, the electrical and thermal properties of the subsurface material can be deduced, which provide information on its compaction. Mars can be studied in a similar way. Its mean temperature is about 200 K and it subtends an angle of 15 arcseconds at closest approach. The submillimeter regime is particularly important to the study of Saturn's rings. The emission from the rings, as opposed to scattered radiation, is undetectable at longer wavelengths because of the strong wavelength dependence of emission from the ring material. Interferometric observations may be important in establishing the sizes and composition of the particles in the rings.

The submillimeter array can be used to probe the molecular emission from the atmospheres of Venus and the Jovian planets and major satellites that have atmospheres, such as Titan. Of particular importance, for example, are CO observations of Venus. Because the surface of Venus is much hotter than its atmosphere, strong (~ 100 K) absorption line profiles are readily observable. Single antenna millimeter-wavelength observations have shown that these profiles have broad wings indicative of pressure broadening (Wilson et al. 1981). Together with the pressure and temperature profiles obtained from space probes, a CO profile can be used to determine the mixing ratio of CO versus altitude. CO is thought to form as a result of ultraviolet decomposition of CO_2 on the sunlit side and to be carried to the nightside of Venus by strong winds. Observations show that the mixing ratio is greater on the nightside than on the dayside. In addition, Clancy and Muhleman (1983) have suggested that chemical fractionation occurs during the day-night transport of CO. The angular size of Venus changes from 10 to 60 arcseconds due to orbital motions so it can be well resolved with the proposed array. Furthermore, observations of

several CO transitions will make it possible to invert the profiles to obtain the mixing ratio versus altitude without knowledge of the temperature and pressure profiles. Thus, with the array it will be possible to measure the CO mixing ratio in three dimensions. It may also be possible to measure the wind speeds and study chemical fractionation. The study of atmospheric conditions on Venus and other planets may have an important relationship to the extensive work being done to understand the earth's atmosphere.

Finally, the molecular constituents of comets can be studied with a submillimeter array. Comets are thought to contain the most primitive material in the solar system and are being studied for clues to the origin of the solar nebula (Whipple and Huebner 1976). Several molecular lines have been detected in the microwave spectrum of comets (Snyder 1982). With a submillimeter array, many new molecular transitions could be measured, and the excitation and abundance of molecular species could be probed in the central regions of comets.

v. Summary

We summarize the four main scientific applications of the array as follows. For star formation, the unique combination of arcsecond resolution at submillimeter wavelengths offers the prospect of detecting and studying long-sought evidence of gravitational infall onto very young stars. High-velocity flows from recently formed stars could be imaged with unprecedented resolution and sensitivity, thus elucidating the flow mechanism that limits the growth of a star. The array could map the structure and motions of protostellar disks and allow the study of their role in forming binary stars and planets. Finally, the array would be far

more sensitive to emission from circumstellar dust than studies at longer wavelengths. In combination with existing far-infrared data, it could measure the luminosities of invisible young stars and could thereby help to estimate the masses of young stars.

Fundamental contributions to the study of galaxies are also anticipated. Emission in rotational lines of CO could be observed with arcsecond resolution, providing new maps of spiral structure in molecular clouds. Observations of emission by warm circumstellar dust would reveal the spiral structure of the youngest stars, still obscured at optical wavelengths. These two new views of galactic structure would add greatly to our understanding of the origin and maintenance of spiral patterns in galaxies and to our understanding of why some clouds are producing stars with high efficiency and others with low efficiency.

The array, because of its high sensitivity, could provide accurate measurements of the submillimeter emission from quasars and active galactic nuclei to clarify the relationship between these enormously energetic objects and to try to learn the mechanism of their energy production. These measurements would be crucial to distinguishing between the mechanisms leading to 'radio-loud' and 'radio-quiet' quasars and would be more sensitive than comparable single-aperture instruments.

The array would give unique new information about the surfaces and atmospheres of planets and other solar system bodies. Array maps of Mercury, Mars, Saturn's rings, and some dozen or more other bodies would reveal their subsurface temperature structure, and would constrain models of their subsurface composition and dielectric properties. Molecular line observations of the atmospheres of Venus, Titan, and other bodies would

give new knowledge of planetary 'weather' -- the structure of atmospheric winds and the variations in chemical constituents.

The remaining sections of this report give a more detailed description of some of the scientific potential of the instrument (Section II); a discussion of the technical issues affecting array performance (Section III); a budget for construction and operation (Section IV); suggestions and recommendations concerning the strategy of developing a submillimeter array (Section V); our main conclusions (Section VI); acknowledgments; two appendices; and references.

II. SCIENTIFIC POTENTIAL

A. Emission by Dust and Molecules

To describe and evaluate the scientific potential of a submillimeter array, we first discuss some basic properties of emission by dust and molecules. Emitters that can be described by a temperature T (e.g., dust that has a kinetic temperature, and molecules whose lines have excitation temperatures) will have their strongest emission at a wavelength λ close to hc/kT, where h is Planck's constant, c is the speed of light, and k is Boltzmann's constant. For such cases the emission intensity falls off much more rapidly on the short-wavelength (Wien) side of the peak than on the long-wavelength (Rayleigh-Jeans) side. Therefore an instrument operating over a fixed range of wavelengths will receive strongest signals from a thermal emitter, of fixed size and distance, whose peak intensity occurs near the short-wavelength end of the operating range.

These considerations allow estimates of the range of temperatures for which the emitted intensity is greatest at submillimeter wavelengths. We make estimates for (1) black-body emitters, whose flux density can be written

$$S_\nu \propto \lambda^{-3} \left[e^{a/\lambda T} - 1 \right]^{-1}, \qquad (1)$$

with a =hc/k = 1.44 cm K; (2) optically thin dust, where the emissivity is assumed to vary as λ^{-2} (e.g., Savage and Mathis 1979), for which

$$S_\nu \propto \lambda^{-5} \left[e^{a/\lambda T} - 1 \right]^{-1}, \qquad (2)$$

and (3) optically thin emission in a rotational line of a linear molecule with excitation temperature T_{ex} and rotation constant B_o, for which the flux integrated over the line is

$$S = \int S_\nu d\nu \propto \lambda^{-4} \left[\frac{c}{2B_o\lambda} + 1\right] \exp\left[-\frac{a}{2\lambda T_{ex}} \left[\frac{c}{B_o\lambda} + 1\right]\right], \qquad (3)$$

where $c/2B_o\lambda = J$, the upper level rotational quantum number. Equation (3) is an expanded form of the familiar equation $P = h\nu An_u$, where P is the radiated power per unit volume, ν is the frequency, A is the Einstein coefficient of the transition, which is proportional to λ^{-3}, and n_u is the upper level population density for the transition. In equation (3) the left-most term in brackets is the degeneracy factor, and the 'exp' function is the Boltzmann factor. In the Rayleigh-Jeans regime the dependence of these expressions on wavelength is (1) $S_\nu \propto \lambda^{-2}$; (2) $S_\nu \propto \lambda^{-4}$; and (3) for $J \gtrsim 3$, $S \propto \lambda^{-5}$. These power laws imply that if submillimeter emission of these types is in the Rayleigh-Jeans regime, it is much more intense than at millimeter or centimeter wavelengths.

Figure 6 shows plots of these relations for (a) CO lines with typical excitation temperatures, T_{ex}, of 10 K and 50 K, (b) a blackbody and a blackbody x λ^{-2} (optically thin dust) at 10 K; and (c) atmospheric transmission for 1 mm of precipitable H_2O, for wavelengths from 3.0 to 0.1 mm. Figure 7 shows the actual dust spectrum of the nearby dust globule B335. These figures show that relatively cool dust (T ~ 10 K) and CO molecules (T ~ 10 - 50 K) will have their strongest emission at the submillimeter wavelengths over which the array is expected to operate. Therefore the submillimeter wavelengths are well matched to the conditions in molecular clouds, where the extended cloud material is at T_{ex} ~ 10 K;

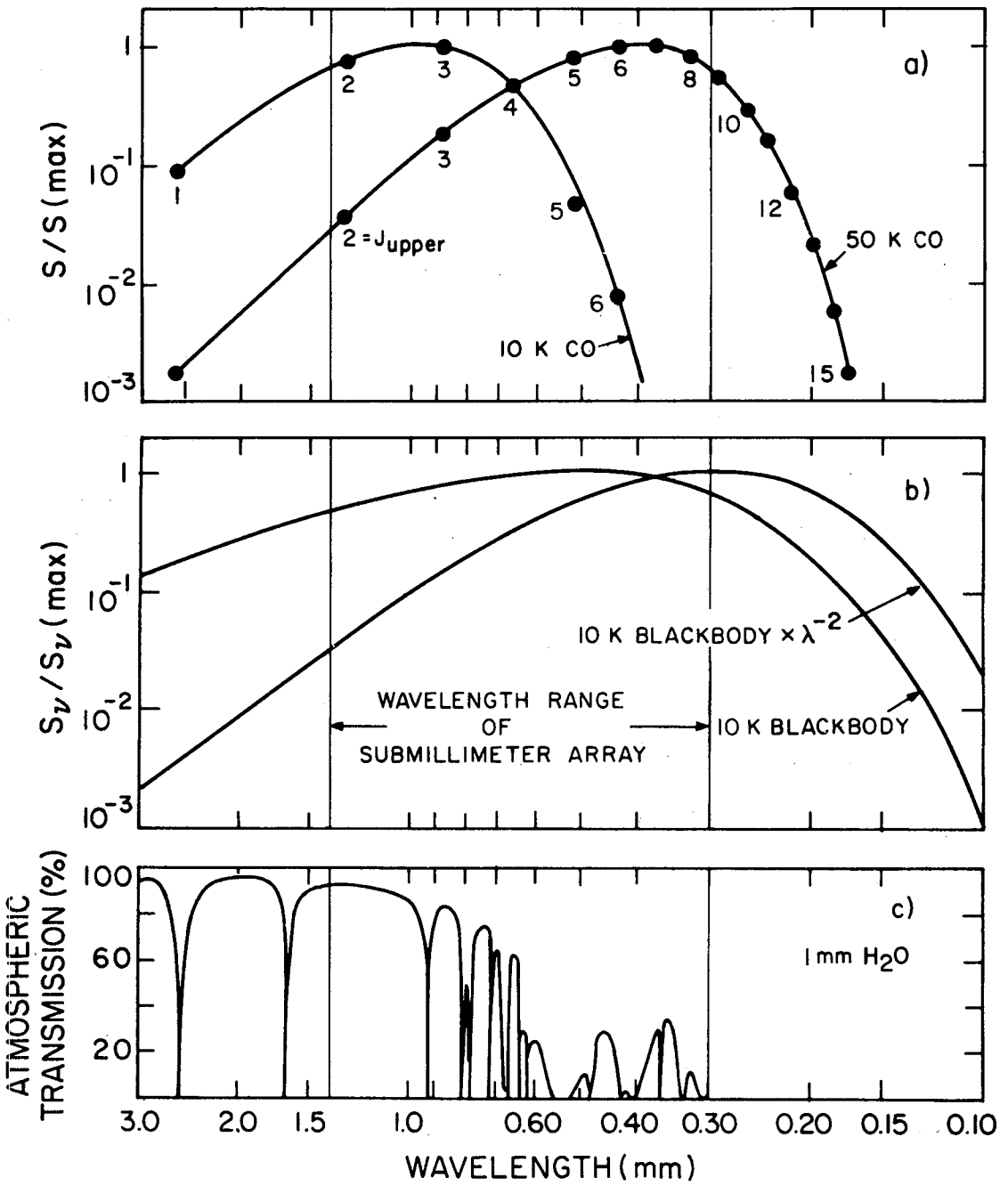

Figure 6. (a) curves of relative integrated flux density in optically thin rotational lines of CO, for excitation temperatures 10K and 50K, as functions of wavelength (see equation (3) and Table 1); (b) relative flux density for a 10K blackbody and for a 10K blackbody x λ^{-2}, the latter to simulate emission by optically thin dust; (c) predicted atmospheric transmission when the column density of precipitable H_2O is 1.0 mm.

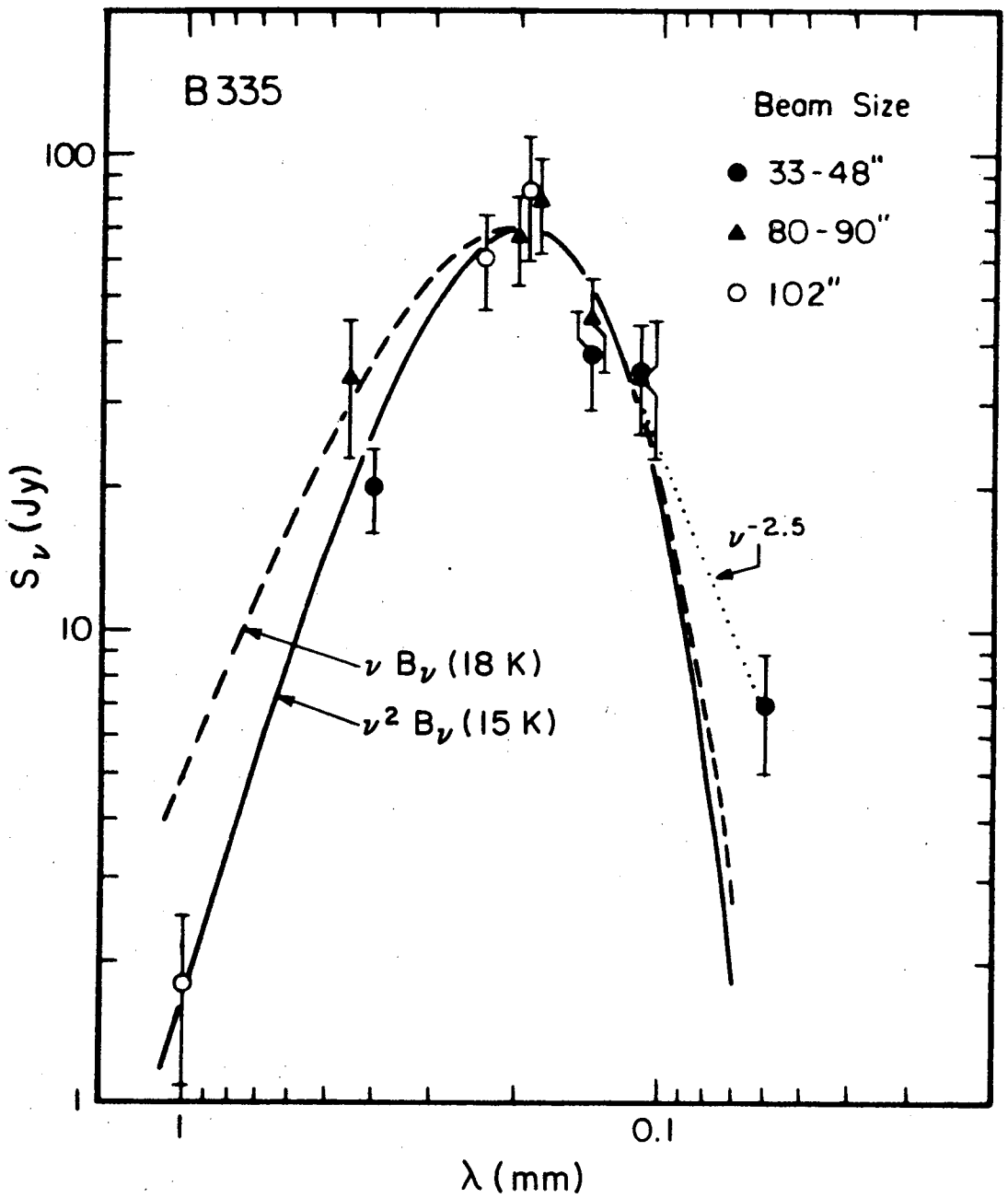

Figure 7. Spectrum of B335, a small isolated dust globule, at a distance of ~300 pc, whose angular size at far-infrared wavelengths is less than 30 arcseconds. Dust emissivity longward of 0.10 mm probably scales as ν^2. The solid line shows a model of a blackbody at 15K times ν^2, and the dashed line a model of a blackbody at 18K times ν. The data are best fit by the dotted curve, labeled $\nu^{-2.5}$, for $\lambda < 0.1$ mm. The emission peaks in the submillimeter region and may represent a young star or protostar of about a solar mass. Data from Keene et al. (1983).

and near young stars in molecular cloud cores, where gas and dust temperatures up to ~ 100 K have been observed. Furthermore, emission at submillimeter wavelengths will be the strongest available to ground-based observations of optically thin dust with temperatures up to ~ 100 K and CO molecules with temperatures up to several thousand degrees, because the wavelength of peak emission for temperatures up to these values will lie in the opaque part of the atmospheric transmission curve between the submillimeter and infrared bands (i.e., from ~ 0.3 to 0.03 mm), and because the submillimeter emission on the Rayleigh-Jeans side of these peaks will be stronger than the infrared emission on the Wien side. These facts make a submillimeter telescope of high angular resolution well-suited to study the tens of thousands of galaxies and young stars recently discovered by the IRAS satellite.

At submillimeter wavelengths CO is one of many linear molecules having rotational transitions with intensity sensitive to temperatures expected in star-forming regions in molecular clouds. For three molecules well-studied at millimeter wavelengths (CO, CS, HC_3N), Table 1 shows the number of available transitions and the wavelengths that maximize the flux in an optically thin line, as given by equation (3), at excitation temperatures of 10, 50, 150, and 600 K. The table shows that one can 'tune' the gas temperature to which one is most sensitive by selecting a line of a molecule with an appropriate rotation constant. Some lines of the molecules in Table 1 have already been detected at short millimeter or submillimeter wavelengths: CO, J=3-2 (Erickson *et al.* 1982); CO, J=6-5 (Koepf *et al.* 1982); and HC_3N, J=30-29 and J=31-30 (Erickson *et al.* 1980).

Table 1

Rotational Transitions of Selected Linear Molecules at Submillimeter Wavelengths

Molecule	Rotation Constant[a] B_o (GHz)	Number of Available Transitions[b]	Wavelength λ_{max}(mm) of Maximum Integrated Intensity[c] When T_{ex} is 10 K	50 K	150 K	600 K
CO	57.5	4 (J=2,3,4,7)	0.87	0.37	(0.22)	(0.11)
CS	24.5	8 (J=5,6,...,10; 14;17)	(1.5)	0.61	0.34	(0.17)
HC_3N	4.55	43 (J=25,...,51;70, ...,75;89,...,97)	(3.0)	(1.4)	0.78	0.39

[a] From Lovas, Snyder, and Johnson (1979).

[b] Number of rotational transitions from J to J-1 in the wavelength range 0.30 mm $\leq \lambda \leq$ 1.30 mm having zenith atmospheric transmission > 0.2 when the column height of precipitable H_2O is 1.0 mm.

[c] For fixed excitation temperature, T_{ex}, the integrated optically thin line intensity S in equation (3) is maximum with respect to transition wavelength λ at λ_{max}. For example, CO at 50 K has maximum S at λ_{max} = 0.37 mm (J = 7-6), as shown in Figure 6. Values of λ_{max} in parentheses are outside the range 0.30 mm $\leq \lambda_{max} \leq$ 1.30 mm.

The dependence of the flux of a thin molecular line on temperature, as described above, becomes less dramatic as the line becomes optically thick. The peaks of ^{12}CO lines are well known to be optically thick in extended molecular clouds. However the array will resolve most of the extended emission. This fact suggests that much of the detected emission will be in line 'wings', which are more nearly thin, and the central parts of the line will tend to be resolved. Indeed, recent observations of the Caltech millimeter-wavelength interferometer with ~ 6-arcsecond resolution in the J=1-0 transition of CO show that the central part of the line is resolved as expected (Claussen et al. 1983).

The potential of submillimeter observations described above is based on known, well-studied molecules. It is also possible that lines of new molecules will be found and will be useful. An important class of such molecules is the diatomic metal hydrides, including NaH (J=1-0 line at 1.0 mm), MgH (0.87 mm),and CaH (1.2 mm). These metal-bearing molecules may prove useful in estimating how much metal depletion onto grains has occurred in interstellar clouds. Such depletion is of interest in its own right for models of clouds chemistry and has influence on the fractional ionization of the gas (Winnewisser, Aliev, and Yamada 1982).

The foregoing estimates refer to dust and gas conditions that give the strongest emission at submillimeter wavelengths. These estimates indicate that cold molecular clouds in our own galaxy and other galaxies are likely to be well-matched to the array wavelengths. However they cannot substitute for detection estimates, which take into account the expected sensitivity of the array. In the following section we make quantitative estimates of the signal-to-noise ratio expected for a wide variety of potential objects of study and briefly describe each type of object.

B. Detection Estimates

We have estimated the sensitivity of an array of six 6-m-diameter telescopes, each with an aperture efficiency of 0.5 and a receiver system temperature 1500 K at 0.87 mm. The system temperature includes the effect of an atmospheric transmission of 0.8 in the zenith direction, which is appropriate for ~ 1 mm of precipitable H_2O. We assume bandwidths of 1 GHz for continuum observations and one-third the line width for line observations. Column 7 of Table 2 shows the signal-to-noise ratio (SNR) expected for a number of interesting solar system, galactic, and extragalactic objects in an integration time of 10^5 s, equivalent to about three nights of observation. Such long-integration observations with an interferometer are practical because the noise from each element, including both atmospheric and receiver contributions, is uncorrelated with that from every other element. In contrast, single-antenna beam-switched systems have not reached their theoretical performance for times longer than typically a few tens of minutes for continuum observations. Column 8 shows the distance to which each such object could be 'moved' so that the signal-to-noise ratio would equal 10. Thus, comparison of column 4 and column 7 shows the range of distance over which the array could detect each type of object within the stated range of signal-to-noise ratios.

The following paragraphs briefly describe each type of object in Table 2. This discussion emphasizes detection estimates; detailed discussion of the scientific importance of the observations of each type of source is given in Section I.

Table 2

Sensitivity of Submillimeter Array[+] at 0.87 mm to Various Types of Astronomical Object

A. Continuum Sources

Object	Emitter	Name	Distance	Angular Diameter	SNR in 10^5 s	Distance[++] (SNR=10)
Asteroid	blackbody	Juno	2.7 AU	0.1"	29	4.6 AU
Planet	blackbody	Pluto	39 AU	0.2	32	70 AU
Star	blackbody	Sirius	2.7 pc	0.01	10	2.7 pc
Circum-stellar Shell	dust	OH 26.5+0.6	800 pc	4	27	1.3 kpc
Solid Circum-stellar Particles	blackbody	Vega	8.1 pc	20	48	18 pc
Low-Mass Protostar	dust	B 335	400 pc	10	63	1 kpc
Massive Protostar	dust	W3 IRS5	2 kpc	10	510	14 kpc
Ultra-compact HII Region	thermal plasma	W3(OH)	2 kpc	2	300	11 kpc
Galactic Nucleus	dust	NGC 253	3 Mpc	<50	1900	42 Mpc
Quasar, Seyfert Nucleus	synchro-tron plasma	3C84	79 Mpc	0.005	9.5×10^3	2.4 Gpc

[+] We assume six 6-m-diameter telescopes, T_{sys}=1500 K, bandwidth=1 GHz (continuum) or linewidth/3, and that the source angular diameter is smaller than the synthesized beam (see Section III C for a discussion of sensitivity). The angular sizes of the protostellar emission regions are assumed to be 10 arcseconds, guided by available coarse-resolution data.

[++] The distance to which the object could be 'moved' so that the signal-to-noise ratio would equal 10.

B. CO J=3-2 Line Sources

Object	Name	Distance	Angular Diameter	SNR in 10^5s	Distance (SNR=10)
Circum-stellar Shell	Betelgeuse	200 pc	<20"	850	1.8 kpc
Low-Mass Protostar	IRAS source in Taurus	140 pc	10	450	940 pc
Massive Protostar	IRAS source in Orion	500 pc	10	5500	13 kpc
Proto-stellar Outflow	Orion IRc2	500 pc	10	600	3.9 kpc
Extra-galactic Cloud	Cloud in M 83	4 Mpc	4	50	8.9 Mpc

i. Continuum Sources

Asteroids -- There are 10 asteroids like Juno, with radii $\gtrsim$ 100 km, within the asteroid belt ~ 3 AU from the Sun. Submillimeter observations can be used to infer properties of an asteroid's surface.

Planets and Satellites -- All nine planets are easily detectable; planets of Pluto's size could be detected at distances three times greater than that of Pluto. There are four satellites of Jupiter, one of Saturn (Titan), and one of Neptune (Triton) larger than Pluto and closer than Pluto, which could be studied easily. For Venus, Jupiter and Saturn, high-resolution observations of molecular constituents may make it possible to monitor the 'weather' on these planets (see Section I C(iv)).

Stars -- Thermal radiation from the photospheres of the brightest of the nearby dwarfs (Sirius) and the nearby giants (Pollux, Arcturus, β Peg) could be detected. It should be possible to compare the submillimeter flux density with the product (brightness temperature) x $(\text{size})^2$ expected from optical spectral classification. This comparison may constrain models of stellar atmospheres, particularly the chromosphere and higher layers, as has been done for the Sun.

Circumstellar Shells (OH 26.5+0.6) -- Dust shells around evolved stars, including OH/IR stars and carbon stars, are bright in the mid-infrared. For OH 26.5+0.6, IRAS observations (Olnon et al. 1984) and the assumption $S \propto \lambda^{-3}$ imply a signal-to-noise ratio of ~ 30 for the array at 0.87 mm. At 0.35 mm the flux will be ~ 15 times greater than at 0.87 mm, and mapping of the shell structure may be fruitful for studies of shell mass and dust emissivity. Maps of the dust emission will complement CO line emission, discussed in (ii) below.

Solid Circumstellar Particles (Vega) -- The circumstellar material around Vega (Aumann et al. 1984) could be detected and its flux compared with that expected for blackbody particles. At least three other such systems, Fomalhaut, ε Eri, and β Pic (Gillett 1984), have been found, and others may be found as the IRAS results are analyzed more thoroughly. There may be many cool systems that IRAS missed, because the IRAS bands would be on the Wien side of the blackbody peak for ~ 30K dust. Depending on the geometric filling factor of the dust particles, the array may detect such dust around some of the nearest stars.

Dust Around Low-Mass Protostars (B 335) -- The IRAS satellite discovered a large number of stellar sources like B 335 that are optically

invisible, but that have a luminosity several times that of the Sun emerging in the far infrared. The properties of B 335 are similar in some respects to those predicted by models of the formation of Sun-like stars by gravitational collapse. The proposed array could map the dust environment of these extremely young stellar objects. The spectrum of B 335, from Keene et al. (1983), is shown in Figure 7. On the radio side of the spectrum the flux increases as $\sim \nu^4$ so that a submillimeter interferometer is well suited to map its structure.

Dust Around Massive Protostars (W3IRS5) -- Highly luminous sources, like W3IRS5, appear to be forming OB stars. Submillimeter luminosity measurements allow estimates of the mass and evolutionary status of each star. The proposed array could detect such objects throughout the Galaxy.

Ultra-Compact H II Regions (W3(OH)) -- A recently formed O star, such as W3(OH), ionizes the dense gas around it, causing intense thermal bremsstrahlung. There are probably $\gtrsim 100$ such objects in the Galaxy that could be studied with the array. The ultra-compact H II region with the highest known emission measure (electron density squared integrated over volume) surrounds the very young massive star known as the Becklin-Neugebauer Object in the Orion nebula. Its electron density is $n_e \sim 10^7$ cm^{-3} and its size is L ~ 40 AU (Moran et al. 1983). A class of even smaller and denser objects with $n_e \sim 10^8$ cm^{-3}, L < 10 AU surrounding even younger stars may also be present. Such objects would be undetectable by the VLA but could be detected with a submillimeter array. The sound crossing time is so short for such an object, < 1 year, that it might be possible to observe motions such as expansion.

Dust in Galactic Nuclei (NGC 253) -- The dust luminosity in galactic nuclei is an important indicator of massive star formation; it can be compared with VLA centimeter-wavelength luminosity measurements to deduce the galactic distribution of massive stars. Probably more than 10 - 100 such galaxies can be studied with the array, including galaxies in the Virgo cluster. Spectra of NGC 253 and other galaxies are shown in Figure 3. In addition, 5,000 - 20,000 IRAS sources are probably spiral galaxies with 0.1-mm flux densities $\gtrsim$ 1.5 Jy. Hence, there is a surprisingly large class of spirals whose structure can be studied at submillimeter wavelengths. The potential of the array for studying spiral galaxies is discussed at greater length in Section I C(ii).

Quasars and Active Galactic Nuclei (3C84) -- There is a major gap, which extends from 3 to 0.02 mm, in the measurement of the spectra of most quasars and active galactic nuclei, such as 3C84. The spectra of many of these objects are expected to peak in the submillimeter band (1.3 to 0.3 mm). The wavelength of this turnover is an important parameter in the models of these sources, from which information about their energy mechanisms, geometry, and magnetic fields can be derived. There are probably at least 40 radio-loud quasars with flux densities at 1 mm greater than 1 Jy (Landau et al. 1983; Owen, Spangler, and Cotton 1980). These well-known radio-loud quasars would be used as phase calibrators for the array. Hence a large quantity of systematically obtained data on the time variability of these sources would be routinely obtained. Extrapolation of the log N - log S curve (see Section I C(ii)) suggests that about 3500 sources will be detectable with the proposed array with a SNR of 10 in 10^5 s.

ii. Spectral Line Emission in the J = 3-2 Transition of CO

Circumstellar Shells (Betelgeuse) -- Molecular-line measurements of emission from gas around evolved stars such as Betelgeuse (M2 supergiant) are useful to determine the stellar mass-loss rate and the stellar velocity. The array would be especially powerful for studies of stars like Betelgeuse, whose CO shell is unresolved in a 30-arcsecond beam and whose emission appears to be optically thin in the 2-1 and 1-0 lines. If so, the 3-2 emission will be ~ 8 times stronger than assumed in Table 2 (see discussion of optically thin lines earlier in this section).

Low-Velocity Molecular Gas near Low-Mass Protostars (IRAS source in Taurus) -- Low-velocity condensations associated with protostars of low luminosity and mass, such as those in B 335 and Taurus, are also easily detectable with the proposed array. As stated earlier, the IRAS satellite has discovered many such regions. The array could study both their continuum emission from dust and their CO line emission.

Low-Velocity Molecular Gas near Massive Protostars (IRAS source in Orion) -- Much of the dense, hot molecular gas near massive protostars, such as those seen by IRAS in Orion, has relatively small velocity dispersion (~ 3 km s^{-1}) and probably is a remnant of the gas clump that formed the protostar. Studies of such regions are important to the understanding of the initial conditions for massive star formation. The array would be extremely well suited to such studies. For the Orion Kleinmann-Low nebula, the proposed array should reach SNR = 10 in a 3 km s^{-1} wide spectral resolution element in less than 10 minutes. In 10^5 seconds, it could reach SNR = 10 for similar regions as distant as the Galactic Center.

High-Velocity Outflow from Protostellar Regions (Orion IRc2) -- The energetic gas flowing away from protostars, such as IRc2 in Orion, at $\gtrsim$ 50 km s^{-1} appears to represent an important phase in early stellar evolution. This motion may help a forming star clear away dense infalling gas and thereby limit the final stellar mass. These outflows tend to be fairly warm and are more optically thin than ambient gas. For example, the wings of the J=3-2 CO line in Orion are considerably stronger than those of the 2-1 and 1-0 lines (Erickson et al. 1982). There are several tens of examples known now; the proposed array would be able to detect such outflow regions throughout the Galaxy.

Giant Molecular Clouds in Nearby Spiral Galaxies (M 83) -- In nearby spiral galaxies, such as M 83, the degree of spiral structure in the molecular gas is unknown because of inadequate angular resolution of current millimeter-wave instruments. If these galaxies have giant clouds like those in our galaxy, these clouds will be detectable and resolvable with the proposed array. Recent observations suggest the presence of hot, optically thin CO in the cores of galaxies (Lo 1984, private communication). Such emission will be stronger at submillimeter than at millimeter wavelengths. Note that the estimate in Table 2 applies to a single cloud in the galaxy.

It is clear from Table 2 and the foregoing paragraphs that the proposed array can detect and study a wide variety of astrophysically significant objects. The sensitivity estimates given here are based on the best existing receiver performance (as of early 1984). The performance of millimeter-wave receivers has improved dramatically in the last several years. This point is discussed at greater length in Section III E. It is reasonable to expect that a similar improvement will occur in the next few

years in the submillimeter range. If so, the detection estimates given here will become even more favorable at 0.87 mm and at shorter wavelengths. The material in Table 2 is presented graphically in Figures 8 (continuum observations) and 9 (CO line observations).

C. Mapping

Table 2 shows the capabilities of the proposed array for detection observations, i.e., the SNR expected when the source is unresolved. The fine angular resolution of the array will best be utilized in making maps, and it is therefore important to identify those types of source that can be most easily mapped. For a 100-pixel map, the peak SNR will range between 0.1 (moderately extended source) and 1 (point source) times the SNR given in Table 2. Therefore, those objects in Table 2 with SNR $\gtrsim 10^2$ and angular size greater than ~ 1 arcsecond are the best candidates for mapping. Hence, dust and CO emission from protostellar regions are most suitable for fast mapping. It is also possible to map dust emission from galactic nuclei and CO emission from nearby galaxies (at 1 pixel per giant molecular cloud) as well as the circumstellar CO around evolved, mass-losing stars.

D. Advantages of Submillimeter Observations over Millimeter Observations

It is important to explain in detail why the main scientific applications of the array, described in Section I, are likely to be distinctly more effective at submillimeter wavelengths than at millimeter wavelengths. To make this comparison, we assume that a hypothetical 'millimeter array' has the same collecting area, atmospheric transmission (0.8), and telescope efficiency as the submillimeter array discussed here;

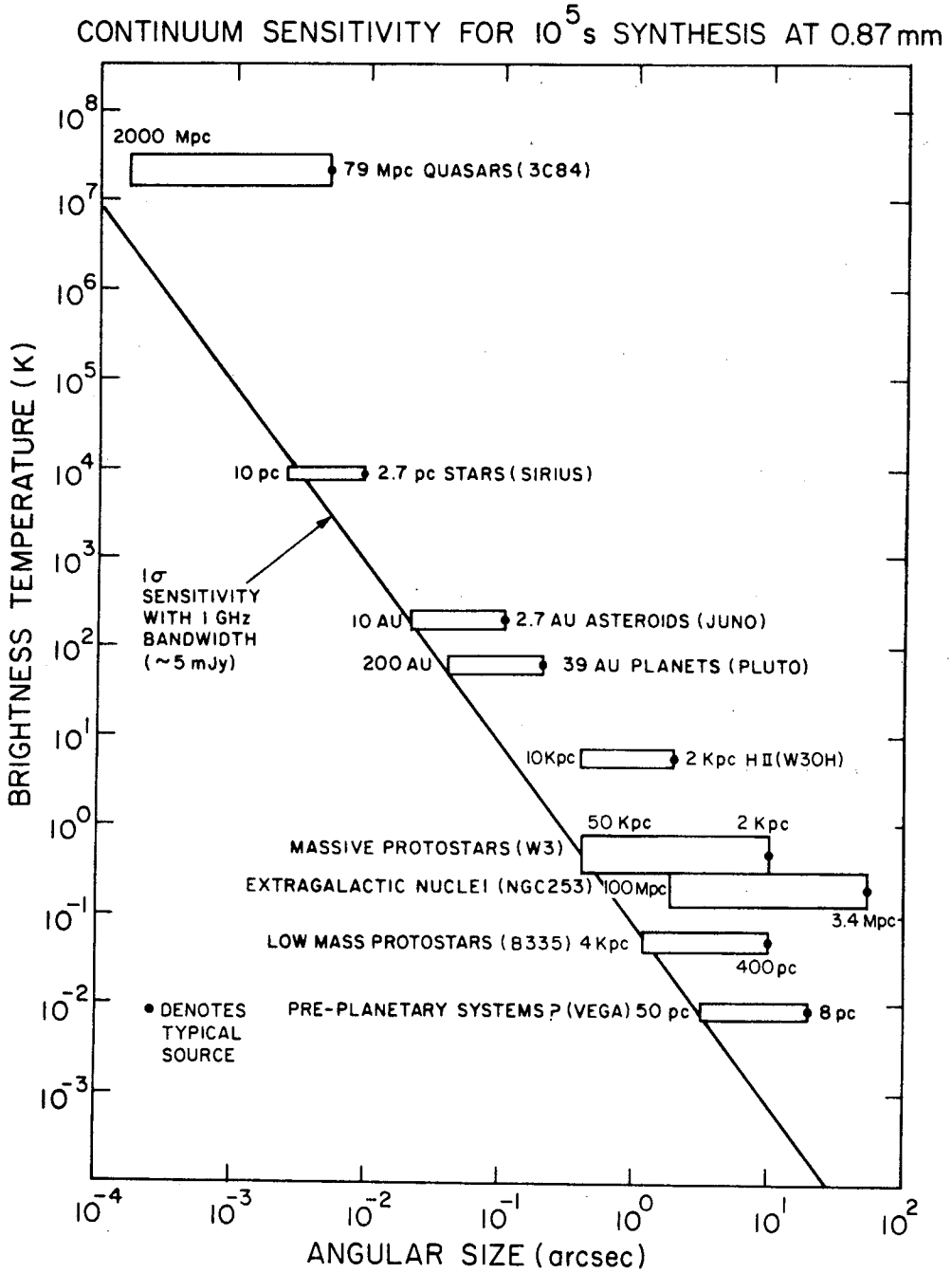

Figure 8. Estimated continuum brightness temperature of well-studied objects (points at right-hand end of each box) as a function of source angular size. The 1-σ sensitivity of the submillimeter array at 0.87 mm in 1-GHz band width in 10^5 sec (~ 5 m Jy) is shown as a line of slope -2. Each point is labeled according to its distance. The height of each point above the sensitivity line is proportional to the signal-to-noise ratio. The label at the left-hand end of each box is the distance to which each source could be 'moved' so that its signal-to-noise ratio is at or near the detection limit. See Table 2.

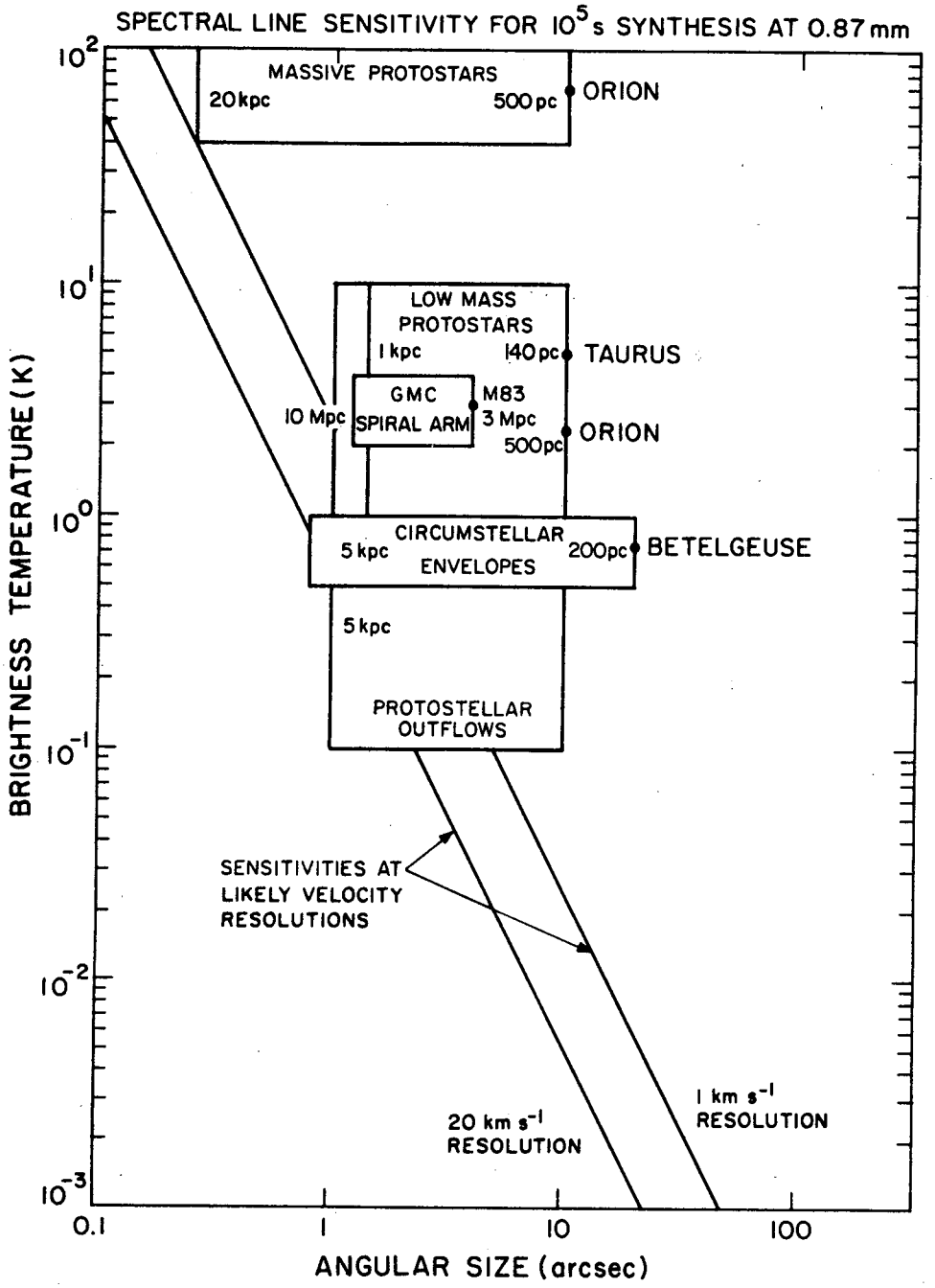

Figure 9. Estimated brightness temperature of the J=3-2 CO line due to well-studied galactic objects, as a function of source angular size. The 1-σ sensitivity of the submillimeter array at 0.87 mm in 10^5 s is shown for velocity resolutions of 1 km s^{-1} and 20 km s^{-1} as lines of slope -2. The labeling of each box is as in Figure 8. See Table 2.

and that the millimeter array is configured with larger baselines to give the same angular resolution as the submillimeter array. We assume that the millimeter array operates at 2.6-mm wavelength (at the J = 1-0 line of CO), with a system temperature, T_s', of 300 K, close to the current state of the art. We assume that the submillimeter array operates at 0.87 mm (at the J = 3-2 line of CO) with T_s' = 1500 K, as assumed throughout this report. These assumptions about receiver performance are conservative in the sense that T_s' for millimeter-wave receivers is now approaching the atmospheric limit, and is thus unlikely to improve much in the future, while there is much room for improvement in submillimeter-wave receivers.

For these assumptions, the relative signal-to-noise ratio is

$$\frac{(SNR)_{submm}}{(SNR)_{mm}} = \left[\frac{\lambda_{submm}}{\lambda_{mm}}\right]^{-4} \frac{(T_s')_{mm}}{(T_s')_{submm}} = 16 \qquad (4)$$

for observations of optically thin dust (Section II A, case 2) and

$$\frac{(SNR)_{submm}}{(SNR)_{mm}} = \left[\frac{\lambda_{submm}}{\lambda_{mm}}\right]^{-4.5} \frac{(T_s')_{mm}}{(T_s')_{submm}} = 28 \qquad (5)$$

for observations of the integrated intensity of an optically thin spectral line (Section II A, case 3). These signal-to-noise ratio advantages, when combined with the signal-to-noise ratio estimates in Table 2, suggest that most of the eight applications involving thin dust and molecular lines would be impossible or impractical with a millimeter array, despite its receiver noise advantage. These estimates indicate that the integration time needed to achieve a given signal-to-noise ratio would be greater for the millimeter array than for the submillimeter array by a factor ~ 250 for optically thin dust and by a factor ~ 800 for optically thin lines. For

most applications, these factors would prohibit millimeter observations if a choice were required.

To illustrate this advantage with recent observational data, we show in Figure 10 a composite of three single-antenna observations of the 'plateau' outflow source associated with the infrared object IRc2 in the Orion Molecular Cloud (Table 2 B, entry #4). The spectra are in the CO J = 1-0, 3-2, and 6-5 lines (Kwan and Scoville 1976; Erickson et al. 1982; and Koepf et al. 1982). The J = 1-0 spectrum is dominated by an intense, narrow 'spike,' which mapping reveals to be extended over many arcmin. In addition, there is a 'plateau' feature, weaker by a factor ~ 10 and broader by a factor ~ 5 than the spike; and mapping shows it to be localized to less than ~ 30 arcseconds.

The 'plateau' feature is thought to trace the energetic outflow motions from IRc2, in optically thin CO emission. Its peak brightness temperature grows dramatically from ~ 10% of the spike in the J = 1-0 transition, to ~ 40% of the spike in the J = 3-2 transition, to dominate the spike in the J = 6-5 transition. The relative increase in peak brightness temperature from 1-0 to 3-2 is ~ 4 rather than the ~ 9 predicted by the optically thin model, although in the wings at ±25 km s^{-1} from line center, the relative increase is consistent with the thin model. Thus the improvement in the signal-to-noise ratio of an integrated line intensity is closer to ~ 20 than the predicted 28, but is still highly significant. The 'plateau' feature dominates the spectrum at submillimeter wavelengths, and the spectrum is quantitatively different from that at millimeter wavelengths. This example illustrates how submillimeter observations can provide different information from that obtainable at longer wavelengths.

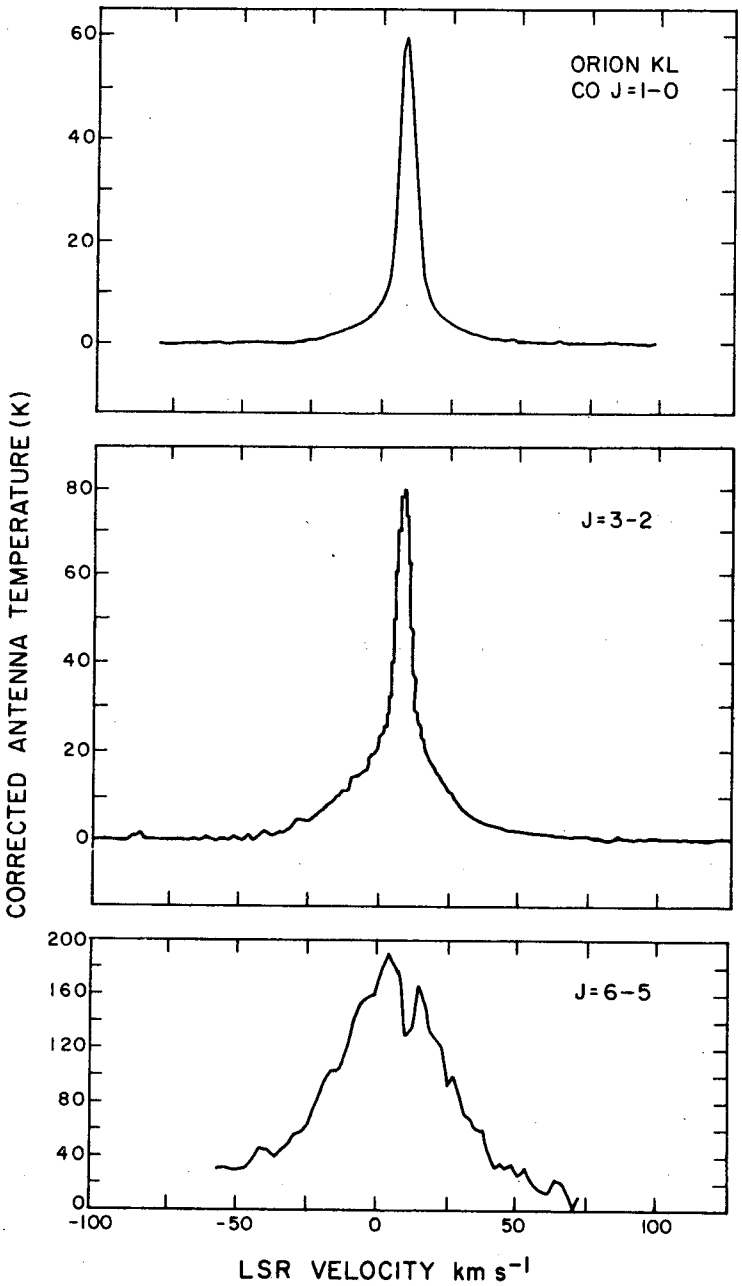

Figure 10. ^{12}CO profiles of the broad wing source in the Orion KL region. (Top) J = 1-0 transition at 3 mm from Kwan and Scoville (1976); (Middle) J = 3-2 transition at 1 mm from Erickson et al. (1982); (Bottom) J = 6-5 transition at 0.4 mm from Koepf et al. (1982). The temperature scales are not comparable because of different calibrations applied by the various authors. Note how the optically thin wings become more prominent at shorter wavelength as expected by the scaling law, $T_B \propto \lambda^{-2}$.

These comparisons suggest that the main applications of the submillimeter array -- studying the gas motions around young stars, and studying the dust emission from nearby galaxies -- will be far more effective at submillimeter wavelengths than at millimeter wavelengths, assuming current receiver performance. In the future, submillimeter receivers are likely to improve faster than millimeter receivers, giving submillimeter observations an even greater advantage.

E. Other Projects

There are a number of potentially important projects for which the results would be marginal with current technology but whose viability will improve with time. Two such projects are the study of fluctuations in the cosmic background and the study of the cores of compact extragalactic sources with very long baseline interferometers.

i. Cosmic Background Measurements

The effect of the Compton scattering of cosmic background photons by hot gas in the intergalactic medium of clusters of galaxies, called the Sunyaev-Zeldovich effect (Sunyaev and Zeldovich 1980), may be detectable with a submillimeter array. The process is expected to distort the 3 K cosmic background spectrum, producing a decrement near 3 mm and an excess near 0.8 mm of about 1 mK. This effect has been long sought, and only recently has it been detected in several clusters with reasonable certainty (e.g., Birkinshaw and Gull 1984). This measurement is very important because, when combined with measurements of the x-ray flux and temperature, it provides a direct estimate of the Hubble constant and the cosmological deceleration parameter. High angular resolution imaging of a cluster is

essential in firmly establishing the reality of the effect because low-level emission from discrete sources can seriously affect the measurement accuracy of such a small effect.

A submillimeter interferometer offers several advantages in the efforts to detect the Sunyaev-Zeldovich effect. An interferometer can achieve its theoretical sensitivity in long integration times whereas a single antenna is presently limited by fluctuations in the sky noise. At submillimeter wavelengths, the effects of synchrotron emission from the galaxies in the clusters will be much less than at lower frequencies. Finally, the opportunity to observe the background deviation with opposite sign by observing at 3 and 0.8 mm will help in identifying the effect in many clusters. The array proposed here would have a sensitivity of 0.8 mK in 10^5s integration with a 1500 K system temperature, 1-GHz bandwidth, and resolution of 10 arcseconds at 0.87 mm. Hence the effect should be detectable in several weeks of observing or less time when better receivers become available.

In principle, the velocity of the cluster perpendicular to the line of sight can be measured (Birkinshaw and Gull 1983). This measurement requires a mapping ability that the array naturally provides. Thus, the three-dimensional velocity distribution of clusters could be found. This information would also be important in the study of the dynamics of multiple clusters (Beers, Geller, and Huchra 1982). The size of the effect is very small but may be measurable in the later stages of the project when receiver technology improves substantially. We stress that although these experiments concerning the cosmic background are very important, they are very difficult because required integration times are so long and because systematic effects can bias the results.

ii. Very Long Baseline Interferometry

The radiation from the central regions of many quasars and radio galaxies has been mapped with very long baseline interferometers (VLBI) (Kellermann and Pauliny-Toth 1981). The technique of VLBI, as currently implemented, requires that the signal received at each element of the interferometer be faithfully recorded on video tape and correlated at a later time with the signals from other elements. Hence, no real time link is needed among the elements, and they can be widely separated. At centimeter wavelengths, multi-element VLBI experiments have yielded detailed images with resolutions as fine as ~ 0.5 milliarcsecond (mas). Preliminary VLBI experiments have been performed at 3-mm wavelength and the sizes of several emission regions estimated (Readhead et al. 1983). The highest resolution that has been achieved with such experiments is 0.1 mas. The correlated flux density of the quasar 3C273B at 3-mm wavelength was found to be 6 Jy, while the total flux density was 55 Jy (Predmore et al. 1984).

High-resolution VLBI observations at millimeter and submillimeter wavelengths are important for several reasons. First, for radiation due to synchrotron radiation from electrons, the wavelength of maximum emission is proportional to $\theta^{\frac{4}{5}}$, where θ is the angular size of the emitting region (Kellermann and Pauliny-Toth 1981). Quasars and radio galaxies exhibit emission from components having a large range of scale sizes. Emission from the smallest components, usually associated with the central core, only becomes prominent at short wavelengths because, at long wavelengths, the radiation is self-absorbed. Second, the resolution of 0.1 mas possible with millimeter and submillimeter interferometers corresponds to a linear size of 0.1 pc at a distance of ~ 200 Mpc. This size is comparable to that

of an accretion disk around a 10^9 $M_\odot$ black hole. Hence, VLBI at the shortest possible wavelengths offers a means of probing the very cores of quasars in the quest to discover their source of energy.

Although millimeter VLBI has just begun, the push to shorter wavelengths is inevitable. There are no fundamental limitations to the performance of VLBI at submillimeter wavelengths other than considerations of sensitivity. The proposed submillimeter array could be operated as an element in a VLBI experiment. If the array were located on Mt. Graham in Arizona, a VLBI experiment could be undertaken, for example, with the Multiple Mirror Telescope, located on Mt. Hopkins, 140 kilometers away. An initial experiment might be undertaken at a wavelength of 0.87 mm where the resolution would be ~ 1 mas. The coherent integration time, determined primarily by the atmospheric stability, can be expected to be about 100 seconds from dry mountain sites (Rogers et al. 1984). The maximum bandwidth with currently available recording systems is 112 MHz (Rogers et al. 1983). With these parameters and an effective system temperature of 1500 K, the sensitivity in one coherent integration period would be about 1.5 Jy, which would be adequate to detect the stronger sources. The system temperatures should decrease and recording bandwidth increase with time, thereby improving the sensitivity. Longer baselines, such as those from Arizona to Hawaii (5000 km), would provide extremely high resolution (0.03 mas at 0.87 mm). Of course, good weather at both sites would be required for such experiments.

The major equipment items needed to make the array into a VLBI element are a recording terminal and a hydrogen maser frequency standard. The total cost for this equipment is about $750 K. We have not included these items in the construction budget because we assume they can be borrowed for exploratory experiments and purchased later if necessary.

III. TECHNICAL DISCUSSION

A. Atmospheric Limitations

Atmospheric water vapor limits the transparency of the submillimeter windows and causes differential phase delays that can destroy the phase coherence of an interferometer. Hence, a very dry site is required for successful operation. Since the scale height of water vapor is about 2 km, high mountains offer the best sites. Some well known sites in the United States that should be considered for the array are Mt. Graham, Arizona; Mauna Kea, Hawaii; and Jelm Mountain, Wyoming.

A reasonable amount of data exists regarding the quantity of precipitable water vapor above most of the likely sites for a submillimeter array (see Section III A(i)). From these data one can infer that atmospheric transparency, although never 100 percent at submillimeter wavelengths, will be acceptable for a reasonable fraction of the time. Further, observations can be scheduled to take advantage of the driest nights for the least transparent submillimeter bands and to observe in the less water-sensitive (longer wavelength) bands at other times. There are several sites with more than 40 days a year that have less than 1 mm column height of precipitable water. These sites can therefore be used effectively for observations at the shortest wavelengths (~ 0.35 and ~ 0.45 mm). This number of days is comparable to the number of dark photometric nights at a good optical site. Furthermore, a good site should provide another 100 or more days a year that are useable at the longer wavelengths (> 0.65 mm).

The major uncertainty in site quality involves the extent to which the atmosphere introduces different propagation delays between the source and the various antennas of the array. At wavelengths shorter than a few millimeters, these differential atmospheric delays (or phase shifts) will usually occur on a time scale too short to allow for their calibration. These phase shifts degrade the interferometer data, reducing the dynamic range of a map and, if severe, blurring the image. Results from existing interferometers demonstrate that atmospheric phase shifts tend to increase linearly with antenna separation, at least up to several hundred meters, and inversely with observing wavelength. Hence, the primary effect is to impose a weather related limit on the maximum useable baseline length measured in wavelengths, i.e., a resolution limit. In practice, therefore, at times of high atmospheric fluctuations (e.g., summer in the southwestern United States), the array need not be shut down, but can be used at longer wavelengths or be reconfigured to shorter baselines. A more detailed discussion concerning questions of weather, opacity, and phase fluctuations follows in Sections III A(i), (ii), and (iii). In Section III A(iv), the problems of site testing are discussed.

i. Weather Statistics at Possible Sites

The evaluation of the quality of a telescope site is a controversial topic. Global surveys show that the mean water vapor content decreases with increasing latitude (Bean et al. 1966). On the other hand, observations at higher latitude sites tend to be made at higher zenith angles, which means increased absorption. Weather conditions at specific sites are variable not only on diurnal and seasonal timescales but also on a timescale of many years. Reported measurements are often inaccurate and are rarely comprehensive. Our purpose here is not to make a precise

comparison between sites but rather to show that there are sites where a submillimeter array could operate for an acceptable fraction of the time.

a) Mt. Graham

Much data exist for Mt. Lemmon, Arizona, about 32 kilometers from Tucson and 95 kilometers from Mt. Graham. Submillimeter observations there are generally impossible in the summer (July - September), but winter conditions are often favorable (Ulich 1983). We have taken the compilation of 18 years of survey data for Mt. Lemmon (2790 m) (Ulich 1984, private communication) and multiplied the column density by 0.8 to predict likely conditions on Mt. Graham (3260-m elevation, 32^{o} latitude). The curve in Figure 11 shows that about 40 days a year on Mt. Graham can be expected to have less than 1 mm of precipitable water vapor.

b) Mauna Kea

The qualities of Mauna Kea (4200-m elevation, 20^{o} latitude) as an observing site were evaluated by Morrison et al. (1973). An early set of measurements of water vapor content were made by Westphal (1974). The Westphal Survey on Mauna Kea consisted of about 270 measurements of mid-day solar absorption taken over a one-year period ending in July 1972. Figure 11 shows these data, which suggest that about 40 days a year have less than one millimeter of precipitable water vapor. Because daytime winds bring moist sea air to the summit, the nighttime water vapor content is usually lower than the daytime content. We also plot in Figure 11 the estimates of the amount of precipitable water vapor made on 105 nights by the University of Chicago group (Hildebrand, Davidson, Keene, and Whitcomb 1984, private communication). These estimates were derived from broadband

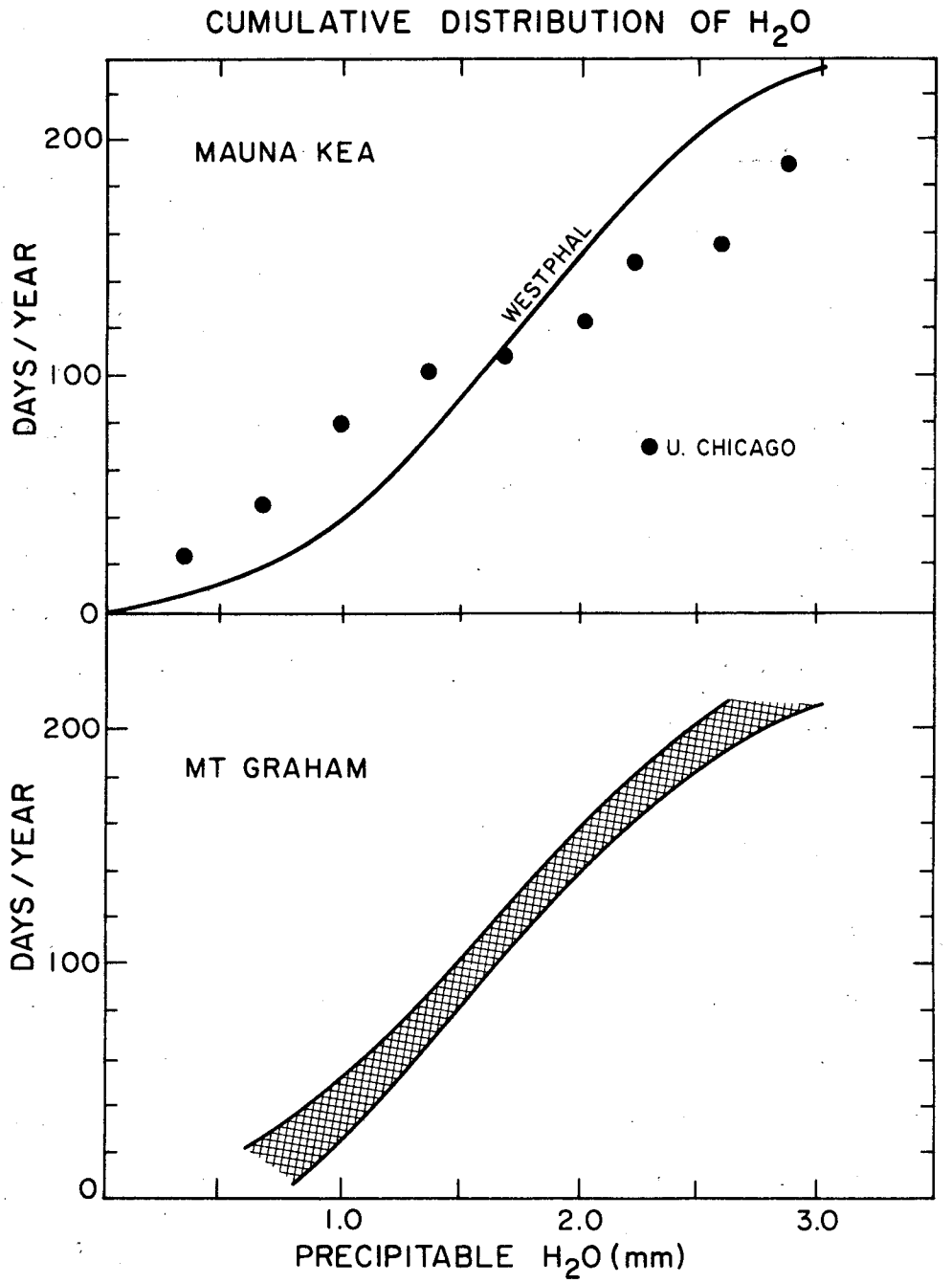

Figure 11. Cumulative probability distribution of the number of days per year versus precipitable water vapor. The top graph shows data for Mauna Kea. A solid line indicates daytime data taken over a period of one year, ending in July 1972 (Westphal 1974). Filled circles are based on the submillimeter data of the U. Chicago group on 105 nights (Hildebrand, Davidson, Keene, and Whitcomb 1984, private communication). The lower graph shows the range of data from five surveys taken over an 18-year period on Mt. Lemmon, scaled to Mt. Graham by the expected reduction for a scale height of 2 km for the water vapor (Ulich 1984, private communication).

submillimeter absorption measurements made during astronomical observing sessions. The data were acquired during 13 sessions, of average length eight days, from November 1979 to May 1984. The periods with low water vapor content tended to last for several days. These measurements suggest that about 80 nights a year on Mauna Kea can be expected to have less than one millimeter of precipitable water vapor and about 120 nights less than two millimeters.

c) Jelm Mountain

The University of Wyoming operates an infrared telescope on Jelm Mountain (2940-m elevation, 41° latitude), 55 kilometers from Laramie, Wyoming. The telescope site is very dry in the winter because of its elevation and latitude (Warner 1977). The high latitude would be a significant disadvantage for observing sources at low declination. For example, sources at the declination of the galactic center, -28°, are above 20° elevation angle for only 1.7 hours per day compared with 5.1 hours at Mt. Graham and 7.3 hours at Mauna Kea. Jelm Mountain may be a suitable site, although severe winter weather conditions could present significant logistical problems.

d) Other Sites

Other sites in the western United States deserve some study. We mention three such sites: the Aquarius Plateau, Utah; Chalk Mountain, Colorado; and White Mountain, California. The NRAO staff suggested that the large flat area called the Aquarius Plateau (3350-m elevation, 38° latitude) located about 160 kilometers northeast of Cedar City, Utah, in the Dixie National Forest near Capitol Reef National Park might be a

potential site for a telescope array. The area is undeveloped. There is an abandoned station of the High Altitude Observatory and an abandoned cosmic-ray station of Louisiana State University on Chalk Mountain (3600-m elevation, 39° latitude) located near Climax and Leadville, Colorado. The mountain has an unusually flat top several kilometers in size. The summit is five kilometers from a paved road. White Mountain (4330-m elevation, 37° latitude) located on the east side of Owens Valley has flat areas near its summit as well. The winter weather at all these locations is often severe.

A possible site outside the United States is the inland portion of Antarctica, for example the south pole (2900-m elevation, -90° latitude), which offers an extraordinarily dry environment. The mean annual temperature is -55°C (Lovering and Prescott 1979). The amount of precipitable water vapor in the summer is typically 0.3 mm (Murcray et al. 1981) and is probably under 0.5 mm for 80 percent of the time (F.H. Murcray 1984, private communication). Winds at the pole are light. Winter operations would be virtually impossible for a complex instrument because outdoor activity is extremely limited, and there is currently no transportation during that season. There would be many operational problems in Antarctica. For example, the array would have to be anchored in the ice sheet, which is moving at the rate of a few meters per year. Despite the summer dryness, we feel the expense and the extreme logistical and personnel problems make it unwise to consider further the operation of a complex developmental instrument such as the submillimeter array in Antarctica.

ii. Opacity

The atmospheric opacity versus frequency for a high mountain site with one millimeter of precipitable water vapor is shown in Figure 12. The plot does not show the effects of narrow ozone lines (see Waters 1976), which are not important for continuum observations and most spectral observations. One millimeter of H_2O gives lower opacity and broader transmission bands on a high mountain site than at a lower site because the contribution of pressure-broadened wings of various lines is less at higher altitude. The zenith opacities for 1 mm of H_2O at a high altitude site are given in Table 3.

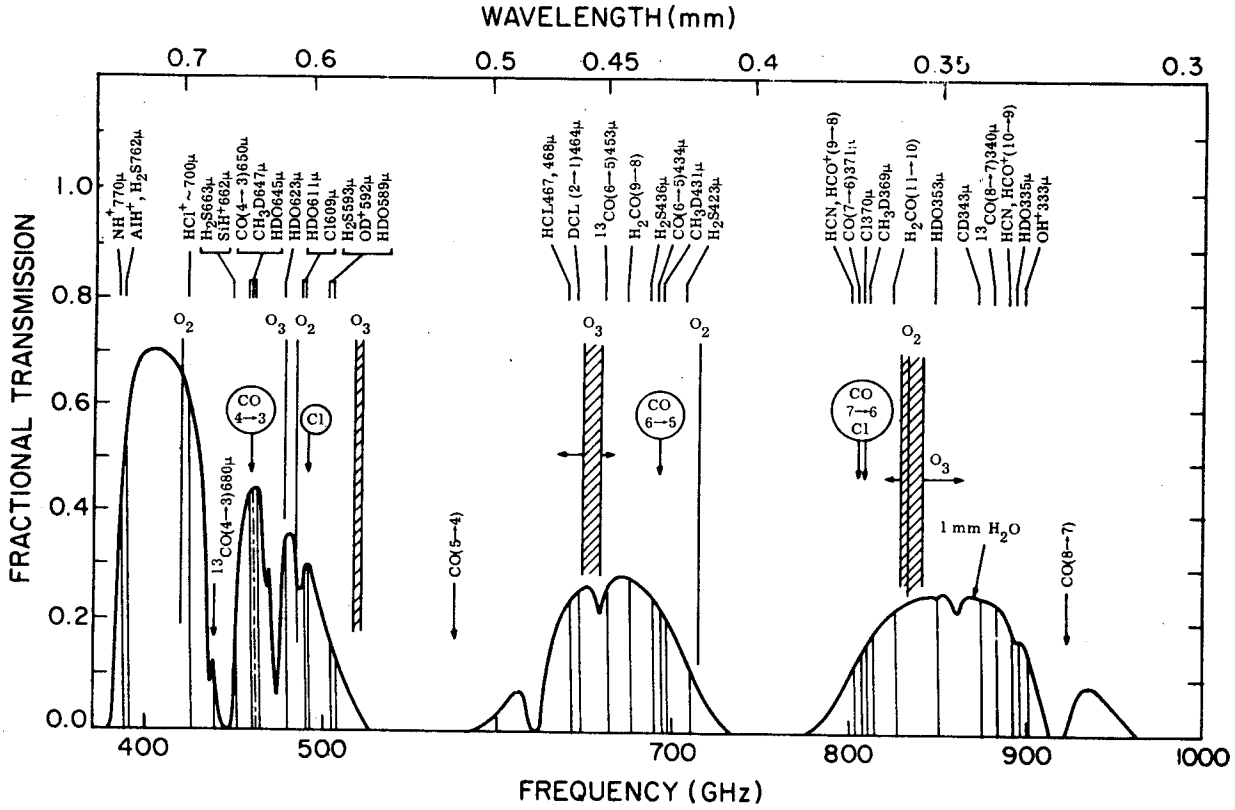

Figure 12. The theoretical zenith transmission of submillimeter radiation through the atmosphere from the top of Mauna Kea, Hawaii at 1 mm of precipitable water vapor. Except for narrow absorption lines due to ozone, which are not shown, the transmission is greater than 0.8 in windows with wavelength greater than 0.7 mm (see Figure 6). Astrophysically significant atomic and molecular lines are indicated. Figure from Roser (1979).

Table 3*

Zenith Opacity, Transmission, and Refractivity with One-Millimeter Precipitable Water Vapor

ν (GHz)	λ (mm)	Optical Depth (nepers)	Fractional Transmission	Dispersive Refractivity (N'_v)**
230	1.30	0.10	0.90	0.03
345	0.87	0.22	0.80	0.05
460	0.65	0.70	0.50	0.10
690	0.44	1.4	0.25	-0.03
850	0.35	1.4	0.25	-0.10

*We list parameters for the observable CO transition wavelengths as well as the shortest wavelength at which ground-based observations are possible (0.35 mm).
**The part of the refractivity of water vapor that depends on wavelength. The nondispersive component of refractivity of water vapor for the stated conditions has a value of 3.0 (see Section III A(iii) below).

iii. Phase Fluctuations

Temporal and spatial fluctuations in the index of refraction of the troposphere introduce fluctuations in the time necessary for signals to traverse the troposphere on their way to the various elements of the array. The fluctuations in these differential delays produce phase fluctuations in the array. The index of refraction of air is nearly constant throughout the radio range for wavelengths longer than 1 mm (Liebe 1981). The refractivity, the index of refraction minus unity times 10^6, is given accurately by the empirical Smith-Weintraub equation (Bean and Dutton 1966), for wavelengths longer than one millimeter:

$$N = \frac{77.6\ P}{T} + \frac{3.73 \times 10^5 e}{T^2}, \qquad (6)$$

where P is the total pressure in millibars, T is temperature in Kelvins, and e is the partial pressure of water vapor in millibars. The first term on the right side of equation (6) is the refractivity of dry air, N_D, which is due to a few strong molecular resonances in the ultraviolet. At sea level under standard conditions, i.e., P = 1013 mb and T = 288 K, N_D is 273. The dry air is very nearly in hydrostatic equilibrium and N_D decreases exponentially with a scale height of about 8 km. Hence the excess propagation path in the zenith direction due to dry air,

$$L_D = 10^{-6} \int N_D \, dh, \qquad (7)$$

is about 2.2 m. At an elevation of 4000 meters, this path length is reduced to 1.3 m. The second term on the right side of equation (6) is the non-dispersive part of the refractivity of water vapor, N_v, which is due to the wings of many infrared resonances. The contribution of any one line is very small. The partial pressure of water vapor is given by (Hess 1959)

$$e = 6.1 \times 10^{[7.5(T_p - 273)/(T_p - 35.7)]} \quad \text{mb}, \qquad (8)$$

where T_p is the dew point temperature in Kelvins. Also of interest is the absolute humidity given by

$$\rho_v = \frac{217\ e}{T} \quad \text{g m}^{-3}. \qquad (9)$$

Atmospheric water vapor is not well mixed, but on the average it is exponentially distributed with a scale height of about 2 km. The column height of precipitable water vapor is

$$w = \frac{1}{\rho_w} \int \rho_v \, dh, \tag{10}$$

where ρ_w is the mass density of liquid water vapor. The excess propagation path length is

$$L_v = 10^{-6} \int N_v \, dh. \tag{11}$$

If the temperature is assumed to be constant at 288 K, then from equations (6), (9), and (10) we find that L_v and w will be proportional, that is,

$$L_v = 6 \, w, \tag{12}$$

where L_v and w are in the same units of length. Hence, if $\rho_v = 0.5$ g m^{-3}, then e = 0.67 mb, $N_w = 3.0$, w = 1 mm, and $L_v = 6$ mm.

The refractivity in the vicinities of the strong submillimeter resonances of water vapor is not entirely negligible, as can be seen in Figure 13, where the dispersive component of the refractivity, N'_v, is plotted. Note that N'_v is the refractivity of water vapor minus N_v, the wavelength-independent part of the refractivity of water vapor. Near the powerful resonance of water vapor at 0.54 mm (560 GHz), where the absorption is 58,000 db through a standard atmosphere, the refractivity reaches 145, about twice the value of the nondispersive refractivity, N_v.

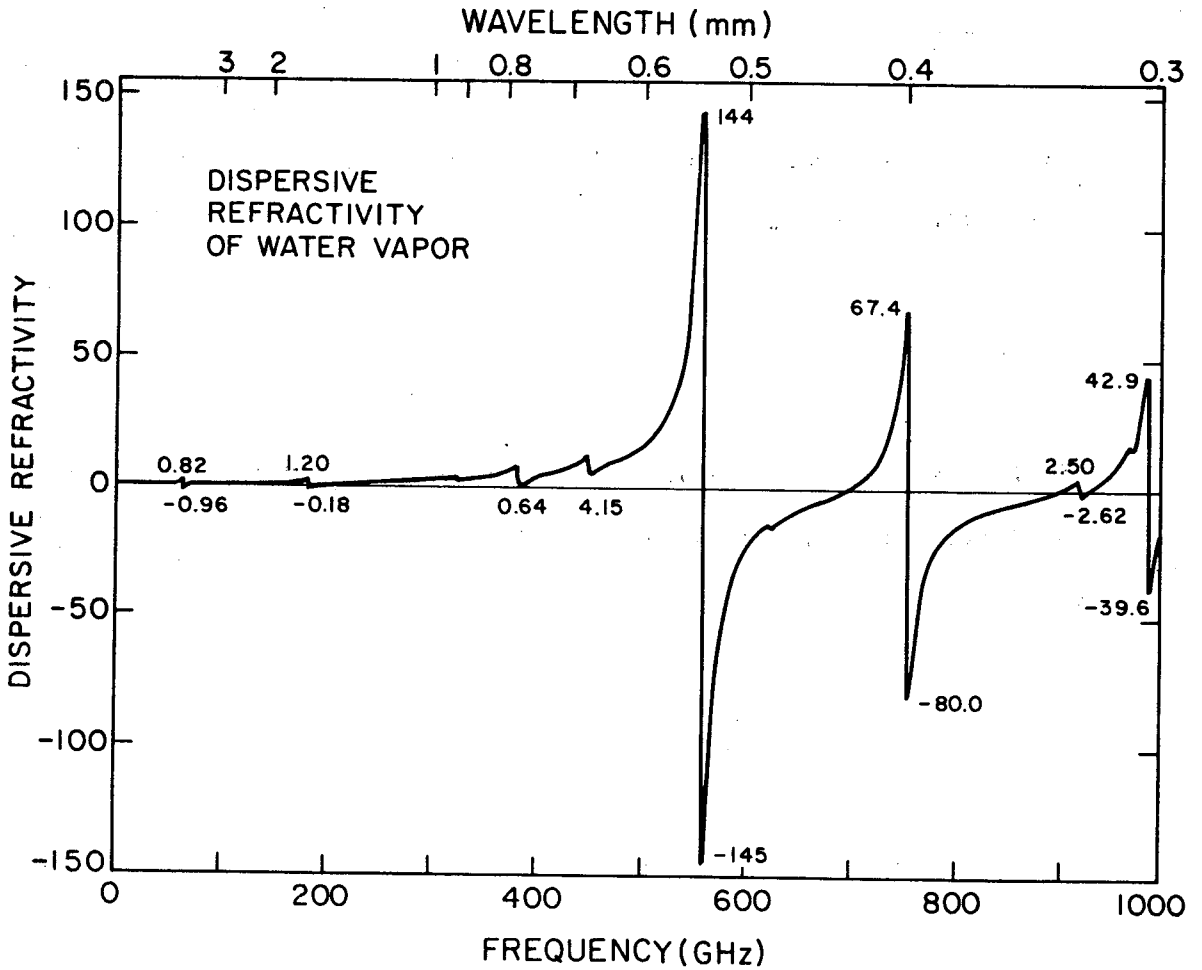

Figure 13. The dispersive component of the refractivity of water vapor, N'_V, for saturated air at sea level and 15°C. These conditions correspond to 26 mm of condensed water vapor, for a scale height of 2 km. The value of the nondispersive component of refractivity of water vapor under these conditions is 77. Hence, in the atmospheric windows, the dispersive component of refractivity is negligible compared to the nondispersive component. Figure adapted from Liebe (1981).

The values of N'_v near the middle of various submillimeter bands are listed in Table 3. Note that N'_v is negative at wavelengths below strong resonances. Hence, for example, the phase fluctuations due to water vapor in an interferometer operating at 0.35 mm (870 GHz) can be expected to be about 4 percent less than those in a millimeter- or centimeter-wavelength interferometer. For practical purposes, the refractivity is independent of wavelength in the atmospheric windows with wavelengths longer than 0.35 mm.

The phase stability of an interferometer depends on the short term fluctuations in the excess path length and their spatial scale. The phase noise in all existing radio interferometers is dominated by fluctuations in L_v. The fluctuations in L_D are very small and are due primarily to fluctuations in the temperature. The situation in the optical and near infrared parts of the spectrum is very different because the refractivity of water vapor is less in those regimes by a factor of about 20 (Thayer 1974).

The simplest criterion for evaluating the performance of an interferometer involves the rms phase noise: it should not exceed one radian. Since phase noise seems to increase monotonically with baseline length, up to some maximum value at a baseline corresponding to the outer scale length (~ 1 km), the maximum usable resolution will be set by the baseline length for which phase noise equals one radian. If the phase fluctuations increase linearly with wavelength, a <u>wavelength-independent</u> value of 'seeing' can be derived (see Appendix A). Let σ_ϕ be the rms deviation in phase for baseline length d where the phase noise is assumed to be a Gaussian random variable. Then the 'seeing', or apparent size (full width at half maximum) of a point source will be given by

$$\theta_s = 2.35 \left[\frac{\sigma_d}{d}\right] \text{ (radians)}, \qquad (13)$$

where σ_d is the rms fluctuation in path length, $\sigma_\phi \lambda/2\pi$.

We can attempt to predict the phase performance of a submillimeter interferometer by scaling the data from existing interferometers. Data from the Hat Creek millimeter interferometer, shown in Figure 14 (Bieging et al. 1984), indicate that σ_ϕ increases approximately linearly with baseline length and has a value of 0.8 radians at a wavelength of 3.5 mm on a 175 m baseline (50,000 λ). Hence, $\theta_s \sim 1.2$ arcseconds. One could expect $\sigma_\phi = 1$ radian at 0.87 mm when d = 50 m. The Hat Creek site, which is at an elevation of 1040 m, typically has 4 mm of precipitable water vapor in wintertime. It could not be used for observations at 0.87 mm on baselines of more than about 50 m. By scaling the Hat Creek data to a site with 1 mm of water vapor we can expect $\theta_s = 0.3$ arcseconds and about 1 radian of phase noise at 0.87 mm on a 200 m baseline, assuming that the phase noise is due primarily to water vapor fluctuations.

Sramek (1983) has studied the phase fluctuations on the VLA at a wavelength of 1.3 cm. With the VLA data the increase in phase noise with baseline length is readily apparent (see bottom part of Figure 14). For integration periods of 16 minutes he finds that the rms phase noise is given by

$$\sigma_\phi = 0.25 \left[\frac{\lambda}{1.3 \text{ cm}}\right]^{-1} \left[\frac{d}{1 \text{ km}}\right]^{0.36} \text{ (radians)}. \qquad (14)$$

Hence at the VLA site (2130 m elevation) one could expect $\sigma_\phi = 1$ radian at 0.87 mm when d = 26 m, which is roughly comparable to the result obtained for the Hat Creek data. Sramek's data were taken on 10 occasions

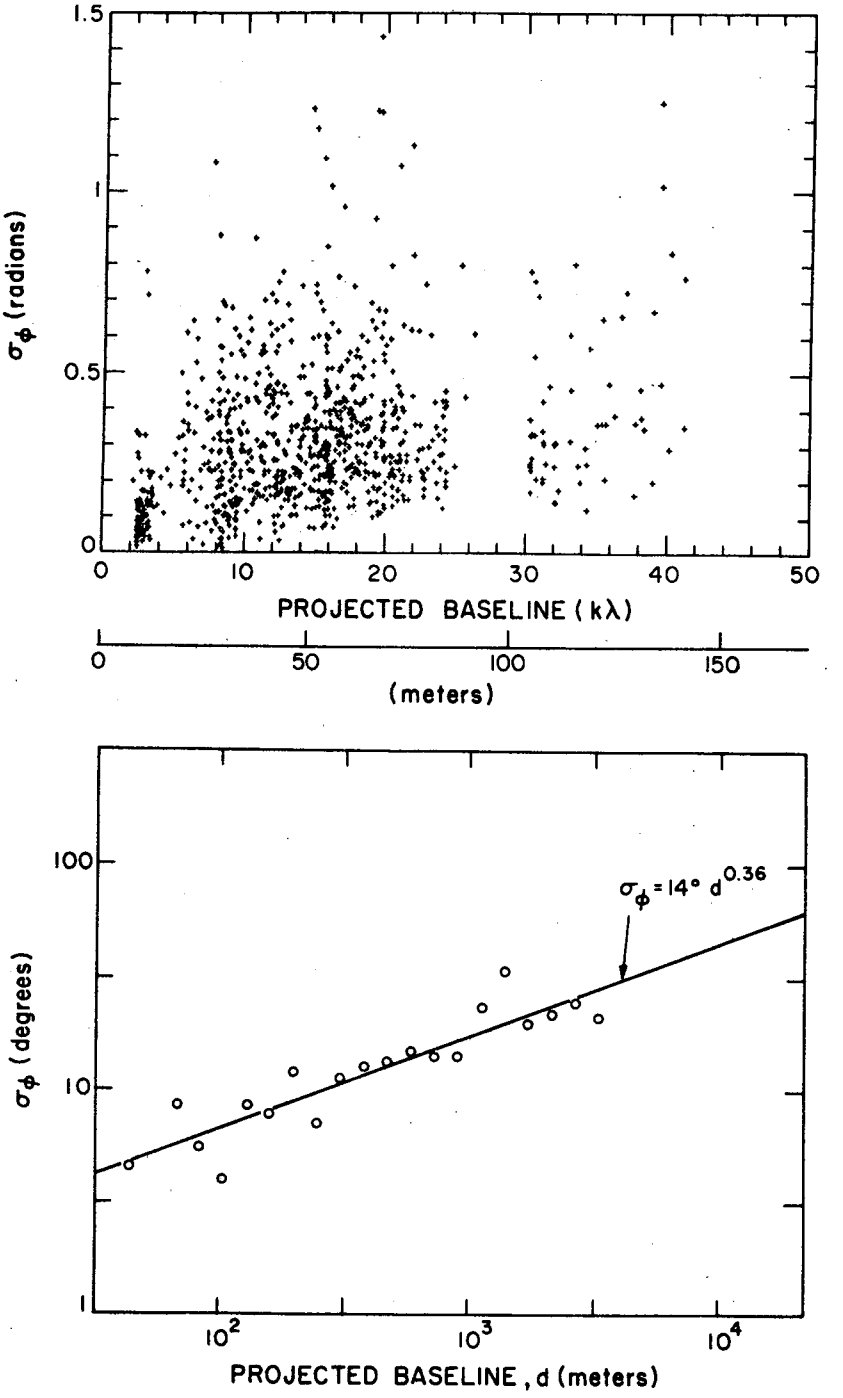

Figure 14. (Top) RMS phase noise on the Hat Creek interferometer at 3.4 mm (88 GHz) versus baseline length (Bieging et al. 1984). Note that the Hat Creek interferometer has only two elements so that only one data point at a time can be obtained. The increase of phase noise with baseline length is partially obscured because the data were obtained under a wide variety of weather conditions. (Bottom) RMS phase noise (Allan standard deviation) on the VLA at 1.35 cm (22 GHz) versus baseline length for 16-minute averaging time (Sramek 1983).

between November 1982 and July 1983. The mean value of the surface partial pressure of H_2O was 3.5 mb, which, for a scale height of 2 km, corresponds to 5 mm of precipitable water vapor. No correlation is apparent between phase noise and surface water vapor among the ten observations, which is not surprising since it is well known that surface water vapor is not well correlated with total water vapor content.

The VLA data also show that the phase fluctuations when the wind speed is 10 m s^{-1} (22 mph) are twice those when the wind is calm. A similar effect has been noted at Hat Creek. If these increased phase fluctuations are due to increased air turbulence, a windy mountaintop site might not perform as well as implied by extrapolation of the Hat Creek and VLA data. Alternatively, the increased phase fluctuations may be due at least in part to physical buffeting of the antennas, which could be measured. This type of antenna motion can be alleviated by the use of antenna enclosures or stiffer support structures.

The above discussion is based on the assumption that water vapor irregularities are the principal cause of phase noise. The turbulence in the dry air, which is responsible for optical seeing limitations, will also contribute at some level to the phase noise. Turbulence theory suggests that dry-air seeing scales as $\lambda^{-0.2}$ (e.g., Townes 1980). Hence the dry and wet components will contribute approximately equally when the optical seeing is 1 arcsec and the amount of precipitable water is 1 mm. This equality suggests that good optical seeing conditions may be an important criterion for selecting a site for a submillimeter-wavelength interferometer.

In conclusion, experience with the VLA at centimeter wavelengths and the Hat Creek interferometer at millimeter wavelengths suggests that atmospheric phase shifts are small enough to allow high-quality submillimeter-wavelength observations at a dry site with good optical seeing. When the water vapor level is low enough for adequate transmission, the phase stability should be good enough for work at least at the 1-arcsecond level of resolution.

iv. Site Testing

The only unequivocal way to test a site for atmospheric-induced phase fluctuations is to operate an interferometer. Fortunately, this need not be done at the same wavelength as would be used with the proposed instrument. Thus, a small test interferometer could be built to observe the strong (10^6 Jy) H_2O line at 1.3 cm in the Orion KL region, or an existing satellite-borne transmitter could be used. Measurements with such an interferometer could directly provide rms phase data versus baseline length. We recommend that the feasibility of deploying such an interferometer be studied.

Other methods may be effective in evaluating sites. The University of Arizona plans to build in the near future a dual-frequency water-vapor radiometer on Mt. Graham to measure the sky brightness of the 1.3-cm water vapor line (Ulich 1984, private communication). The sky brightness, T_B, at 1.3 cm is closely related to the atmospheric water vapor content, w. The relation is approximately (Moran and Rosen 1981)

$$T_B \sim 1.3 \text{ w K}, \qquad (15)$$

where w is in millimeters. The data from dual-frequency water-vapor radiometers can be used to predict interferometer phase fluctuations with reasonable accuracy (e.g., Resch et al. 1984). It should be possible to use the variations in the brightness temperature and the wind speed to estimate the spatial correlation in water vapor, if the structure of the turbulence does not change in the time required for it to drift over the desired spatial scale length. The usefulness of this technique could be checked by comparing water vapor radiometer data and interferometric data from the VLA. If the method is viable, a water vapor radiometer could be used to test possible sites. We strongly urge that a water vapor radiometer be built (or borrowed) by SAO as soon as possible for these studies.

The UK/Dutch group has been making sky brightness temperature measurements on Mauna Kea at various elevation angles at 1.2, 0.45 and 0.35 mm wavelengths many times a day for the past year (Hills 1984, private communication). The estimates of the transmission coefficients will be available shortly.

Some skepticism may be justified concerning the value of site testing over short periods since the long-term weather variations introduce fluctuations that are greater than the differences among 'good' sites. For example, in a study of records over a 30-year period, Roosen and Angione (1977) found variations of about a factor of two in the annual mean precipitable water vapor content at mountaintop observatories with a characteristic time scale of about 5 years. We feel, however, that it is essential for a program of this magnitude to conduct a 'proof test' of at least one site in order to establish that good astronomical data can be obtained for an acceptable fraction of the time. Clearly these tests

should begin as soon as possible in order to provide the maximum amount of data.

B. Physical Locations for the Array

i. Mt. Graham

There are several viable sites for an array on Mt. Graham. Figure 15 is a section of a topographical map of the Mt. Graham area. We consider 'Mt. Graham' to be the whole of the long ridge that extends 5 kilometers north from near Heliograph Springs to High Peak (which is labelled Mt. Graham). The ridge is almost all above 2900 m (9500 ft). Around High Peak, the principal summit at 3267 m (10,720 ft), the three circled x's mark the sites under consideration for the University of Arizona/Max-Planck-Institute submillimeter telescope (UA/MPI SMT). Possible sites for the National New Technology Telescope (NNTT) are High Peak, or Hawk Peak. Hawk Peak may have better seeing since it is upwind from High Peak.

A possible site for a large submillimeter array with three arms is shown on the map in Figure 15 (site 1). It allows arm lengths of 850 meters (SE), 800 meters (SW), and 450 meters (N), sufficient for the currently conceived array and possible future expansion. The center of this array is near the saddle between High Peak and Hawk Peak. The array would straddle the road near the 10,440 foot (3182 m) contour level. Elevation deviations are less than $\pm$ 12 meters. The worst horizon blockage from the center of this array is about 13^{o} and is in the NE direction over High Peak. The worst blockage from any point in the array is about 18^{o} and occurs midway in the SW arm looking northwest over Hawk Peak. Since

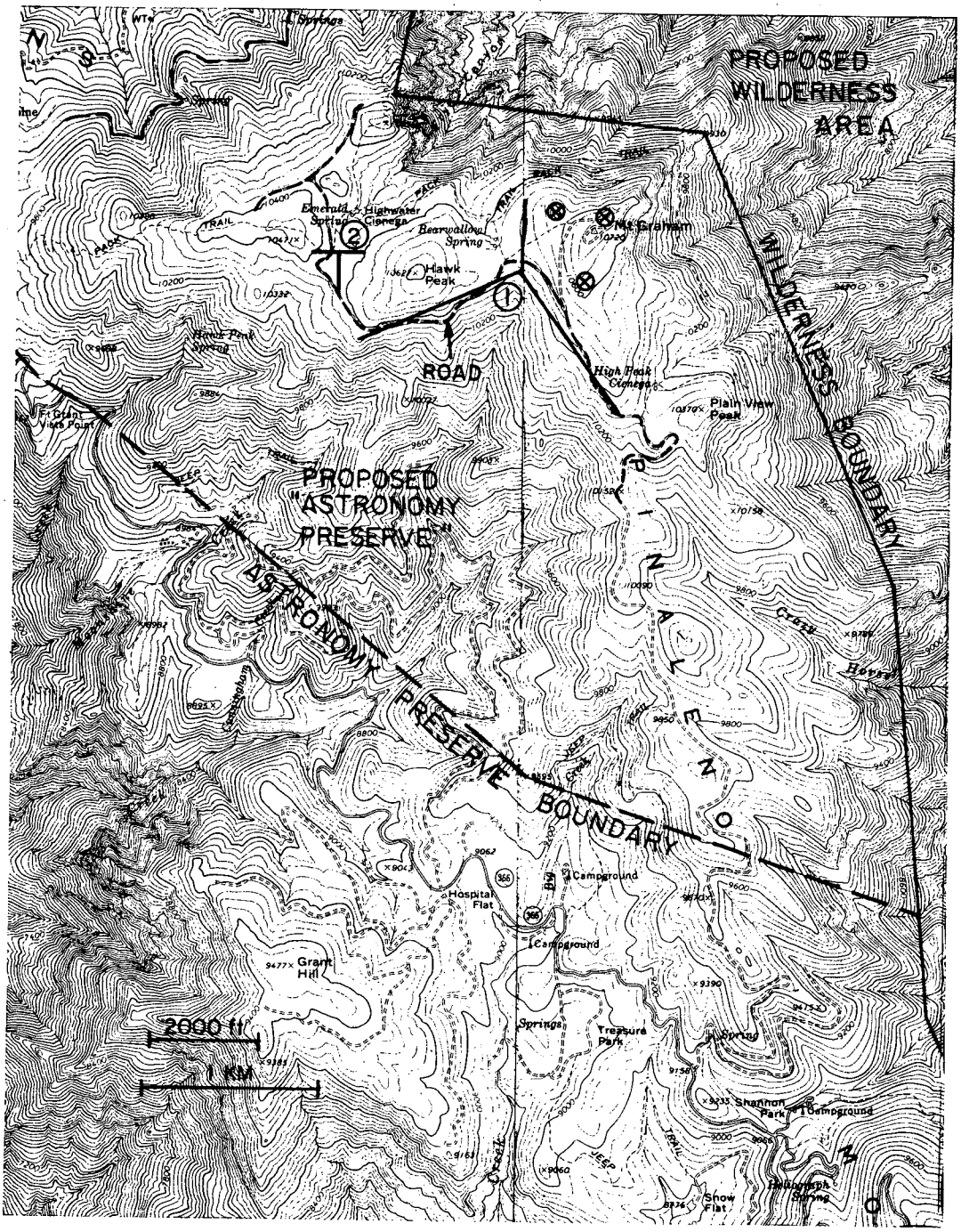

Figure 15. Region near the summit of Mt. Graham, Arizona (130 kilometers northeast of Tucson, near Safford, Arizona), from the U.S. Geological Survey topographic maps of Mt. Graham and Webb Peak quadrangles. The elevation contour interval is 40 ft (12 m). The interval between heavy contours is 200 ft (61 m). A large 'Y'-shaped array, marked '1' with arms of up to 1 km in length could be built close to an existing dirt road near the 10,440 foot (3182 m) level. The maximum horizon blockage at the center of the 'Y' is 13 degrees. A smaller 'T'-shaped array, marked '2', could be built near Emerald Spring.

submillimeter observations are very sensitive to atmospheric attenuation and are unlikely to be made at low elevation angles, it is unlikely that these physical elevation limits would be restrictive.

A smaller array with 250 meter arms (Figure 15, site 2) could be located just south of Emerald Spring. Another potential site is along the road near the 'T' road junction just north of Emerald Spring. It may be necessary, for environmental reasons, however, to avoid building too near to Emerald Spring, Highwater Cienega (marsh), and Bearwallow Spring, which are beautiful and ecologically fragile areas.

ii. Mauna Kea

The summit of Mauna Kea, including all the land above 12,000 feet (3658 m), has been leased to the University of Hawaii during the period 1968 - 2033 for use as an astronomical observatory. The area is known as the Mauna Kea Science Reserve. The Institute of Astronomy of the University of Hawaii and several other cooperating institutions have built six telescopes near the summit. The state of Hawaii has recently approved a development plan called the 'Science Reserve Complex Development Plan' (SRCDP), which sets guidelines for future expansion of facilities through the year 2000 (Oda et al. 1983). The plan calls for a total of 13 telescopes: six existing telescopes; three telescopes to be built in the near future (the Caltech 10-m-diameter submillimeter telescope, the UK/Dutch 15-m-diameter millimeter telescope, and the University of California 10-m-diameter optical/infrared telescope); and four additional telescopes. The SRCDP is flexible with regard to the type of telescopes that can be built, as long as the total does not exceed 13. The Caltech and UK/Dutch radio telescopes are under construction in area II (see

Figure 16), which is relatively flat (± 30 m) and has dimensions of 250 x 450 m. It is located at 4053 m (13,300 ft) elevation, about 150 m below the summit, and is shielded from the wind by the surrounding cinder cones. This area, or area III, would be the best location for a submillimeter array. There are two archaeological sites in area II that would have to be avoided.

C. Array Sensitivity

The sensitivity of a submillimeter telescope, with currently available instrumentation, will be limited by the additive Gaussian random noise of the receiver. In the next decade this noise contribution may be reduced enough so that the additive atmospheric emission will limit the sensitivity. The total noise temperature, T_R', the combination of the receiver noise temperature, T_R, and atmospheric brightness temperature is $T_R + T_o(1 - 1/L)$, where T_o is the ambient temperature (~ 290 K) and L is the transmission loss of the atmosphere ($1 \leq L < \infty$). Note that L is equal to $\exp(\tau_o)$, where τ_o is the opacity of the atmosphere. The system temperature, T_s, referred to a point outside the atmosphere in order to account for the effect of atmospheric absorption, is $T_R'L$ or

$$T_s = T_R L + T_o(L-1). \tag{16}$$

A two-element interferometer will have an rms fluctuation in system temperature given by

$$\Delta T_A = \frac{1.2\ T_s}{\sqrt{2B\tau}}, \tag{17}$$

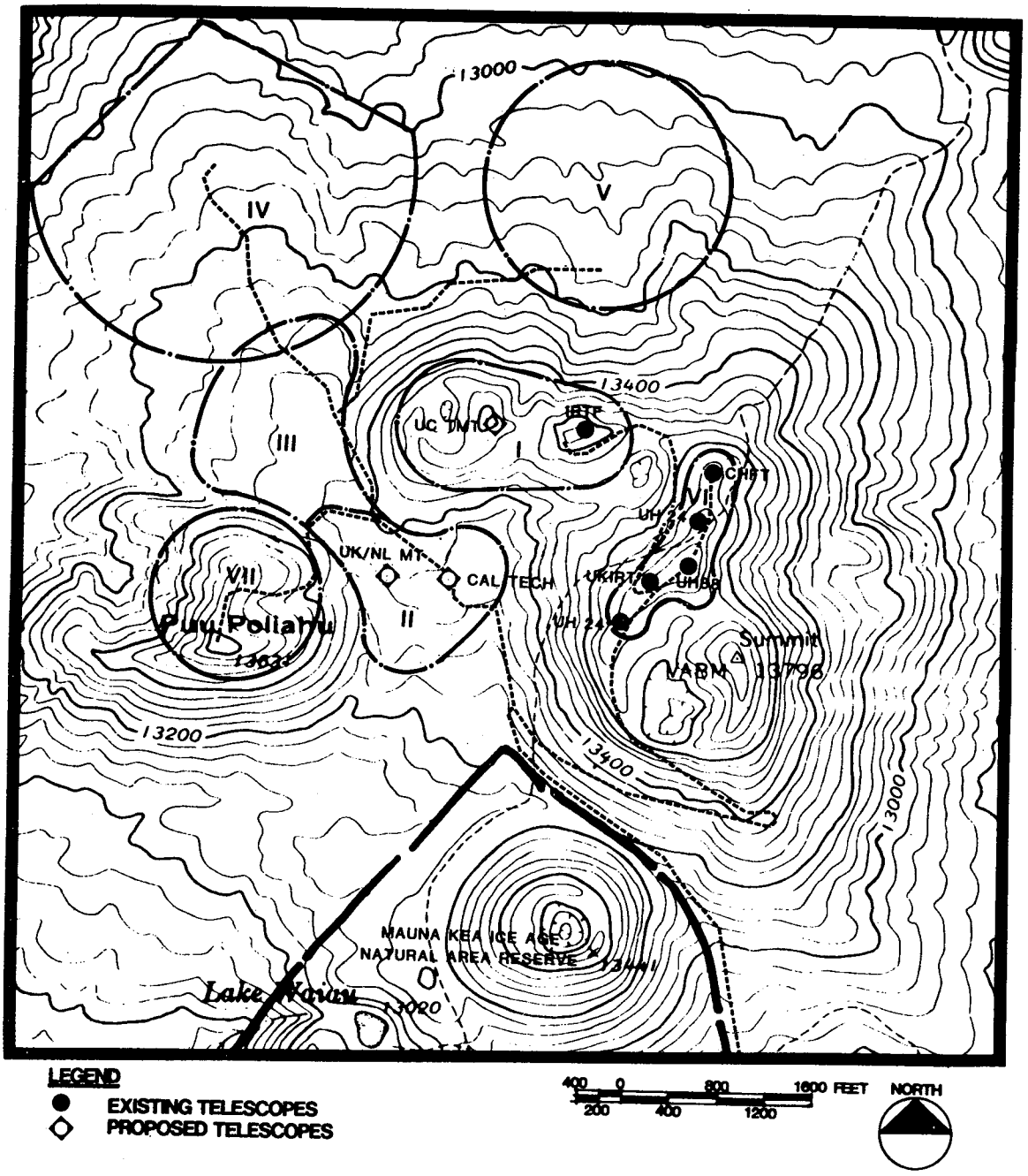

Figure 16. Topographic map of the region near the summit of Mauna Kea taken from the Mauna Kea Science Reserve Complex Development Plan (Oda et al. 1983). The elevation contour interval is 40 ft (12 m). The interval between the heavy contours is 200 ft (61 m). Areas II and III offer relatively flat regions, which are shielded from the wind, where a submillimeter array could be built. The Caltech and UK/Dutch radio telescopes are being built in area II.

where B = radio frequency bandwidth and τ = integration time. The 1.2 factor in the numerator is a typical value representing the loss due to digital signal processing approximations. Hence, the effective system temperature will be

$$T_s' = 1.2\ T_s. \tag{18}$$

The flux density is related to the antenna temperature by the equation

$$S_\nu = \frac{2kT_A}{A_1}, \tag{19}$$

where k = Boltzmann's constant and A_1 = the effective collecting area of one antenna. For a circular antenna,

$$A_1 = \eta\ \frac{\pi}{4}\ D^2, \tag{20}$$

where D = diameter and η = aperture efficiency. The aperture efficiency will be ~ 0.5 for an antenna whose surface matches a paraboloid to an rms accuracy of ~ $\lambda/20$.

The rms variation in estimated flux density will be

$$\Delta S_1 = \frac{2k}{A_1}\ \Delta T_A. \tag{21}$$

The sensitivities of the basic two-element interferometer for reasonable parameters are given in Table 4. Interferometers can be expected to reach their theoretical sensitivities. The sensitivities given in Table 4 are useful for evaluating the performance of a two-element interferometer observing a calibrator source.

Table 4

Sensitivity of Two-Element Interferometer*

	Antenna Diameters		
	10 m	6 m	
ΔT_A	1.4	1.4	mK
ΔS_1	95	260	mJy
$\Delta S_1/\Delta T_A$	70	195	Jy/K

*Parameters: $T_s' = 1500$ K (e.g., $T_R = 950$ K, $L = 1.25$ at 0.87 mm), $B = 1$ GHz, $\tau = 600$ s, $\eta = 0.5$

The sensitivity of an array of N antennas when observing a point source (i.e., a source that is unresolved on all baselines) will exceed that of a two-element interferometer by a factor equal to the square root of the number of baselines, $N(N-1)/2$. Hence, by combining equations (17), (18), and (21), we obtain

$$\Delta S_N = \frac{2kT_s'}{A_1}\left[N(N-1)B\tau\right]^{-\frac{1}{2}} \tag{22}$$

or

$$\Delta S_N = \frac{2k}{A_e}\frac{T_s'}{\sqrt{B\tau}}, \tag{23}$$

where

$$A_e = NA_1\left[\frac{N-1}{N}\right]^{\frac{1}{2}}. \tag{24}$$

Equation (24) shows the important result that the effective area, A_e, of an array is less than the total area, $A_T = NA_1$. A_e is less than A_T because the array does not process the self-product terms, but only the cross-product terms in the received electric field, and hence does not achieve the full sensitivity of a hypothetical 'phased array.' The ratio A_e/A_T is like an efficiency factor and has a value of 0.71 for N = 2, 0.91 for N = 6, and approaches unity slowly as N becomes large. An array of six 6-m-diameter antennas will have $A_T = 85\ m^2$ and $A_e = 77\ m^2$ whereas a two-element interferometer of 10.3-m-diameter antennas also has $A_T = 85\ m^2$, but $A_e = 59\ m^2$. The former array is nearly twice as fast in terms of integration time required to achieve a certain sensitivity.

A small submillimeter array is remarkably sensitive in terms of brightness temperature. The flux density of a source, in the Rayleigh-Jeans approximation, is related to its brightness temperature, T_B, by

$$S = \frac{2k}{\lambda^2} T_B \Omega_s, \tag{25}$$

where Ω_s = source solid angle. Hence the rms sensitivity for observations of an unresolved source in terms of brightness temperature is, from equations (23) and (25),

$$\Delta T_B = \frac{\lambda^2}{A_e} \frac{T'_s}{\sqrt{B\tau}} \frac{1}{\Omega_s}. \tag{26}$$

For spectral line measurements sensitivities should be compared at constant velocity resolution, Δv, which, from the Doppler equation, is related to the frequency resolution B by the equation

$$B = \frac{\Delta v}{\lambda}. \tag{27}$$

Hence,

$$\Delta T_B = \frac{\lambda^{2.5}}{A_e} \frac{T'_s}{\sqrt{\Delta v \tau}} \frac{1}{\Omega_s}. \tag{28}$$

The rms sensitivities in terms of brightness temperature (appropriate for spectral line observations) and flux density (appropriate for continuum observations) are

$$\Delta T_B = 0.57 \left[\frac{\lambda}{0.87\ \text{mm}}\right]^{2.5} \left[\frac{A_e}{77\ \text{m}^2}\right]^{-1} \left[\frac{T'_s}{1500\ \text{K}}\right] \left[\frac{\Delta v}{1\ \text{km/s}}\right]^{-\frac{1}{2}} \left[\frac{\tau}{10^5\ \text{s}}\right]^{-\frac{1}{2}} \left[\frac{\theta}{2''}\right]^{-2} \text{K} \tag{29}$$

and

$$\Delta S_N = 5.4 \left[\frac{A_e}{77\ \text{m}^2}\right]^{-1} \left[\frac{T'_s}{1500\ \text{K}}\right] \left[\frac{B}{1\ \text{GHz}}\right]^{-\frac{1}{2}} \left[\frac{\tau}{10^5\ \text{s}}\right]^{-\frac{1}{2}} \text{mJy}, \tag{30}$$

where θ is the angular size of the source, which is assumed to be a uniformly bright circular disk so that $\Omega_s = \pi\theta^2/4$. Table 5 shows the sensitivity of a hypothetical submillimeter array and several existing arrays at various wavelengths. As can be seen, such a submillimeter array could detect objects with lower brightness temperatures than can the VLA.

Table 5

Sensitivities of the Proposed Array and Selected Operating Interferometers at Various Wavelengths

						Spectral line		Continuum	
Instrument[a]	Line	λ (mm)	ν (GHz)	T_s' (K)	A_e (m^2)	B_s[b] (kHz)	ΔT_B[c] (K)	B_c[d] (MHz)	ΔS[e] (mJy)
VLA(B)	H	210	1.4	70	7800	5	240	200	0.006
VLA(D)[f]	NH_3	13	23	850	5200	77	4.1	200	0.10
VLA(D)[g]	NH_3	13	23	180	5200	77	0.9	200	0.022
OVRO[h]	CO(1-0)	2.6	115	300	96	385	1.4	300	1.6
Hat Creek[i]	CO(1-0)	2.6	115	300	77	385	1.7	300	2.0
SMA[j]	CO(3-2)	0.87	345	1500	77	1150	0.5	1000	5.4
SMA[k]	CO(4-3)	0.65	460	1500	77	1540	0.2	1000	5.4

a) VLA(B) = Very Large Array in B configuration: array diameter = 12 km; VLA(D): array diameter = 1.3 km; OVRO = Owens Valley Radio Observatory of California Institute of Technology; Hat Creek = Hat Creek Millimeter Observatory of the University of California, Berkeley; SMA = proposed Submillimeter Array discussed in this report.
b) Spectral resolution corresponding to Δv=1 km s^{-1}.
c) Rms brightness temperature for a resolution of 2 arcsec, bandwidth B appropriate for a spectral resolution of 1 km s^{-1}, and integration time of 10^5 s (equation (29)).
d) Continuum bandwidth.
e) Rms flux density for bandwidth B_c (equation (30)), and integration time of 10^5 s.
f) Present mixers.
g) System temperature performance expected in 1986.
h) Three 10-m-diameter antennas at 50% efficiency.
i) Including proposed extension from three to six antennas.
j) Six 6-m-diameter antennas, existing receiver technology.
k) Six 6-m-diameter antennas, improved receiver technology (see Figure 18).

D. Array Configuration

i. Instrument Design

The instrument under consideration here will be used to make high-resolution images of astronomical sources using the techniques of aperture synthesis, also known as Fourier synthesis (Ryle 1975). The correlation of the received electric fields for each pair of antennas in an array produces a Fourier coefficient of the image. These complex Fourier coefficients are functions of the baseline length, in units of wavelength, projected in the direction of the source. These projected baseline components, called u and v, correspond to projection in two orthogonal directions on the sky, right ascension and declination, which change as the earth rotates. The locus of points in the (u,v) plane sampled by a two-element interferometer is called a (u,v)-plane track. Some basic design considerations for an array can be summarized as follows.

(1) The resolution is set by the maximum element spacing. A resolution of 1 arcsec at 0.87 mm requires a baseline of 120 m, whereas at 0.35 mm a baseline of 50 m is required.

(2) The field of view is ultimately limited by the size of the individual telescopes. At 0.87 mm a 6-m-diameter dish has a beam of ~ 36 arcsec. Since many molecular clouds are large, the antennas should be as small as practical. As discussed below, antennas of diameter less than ~ 4 meters would lead to unreasonably high receiver costs with current technology and difficult calibration problems.

(3) An interferometer alone cannot reliably map a source that fills more than about one-half (in one dimension) of the primary beam of the interferometer elements because the elements cannot be placed close

enough together to measure the required Fourier components (Clark 1982). If larger fields are to be mapped, data from a single antenna at least twice the size of the interferometer elements are required. These data can be used to provide measurements of the Fourier components of the image corresponding to baselines shorter than D/2. Maps made without the required short spacings show 'bowl'-shaped distortions. For a detailed discussion of the problem, see Vogel et al. (1984).

(4) The antennas need to be large enough to be able to detect calibration sources within a reasonable integration time.

(5) The antennas should be numerous enough so that many Fourier components can be measured simultaneously and an image can be obtained quickly.

The following configurations are representative.

(a) One-baseline interferometer. By linking a single 10-m-diameter antenna to that of another institution, a one-baseline interferometer could be formed. It would be a relatively inexpensive exploratory instrument. It has a serious problem of being very slow to produce images, since the best observing time might not be available for interferometry, and since images could be synthesized only after many baseline moves.

(b) 'Conventional array'. This array would consist of N antennas each of diameter D, where N and D are chosen to satisfy budgetary, field of view, and optimum sensitivity constraints.

(c) 'Novel configuration'. Such a configuration might consist of one large antenna and many small ones. The large antenna would have an

array of feeds whose outputs would be correlated with the signals from the small antennas. This configuration has advantages of giving high SNR on calibrators, providing a large field of view, and solving the problem of obtaining data at short baselines (Welch 1984, private communication).

We confine the discussion primarily to the conventional array approach (b), pending further study of option (c). The advantages of the 'conventional array' approach (b) over the 'one baseline interferometer' approach (a) are as follows:

(1) Data on N(N-1)/2 baselines can be obtained simultaneously, and a map can be made from one night's observations.
(2) With simultaneous measurements of many Fourier components, that is, (u,v)-plane points, calibration is better.
(3) The ratio of effective collecting area to physical area is larger (see page 85).
(4) Closure phase and hybrid mapping techniques can be used on strong sources (Pearson and Readhead 1984).
(5) The field of view is larger.
(6) Data from one of the larger telescopes (e.g., UA/MPI 10-m-diameter) can be used to fill in the zero and short spacings in the (u,v) plane, allowing a still larger field of view.

The disadvantages are as follows:

(1) It is more expensive.
(2) The SNR for a single baseline for observing calibrators is smaller.

This effect should be less significant with 'global' calibration techniques (see Section III G).

ii. Resolution and Size of Antennas

The interferometer resolution, the full width at half maximum of the beam or point source response function, is given by the equation

$$\Theta_R \simeq 0.7 \frac{\lambda}{d}, \tag{31}$$

where the (u,v) plane is uniformly covered out to a maximum antenna spacing, d (Bracewell 1965). Values of Θ_R are given in Table 6.

Table 6

Resolution for Antenna Spacings up to 100 m*

ν (GHz)	λ (mm)	Θ_R (")
230	1.3	1.8
345	0.87	1.2
460	0.65	0.9
690	0.43	0.6
860	0.35	0.5

*Equation (31).

Hence matching the VLA's maximum resolution at 6 cm (~ 0.25 arcsec) would require a baseline of ~ 350 m at a wavelength of 0.65 mm.

The field of view is limited by the diffraction beam of the individual antennas, which is given by

$$\theta_D \simeq 1.2 \frac{\lambda}{D}. \qquad (32)$$

Values of θ_D are given in Table 7.

Table 7

Antenna Beam Sizes

ν (GHz)	λ (mm)	Beam Size for Antenna Diameter: 6m	10m
230	1.3	52"	31"
345	0.87	36	22
460	0.65	26	16
690	0.43	18	11
860	0.35	14	9

The proper choice of antenna size is important because many molecular clouds are large. Sources that are larger than the primary beams of the interferometer elements can be mapped by combining separate maps in a

mosaic. Data from other instruments must be added to the interferometer data to supply the missing information at short spacings in order to prevent map distortions as described above (Section III D(i)).

An idea of the optimum size of the antenna elements from an economic point of view can be obtained from minimizing the array cost for a given collecting area. A very simple cost model for the antenna and receivers is (see Moran 1983)

$$C = NF_1 D^{\beta} + NF_2, \tag{33}$$

where the first term on the right side is the cost of antennas and the second is the cost of electronics and feeds and C = cost, N = number of antennas, β = power law index for antenna cost, F_1 = constant for antenna cost, and F_2 = cost of electronics and feed per antenna. The collecting area of the array, $\pi ND^2/4$, is fixed, and the optimum antenna diameter is found by minimizing C with respect to D. The optimum value of D is

$$D = \left[\frac{F_1}{F_2}\left(\frac{\beta}{2} - 1\right)\right]^{-\frac{1}{\beta}}. \tag{34}$$

Then, for a given budget, C, the number of antennas that can be built is

$$N = \frac{C}{F_2}\left[1 - \frac{2}{\beta}\right]. \tag{35}$$

Note that D does not depend on the total budget C, but only on the relative costs of receivers and antennas. In other words, the optimum value of D depends only on the constants F_1, F_2, and β. The number of antennas is set by the collecting area desired, or alternatively by the total budget C.

For an antenna that is diffraction limited to 0.35 mm, Weinreb (1983) gives the values $F_1 = 4350\$\ m^{-\beta}$ and $\beta = 2.7$. The resulting optimum antenna diameter as a function of F_2 is given in Table 8.

Table 8

Optimum Antenna Size That Minimizes Array Cost [Equation (33)]

F_2 (K$)	D (Meters)
100	4.8
200	6.2
300*	7.2
400	8.0
500	8.7
600	9.3
700	9.8

*reasonable for a state-of-the-art three-band receiver

This calculation is admittedly naive, but it suggests that for any 'reasonable' receiver cost, considering the current technology, the optimum antenna size is in the range 4 - 10 m. However, in the lifetime of the project many generations of receivers could be required as the technology improves, which would suggest the use of larger antennas. On the other hand, past experience suggests that receivers will become cheaper in the future. If an antenna enclosure is required, F_1 may increase since enclosure costs scale about as antenna costs. This consideration would

drive the antenna size down. Correlators and some processing costs scale as N^2 and would drive the antenna size up, but only slightly since the correlator cost is small with respect to the antenna cost (see Table 12).

iii. (u,v)-Plane Coverage

The quality of interferometer imaging depends upon how well the observations sample the (u,v) plane. We conducted a preliminary study to determine possible antenna configurations for a submillimeter wavelength array. Experience with the VLA at centimeter wavelengths has shown that a 'Y'-shaped antenna configuration produces high quality images over a wide range of source declinations for a fixed number of antennas. Therefore, we adopted such a configuration for the purposes of this report. Other configurations are possible, as are improvements on the examples given below. Our examples demonstrate the general characteristics of an array.

Examples of the (u,v)-plane coverage for a six element array are given in Figures 17a and 17b. In all of the examples, antenna locations are specified as Nn, An, or Bn. The first letter indicates the offset direction toward the North, South-West (i.e., 30° South of West) and South-East (i.e., 30° South of East), respectively; the number, n, indicates the distance from the array center in units of 10 m. Sources at three declinations were considered: a high declination source at 60° (e.g., W3), a near-zero declination source (e.g., Orion), and a low declination source (e.g., the Galactic Center). The array was assumed to be at a north latitude of 32° (e.g., Arizona). Elevation limits for the observations were set at 30° except for the -28° declination source where 20° limits were used. Clearly, a lower latitude site such as in Hawaii would produce longer (u,v)-plane tracks at higher elevation angles for the low declination cases.

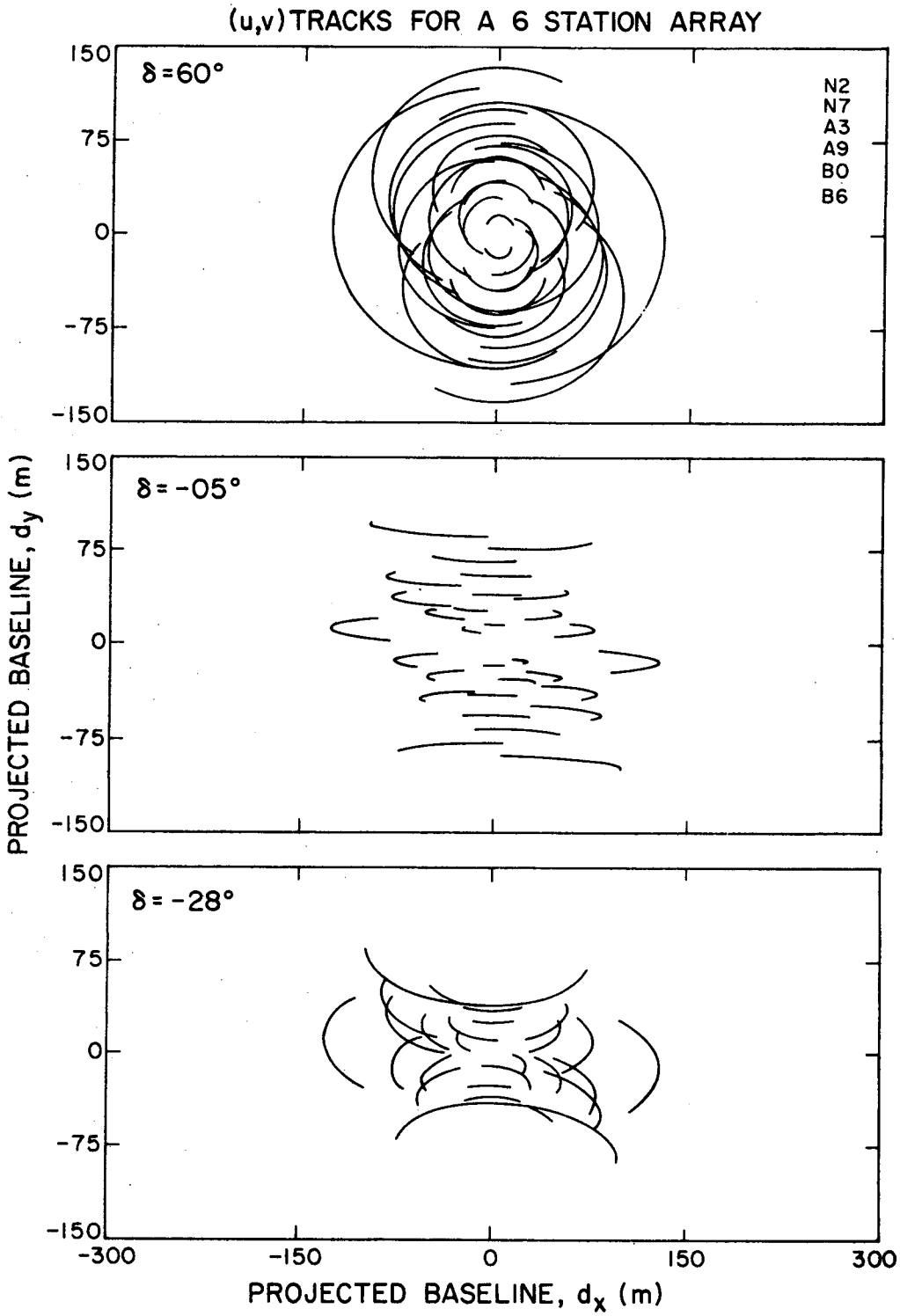

Figure 17(a). (u,v)-plane coverage at declinations, δ, of 60°, -5°, and -28° for a 6-element 'Y'-shaped array in one configuration where $u = d_x/\lambda$ and $v = d_y/\lambda$. Antenna locations are indicated in the upper right corner; N, A, and B refer to the North, South-West, and South-East arms, respectively, and the following number indicates the distance from the array center in units of 10 meters. Plots are full tracks above 30° elevation (except δ = -28° where 20° elevations were allowed) for a site at 32° north latitude. (a) A single array configuration with 15 baselines.

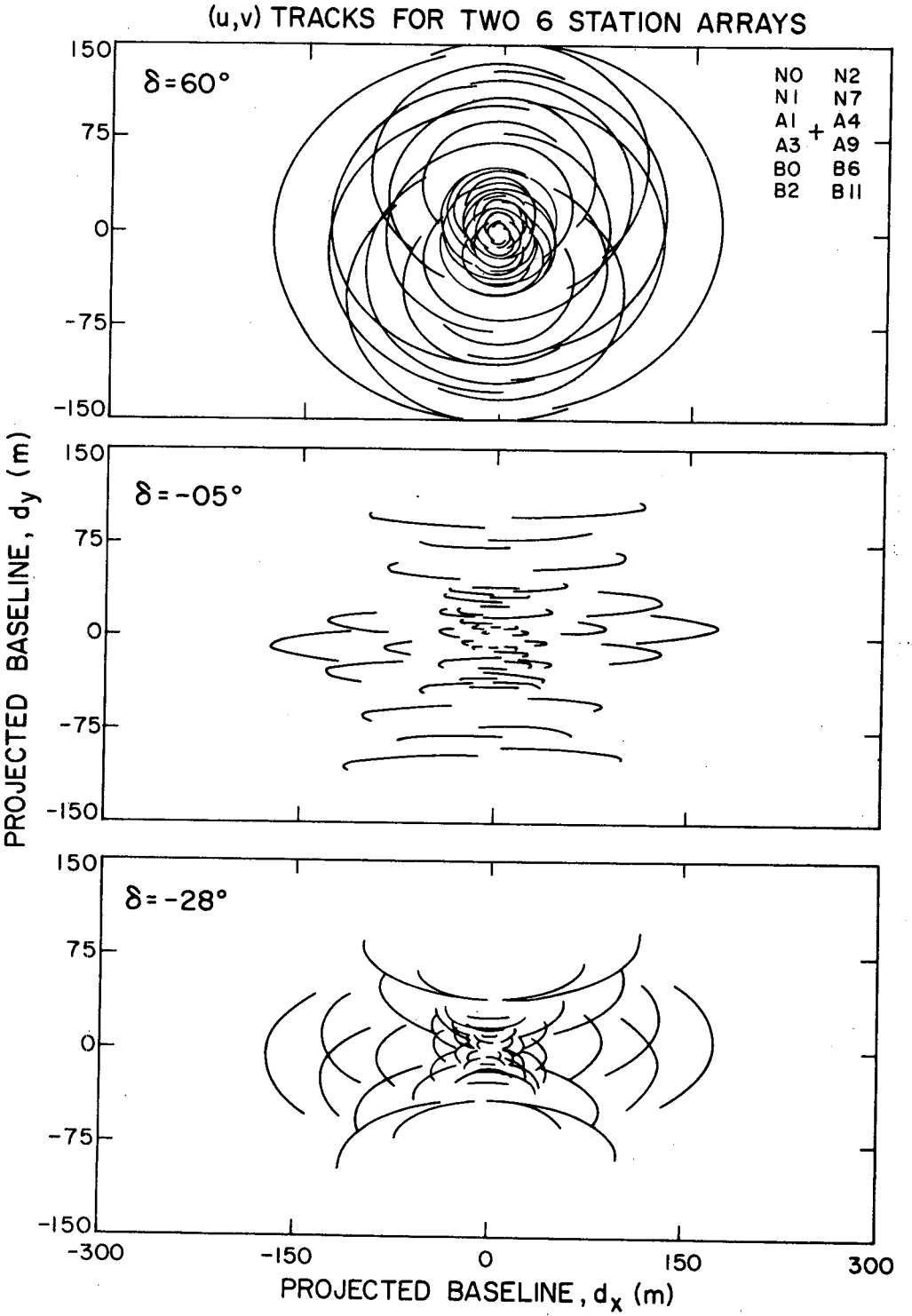

Figure 17(b). Same as (a), except that there are two array configurations yielding a total of 30 baselines.

Figure 17a demonstrates the (u,v)-plane coverage obtainable with a six-element array observing a source continuously for the portion of one day while the source is above the elevation limits. This figure demonstrates that the (u,v) plane can be fairly well sampled with six antennas, and that images with high quality (e.g., dynamic range greater than about 10:1) could be made at all declinations greater than -30° with a single configuration. With fewer than six antennas there would be significant degradation in image quality and a single configuration would not be very good for all declinations.

With a two-dimensional array and only six antennas in a single configuration, it is not possible to cover, in a uniform manner, interferometer spacings spanning a range greater than about a factor of about ten. This constraint limits the sensitivity of the instrument to sources with structure over roughly one decade in angular size. Since many interesting sources have structure on a wider range of angular sizes, it is important to be able to cover more of the (u,v) plane than shown in Figure 17a. Figure 17b shows the (u,v)-plane coverage obtainable by observing a source with two different array configurations. With the (u,v)-plane coverage obtained in this mode of observation, the instrument would be sensitive to more than twice the range of angular scales. Supporting this mode of observation, however, requires moveable antennas and 12 antenna pads. Experience with most radio interferometers suggests that this increase in (u,v)-plane coverage is well worth the extra expense.

iv. Number of Antennas

In this section we summarize the main technical considerations for the choice of the number of antennas. The primary requirement for a

submillimeter-wavelength array is that high quality images be obtainable in one, or at most a few, days of observations for two reasons. First, the number of days available for observations with low atmospheric opacity (e.g., < 1 mm precipitable H_2O) will be limited. For the instrument to be effective in mapping more than a few sources per year it must be fast. Second, calibration of atmospheric absorption may not be very accurate. This inaccuracy may make it complicated to mix data taken with different array configurations on many different days under widely differing weather conditions.

The array should have the largest possible number of antennas for three reasons. First, the number of (u,v)-plane tracks on which data can be obtained in one configuration is $N_t = N(N-1)/2$. Hence the number N_t is proportional to the speed at which data for high-quality images can be acquired. Second, in many cases, the phase closure information, obtained from the data on sets of three antennas, is important in eliminating the effects of phase fluctuations (Readhead and Wilkinson 1978). The ratio of the number of phase-closure data points to the total number of phase data points is $f_{pc} = 1-2/N$. Finally, the collecting area, A_e, given by equation (24), increases with N. The number of antennas is limited primarily by the budget and system complexity. The summary of the cost estimate in Section IV A shows that the marginal cost for one additional or one less antenna is about $2.5M. These considerations are summarized in Table 9.

Table 9

Considerations for the Choice of Number of Antennas

N	Number of (u,v) Tracks (N_t)	f_{pc}*	A_e** (m)	Cost+ ($M)
3	3	0.33	35	--
4	6	0.50	49	--
5	10	0.60	63	22.5
6	15	0.67	77	25.0
7	21	0.71	91	27.5
8	28	0.75	105	--

*Ratio of phase closure to total phase data.
**For 6-m-diameter antennas.
+Including a 20% contingency fund.

We feel that a reconfigurable six-element array is close to optimal in terms of image quality and speed versus cost and complexity for submillimeter-wavelength observations.

E. Receivers

No amplifiers are yet available for submillimeter wavelengths, and all heterodyne receivers have mixer first stages. Several types of mixers are available. Superconductor-Insulator-Superconductor (SIS) mixers are now being developed and have great promise: in principle, they can have gain and they require little local oscillator power (~ 1 μw). However, the

performance of SIS mixers degrades as frequencies approach the band gap energy divided by Planck's constant (about 700 GHz (0.4 mm) for lead alloy material), where the Josephson junction noise becomes important. This limitation may not be fundamental. SIS mixers must be operated at 4 K. Cooled (20 K) Schottky mixers are an alternate possibility. They require ~ 0.1 mw of local oscillator power. InSb bolometer mixers are not appropriate for our application because of their narrow bandwidth. Refrigerators needed to cool the mixers, typically 0.03 m^3 in volume and capable of dissipating 1 watt, are readily available.

Obtaining an adequate source of local oscillator power in the submillimeter range has also been a problem. Some receivers use carcinotrons or lasers, which are probably impractical for an interferometer. High efficiency multipliers are under intensive development and systems with klystrons or Gunn oscillators followed by diode multipliers that can supply ~ 0.5 mw at 300 GHz (1 mm) have been operated successfully (Wilson 1983).

Comprehensive reviews of the state of the art in submillimeter receivers have been written by Wilson (1983) and by Phillips and Woody (1982). A plot of receiver temperature versus frequency from Archer (1984) is given in Figure 18. The effective system temperature, T'_s, will be substantially higher than the receiver temperature because of the loss in the atmosphere and the loss in the electromagnetic coupling to the mixer. Below ~ 300 GHz (1 mm), waveguide mixers are used, which have a coupling factor, α, close to unity. Above that frequency corner reflectors and biconical antenna mounts result in coupling factors of about 0.5. Combining the coupling factor with equations (16) and (18) yields the effective system temperature,

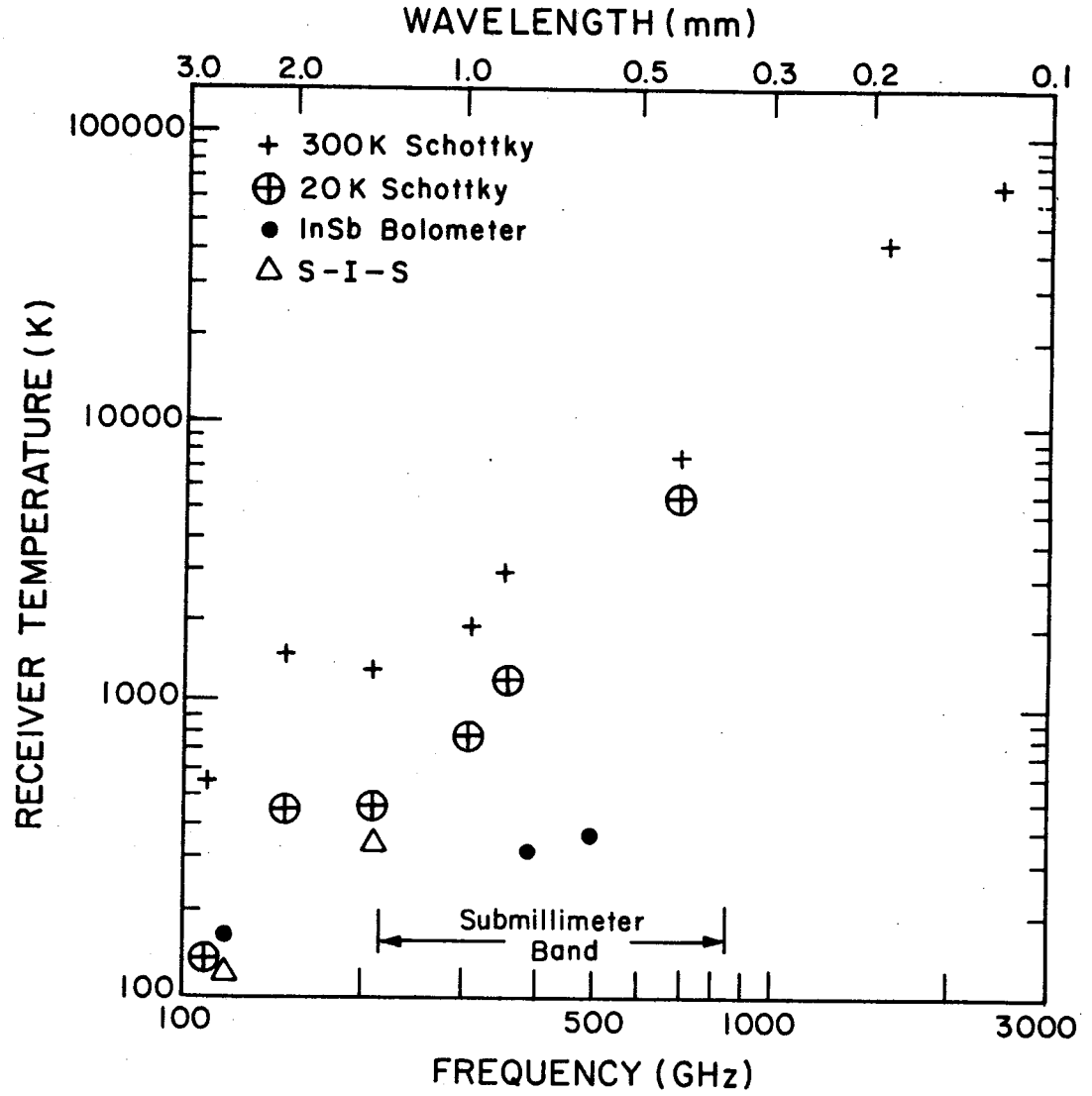

Figure 18. Receiver noise temperature versus frequency for various cooled and uncooled devices. Only the Schottky mixers and SIS mixers are appropriate for a broadband heterodyne interferometer (Archer 1984).

$$T'_s = 1.2 \left[T_R L + T_o (L-1) \right] / \alpha . \qquad (36)$$

The data on the performance of the cooled Schottky receivers suggest that the system temperatures listed in Table 10 represent reasonable state-of-the-art values. Note that L, the atmospheric loss, has been evaluated for the zenith direction. The actual loss will be L times the secant of the zenith angle.

Table 10

Effective System Temperatures of 'Currently' Available Cooled Receivers for Observations in the Zenith Direction

ν	λ	L	α	T_R	T'_s
GHz	mm			K	K
		(1)	(2)	(3)	(4)
230	1.3	1.1	1	300	370
345	0.87	1.2	1	900	1500
460	0.65	2	0.5	2000	10000
690	0.43	4	0.5	5000	26000
860	0.35	4	0.5	8000	77000

(1) Atmospheric loss at zenith for 1 mm of precipitable H_2O.
(2) Antenna-mixer coupling factor.
(3) Receiver temperature.
(4) Effective system temperature single sideband outside the atmosphere (equation (36)).

Submillimeter technology is being developed primarily for research in radio astronomy, atmospheric science, plasma diagnostics, and laboratory spectroscopy. Progress in instrumentation will undoubtedly accelerate with the large number of groups and new instruments being constructed. As an example of the rapid improvement in technology, Figure 19 shows the progress in the development of receivers at 3 mm (100 GHz) wherein the system temperature decreased from 5000 K in 1971 to 80 K in 1983. The current technology is adequate for an interferometer at 0.87 mm (345 GHz). Within 10 years, 1000 K performance at 0.35 mm (870 GHz) seems a realistic expectation. Ultimately, it should be possible to reach the fundamental quantum noise temperature limit, $T_R = hc/\lambda k$, which is 40 K at 0.35 mm. Of course, when T_R dips below T_o, the fractional decrease in system temperature with further decreases in T_R tends to zero. Further, for moderately high zenith angles, the system temperature will tend to scale directly with the secant of the zenith angle for the shorter wavelength observations.

F. Signal Transmission, Processing, and Correlation

The bandwidth for continuum observations should be as wide as possible for maximum sensitivity. The limiting factor is the bandwidth of the intermediate-frequency amplifiers. These amplifiers must have low noise because of the importance of second stage contributions to overall system performance. FET amplifiers with 500-MHz bandwidth and 10 K noise temperature are currently available. Amplifiers with the same noise temperature and 2-GHz bandwidth (operating frequency of 2 to 4 GHz) are being developed by NRAO. The total system bandwidth could be increased by processing two polarizations. In the future, wider bandwidth IF amplifiers with low noise temperatures will doubtlessly become available.

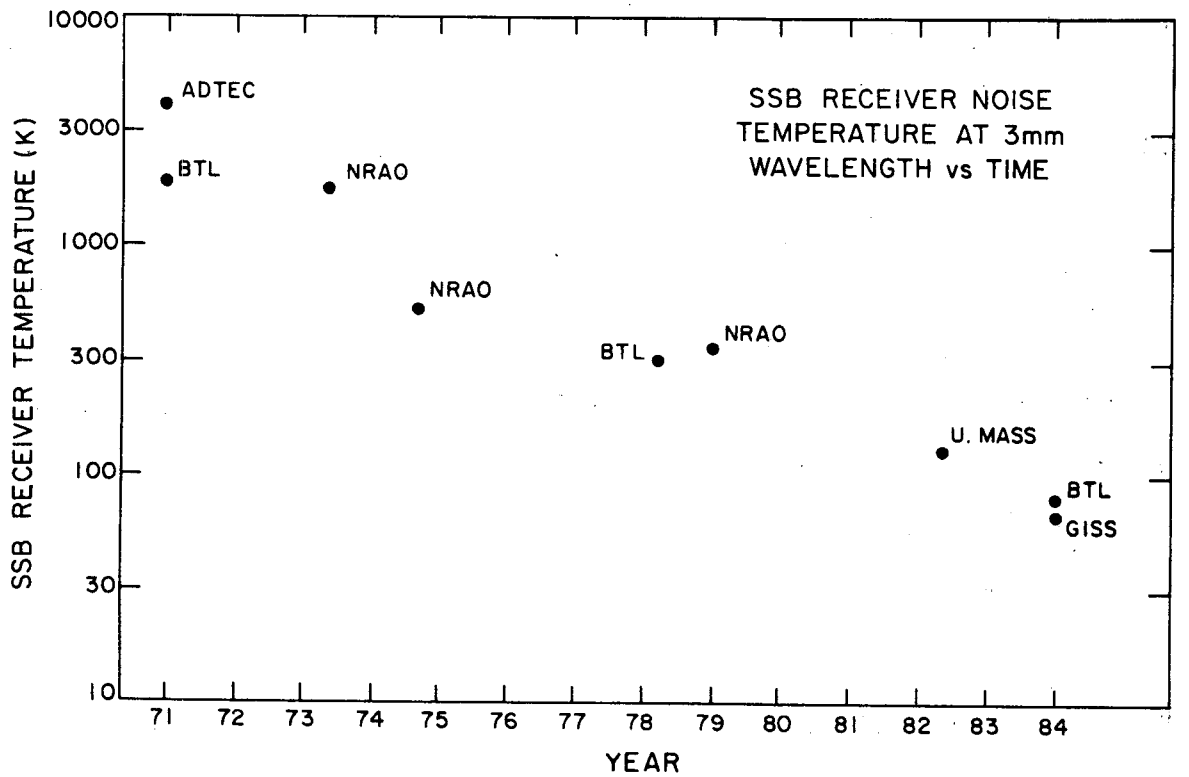

Figure 19. The best receiver noise temperature at 3-mm wavelength (100 GHz) versus year. BTL = Bell Telephone Laboratory; NRAO = National Radio Astronomy Observatory; U. Mass = University of Massachusetts; GISS = Goddard Institute for Space Studies (NASA). (Adapted from Weinreb 1984, private communication.)

The distribution system for the local oscillator reference system and the IF signal could be made from waveguide, optical fibers, or cables. Waveguide may be impractical since the array may not be on level ground. Use of optical fibers would be an innovation in radio astronomy. The microwave signals would have to be modulated on laser signals and read out on photodiode receivers. However, ordinary low-loss heliax cable with an attenuation of ~ 3 db per 30 m should be perfectly adequate for cable lengths of the order of 1 km or less, the same as for the planned instrument.

Delay compensation and fringe rotation can be handled with normal techniques. For a 1 km baseline, the delay range is 3000 nsec, which can be spanned adequately with steps of 0.05 nsec (9 degree phase jumps per step at mid-band for a bandwidth of 1 GHz). Note that baselines of only about 200 m are required to reach 1-arcsec resolution -- the design goal of the instrument. However, the electronics, processor and computer software should be planned to accommodate future expansion to 1 km baseline lengths. Delay compensation as described above can be achieved with a set of 16 analog delay lines arranged in powers of two under computer control. The maximum fringe rate on a 1-km baseline at 0.35 mm is about 180 Hz. This rate can be compensated with standard techniques.

Spectral analysis of very wide bandwidths is necessary. A velocity of 1 km s^{-1} produces a Doppler shift of 3 MHz at 0.35 mm (860 GHz). Hence a spectrometer with a bandwidth of 1 GHz would be required to cover 300 km s^{-1}. This bandwidth is somewhat high to implement with pure digital techniques. The processing of spectral-line data could be accomplished instead with an acousto-optical analog spectrometer, filter banks followed by analog correlators, or a hybrid filter bank-digital

correlator. The last system may be the most economical and flexible. In the hybrid system the signals are filtered in narrow bands (say, ~ 20 MHz) and then spectroscopically analyzed using digital techniques. The spectrometer would be a major cost item in the array (see Section IV A(iv)), and the data from it would be a major load on the computers.

G. Calibration

Strong, unresolved radio sources are the best to use for calibrating an interferometer. Suitable sources for calibration are usually extragalactic continuum sources. Periodic observations of these sources can be used to calibrate the amplitude sensitivities and the instrumental phase shifts of the elements of the interferometer. Experience at the VLA has shown that unless a calibrator is very close to the source under investigation ($< 5^{o}$) and is measured very frequently (~ every 10 minutes), only the effects of the 'static' atmosphere are removed.

The flux densities of extragalactic continuum sources are not well known in the submillimeter range. Owen, Spangler, and Cotton (1980) give flux densities for well-known sources at 10 and 3 mm. The numbers of these sources exceeding various flux density thresholds are given in Table 11.

Table 11

Number of Sources with Flux Density Greater than S_o at 10- and 3-mm Wavelength*

S_o	N(10 mm)	N(3 mm)
1 Jy	46	44
2	27	22
3	14	11
5	6	6
10	2	2

*Owen et al. (1980). There could be substantially more sources that have not been discovered.

The statistics do not seem to be strongly frequency dependent. Therefore, we assume that at 0.87 mm (345 GHz), there will be about 40 sources stronger than 1 Jy observable from the sites under consideration. This extrapolation seems reasonable since Landau et al. (1983) observed a small sample of sources at 1.4 mm and found 20 with flux densities greater than 1 Jy. Hence, the mean distance between calibrators with flux density greater than 1 Jy is expected to be about 30° or less, given the likelihood that more sources will be discovered. These sources can be detected with SNR = 5 in 15 minutes on each baseline of an array with 6-m-diameter antennas with $T_S' = 1500$ K and B = 1 GHz (see Table 4).

The array can be calibrated using 'global' fringe fitting techniques, that is, instrumental parameters can be found from the entire data set

simultaneously, rather than from the data on each baseline individually (Schwab and Cotton 1983). With these techniques the data from all baselines are combined and instrumental parameters for each antenna are solved for in a least-mean-square analysis. Hence, with N antennas, a calibration measurement would yield N(N-1) numbers (amplitude and phase) from which 2(N-1) instrumental parameters would have to be estimated. Assuming that amplitude and phase measurements can be treated separately, analytic models (Cornwell 1983; Herring 1984, private communication) show that the amplitude signal-to-noise ratio, SNR, is

$$SNR = SNR_o \left[\frac{(N-1)(N-2)}{N-1.5}\right]^{\frac{1}{2}} \sim N^{\frac{1}{2}}\, SNR_o, \qquad (37)$$

where SNR_o is the signal-to-noise ratio on one baseline, and the rms phase noise, σ_ϕ, is

$$\sigma_\phi = \frac{1}{SNR_o}\left[\frac{2}{N}\right]^{\frac{1}{2}}. \qquad (38)$$

The SNR increases as $N^{\frac{1}{2}}$, rather than as N, because each measurement contributes to the instrumental parameters of only two antennas. With $N = 6$ and $SNR_o = 5$, SNR ~ 11 and the rms uncertainty in the calibration phase will be ~ 1/9 radian or 7^o, which is adequate for most applications.

IV. COST ESTIMATE

A. Summary of Construction Budget

At this time we can make a preliminary estimate of the construction budget. There is some experience in building most of the components in the array, so reasonable cost estimates can be made. A more accurate budget will require a final design, a site choice, and an engineering study. The budget we have prepared is for an array with six moveable 6-m-diameter antennas, receivers at three frequencies, and a 1000-channel spectrometer with a bandwidth of 1 GHz. The budget summary is given in Table 12, and more details are given in Appendix B. Cost estimates for individual items are given in the following section.

The principal assumptions in this budget are the following.

(1) No allowance for inflation has been included; all figures are in FY84 dollars.

(2) No indirect overhead is allocated or expected. We have included all known direct costs in the budget, including those for increments in administrative support.

(3) The telescope will be placed at a relatively well-developed continental site with roads and utilities. Construction costs on Mauna Kea, a well developed site, are higher than on continental sites. The extra expense of building on Mauna Kea could be substantial (~ $5M). Mt. Graham currently has no facilities. We assume that this site will be developed jointly by the Smithsonian Institution and the University of Arizona with major support from the State of Arizona. The cost for opening

this site (power line, 5 miles of road paving, environmental impact statement) is about $1.5M (Criswell 1984, private communication).

(4) Only new personnel dedicated to the construction of the instrument are included. We assume that many present members of the SAO federal scientific staff will also contribute substantially to the design and construction of the array.

Table 12

Cost of a 6 Element Array (all figures in 1984 K$)

1. DESIGN AND DEVELOPMENT		2250
a. Basic design	750	
b. Nonrecurring development cost for antennas	500	
c. Receiver laboratory setup	500	
d. Digital electronics laboratory setup	150	
e. Site testing equipment and site visits	350	
2. TELESCOPES		6600
a. Six 6-m-diameter antennas λ_m=0.3 mm($800K each)	4800	
b. Six antenna enclosures ($300K each)	1800	
3. RECEIVERS AND SIGNAL PROCESSING		3500
a. Seven receivers x three frequencies ($100K each)	2100	
b. IF transmission and LO distribution	400	
c. Hybrid-filter bank correlator	1000	
4. COMPUTERS		700
a. On-line	200	
b. Off-line	500	
5. CONSTRUCTION AND VEHICLES		2000
a. Site preparation	500	
b. Control building, office building, dormitory	800	
c. 12 antenna pads and distribution network	600	
d. Vehicles and antenna transporter	100	
6. CONSTRUCTION STAFF SALARIES AND BENEFITS (146 person-years x $37K each)		5400
7. MAINTENANCE, UTILITIES, AND TRAVEL (1986-1990)		630
8. CONTINGENCY FUND (about 20 percent of project)		4000
TOTAL		25080

B. Details of Budget

i. Antennas (Table 12, 1a, 2a)

Antenna costs are generally thought to scale as $D^{2.7}$ and λ_m^{-1}, where D is the antenna diameter and λ_m is the minimum operating wavelength, nominally twenty times the rms surface accuracy (Meinel 1979). The power law scaling ignores fixed costs and the exponents assumed are usually valid for coarse scalings over large ranges of the parameters. More elaborate scaling models are described by von Hoerner (1975). Table 13 lists the expected cost associated with the construction of several proposed antennas. We consider only the cost of the antenna and its mount and pointing control system.

Table 13

Cost of Proposed Antennas in 1984 Dollars

Telescope	D (m)	λ_m[a] (mm)	C (K$)	Source
UA/MPI	10	0.35	1800	Hoffmann 1984, private communication
NRAO	10	1.4	800	NRAO Millimeter Array Memo 5
Berkeley	6	1.0	350	Welch 1984, private communication
IRAM	15	1.0	2400	Downes 1984, private communication

[a] λ_m is 20 times the rms surface accuracy. At this wavelength, the aperture efficiency due to surface roughness is 0.5 (Ruze 1966).

The four entries in Table 13 can be crudely fit by the equation

$$C = 9.3 \frac{D^{2.0}}{\lambda_m^{0.7}} \quad (K\$), \tag{39}$$

where D is in meters, λ_m is in millimeters, and C is in thousands of dollars (see Figure 20). This equation gives about the same results as the equation given by Weinreb (1983) (see discussion below equation (35)). With this formula the cost of a 6-m-diameter antenna, with a minimum wavelength of 0.3 mm would be $780 K.

There would also be a nonrecurring cost for machine tooling and testing of the panels, which we estimate to be $500 K. This is the amount budgeted in the NRAO study for a 10-m-diameter millimeter antenna (NRAO Millimeter Array Memo 5). Hence the cost of the first antenna, not including the design study, is $1300 K.

ii. Antenna Enclosure (Table 12, 2b)

Because of the hostile environment in which the array would be sited, antenna protection may be advisable. Several options are available:

(1) An astrodome (a building or dome that rotates with the telescope and has a slit through which radiation can reach the telescope) similar to the ones planned for the Caltech or UA/MPI telescopes. These enclosures cost about as much as the antennas themselves. ($800 K each).

(2) A roll-off shed, which can be moved with each antenna to the various pads. (~ $300 K each).

(3) A radome. New materials such as woven teflon make radomes possible at submillimeter wavelengths. GORE-TEX (a registered trademark of

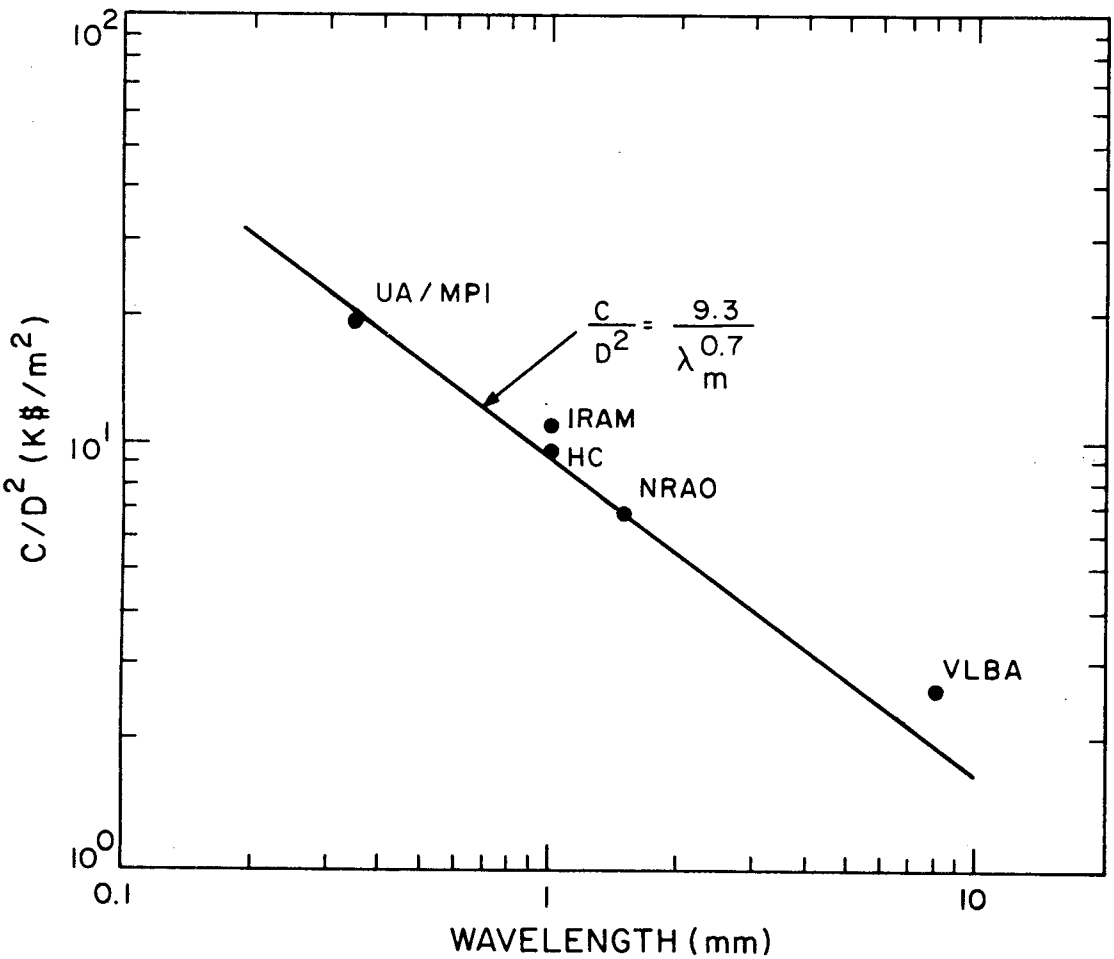

Figure 20. Data for a power law cost model for millimeter-submillimeter antennas. (UA/MPI = U.-Arizona/Max-Planck-Institute's 10-m-diameter antenna; HC = Hat Creek Observatory's 6-m-diameter antenna; NRAO = National Radio Astronomy Observatory's proposed 10-m-diameter antenna; IRAM = Institut de Radio Astronomie Millimetrique's 15-m-diameter antenna; VLBA = NRAO's 25-m-diameter antenna, not used in cost estimate). (See equation (39) and Table 13.)

W.L. Gore, Inc.), a woven teflon material with a thickness of 0.30 mm and tensile strength of 60 kN m^{-1}, has been tested at submillimeter wavelengths by Birch, Nicol, and Street (1983). The transmission is better than 0.9 at frequencies below 500 GHz. The transmission decreases to about 0.8 at 1000 GHz. The cost of the material is $17 per square foot (Gore Associates 1984, private communication). With a radome, the antenna structure can be made lighter since there is no wind or ice loading. Thermal gradients can be controlled more easily. There are disadvantages. Optical pointing would not be possible with a radome. Also, shadowing of some antennas by radomes of other antennas would occur in close configurations. This latter limitation also applies to astrodomes. A 9-m-diameter, 5/8 sphere, radome costs about $300K (Hensel, ESSCO, 1984, private communication).

(4) A flexible, removable shelter (like the sun shade on a baby carriage) (~ $150K each).

(5) A central large shelter into which the antennas can be moved during periods of severe weather (~ $1M total).

We chose the intermediate cost options (2) or (3) for budgetary calculations. We note that the choice of shelter influences other budget items. The cost of the antennas would be less if they were protected by a radome since they need not be as stiff. On the other hand, if a central shelter were used, the transportation system would have to be augmented to allow rapid movement of the antennas when necessary.

iii. Receiver Front Ends (Table 12, 3a)

The technology is moving so rapidly in receiver development that it is essential to have an in-house staff and laboratory to provide continually the best possible receivers in a timely and economic fashion. Starting an appropriate laboratory would cost about $500 K. We estimate that each receiver (feed, mixer, local oscillator, IF amplifier, and refrigerator) will cost about $100 K. We have allowed for a spare receiver (i.e., the prototype) at each wavelength.

iv. Correlator (Table 12, 3c)

The cost of the hybrid filterbank-correlator can be approximated by the equation (Weinreb 1983)

$$C = \frac{BMN^2}{J} + 0.6\ JN + 200 \quad (K\$), \tag{40}$$

where B is the total bandwidth in GHz, M is the total number of spectral channels, J is the number of filters per antenna, and N is the number of antennas. The first term accounts for the digital correlator, assuming 10^9 multiplications per second per dollar. Note that $2BMN^2/J$ is just the bit multiplication rate needed for cross- and auto-correlation. The second term accounts for the analog filters and the third term for fixed costs. A reasonable system might be one with B = 1 GHz, J = 100, N = 6, and M = 1000, which would cost $920 K. This spectrometer would provide 0.35 km s^{-1} resolution over a range of 350 km s^{-1} at 0.35 mm (860 GHz) or 0.87 km s^{-1} resolution over 870 km s^{-1} at 0.87 mm (345 GHz).

v. Computers (Table 12, 4a, 4b)

We can estimate the rate of acquisition of raw data by the array. To map a field of view of 36 arcseconds at a resolution of 1 arcsecond requires an averaging time of about 1 minute or less (this allows less than 1 radian of smearing for a source at the edge of the field). With 15 baselines and 4 bytes (1 byte = 8 bits) per complex data sample (amplitude and phase), the data rate in the continuum mode will be 86 Kbytes/day. In the spectral line mode with a 1000-channel correlator, the rate will be 86 Mbytes/day (two 1600 bpi tapes/day). Typical map sizes, given about 3 points per resolution element, will be 128 x 128.

We estimate that the array will need the capacity of about three Vax 11-750 computers, one on-line and two off-line. This particular model will undoubtedly be obsolete when this array is constructed. The on-line computer would control the array, acquire the interferometer data and monitor information. One off-line computer would be used as a backup for the on-line system and for data processing. The second off-line computer would be located in Cambridge for image processing. The off-line computers will require image displays and substantial disk storage (> 1 Gbyte each). The budget is given in Table 14.

Table 14

Computer Facilities

Item	Number	Cost
Vax 11-750 system	3	$450 K
500 Megabyte disk	5	125 K
6250 bpi tape drives	4	80 K
Image display systems	2	45 K
		$700 K

vi. Buildings (Table 12, 5b)

A control building with office and laboratory space of about 3000 square feet will be required. If we assume construction cost at $150 per square foot, this building will cost $450K. A second building at the site with dormitories and kitchen facilities covering 1500 square feet will cost $225K. (This second building may not be required on Mauna Kea.) Furthermore, a local office of about 1500 square feet in a nearby town will be needed, which at $80 per square foot, will cost $120K.

C. Operating Budget

We have studied the personnel requirements and operating budgets of three observatories, the NRAO-VLA, the Whipple Observatory, and the Hat Creek Observatory, in order to estimate the operating costs for the

submillimeter array. These observatories have staffs of 107, 45, and 33, respectively, and range in size from larger to slightly smaller than the proposed array. We estimate that a staff of 35 people will be required at an annual cost of about $2M. Breakdowns of the staff and budget are shown in Table 15 and Appendix B. We have not included the contributions of present federal SAO scientific staff members in the project.

Table 15

Operations Staff and Budget

Operations Staff	number
Project manager	1
Project scientist	1
Site director	1
Receiver (2 engineers, 3 technicians)	5
Digital (2 engineers, 2 technicians)	4
Computer programmers	4
Mechanical maintenance	2
General technical support (1 engineer, 3 technicians)	4
Secretaries	2
Telescope operators	5
Miscellaneous (1 contract manager, 1 shipping clerk, 1 general laborer, 2 cooks/cleaners, 1 post doc)	6
	35

Operations Budget	K$
Staff salaries (35 people at an average of $37K each, including benefits)	1300
Utilities	140
Maintenance materials and spare parts	115
Maintenance contract on computers	105
New equipment	250
Travel (staff and outside users)	60
	1970

For more details, see Appendix B.

V. STRATEGIC CONSIDERATIONS

A. Timescale

The developments in millimeter-wave and far-infrared astronomy in the past decade have highlighted the importance of submillimeter astronomy. The productivity of the VLA and millimeter arrays shows the importance of arcsecond resolution as achieved by interferometry. The rapid pace of technological development in the past decade suggests that building a submillimeter array is feasible at this time. By estimating the time required for construction and development of the various components of such an instrument, we conclude that a five-year construction program is optimal.

Figure 21 shows the possible time scales for further study, funding, and construction of the array. Without more detailed studies, these estimates, especially with regard to antenna construction, are only illustrative in nature. A number of points, however, are important to emphasize: (1) Further in-house study and consultations within the community should proceed even before design funding is available. (2) A receiver group should be assembled and their laboratory set up as quickly as possible. (3) Testing of a working interferometer and the vigorous shake-down of all components should be conducted in the Cambridge area. These steps will be most important for completing the submillimeter array within the proposed timescale. They are discussed in more detail in the next sections.

SMITHSONIAN ASTROPHYSICAL OBSERVATORY
SUB-MILLIMETER ARRAY

I) BUDGET SUMMARY
(in thousands of 1984 dollars with no allowance for inflation)

Description	FY 84	FY 85	FY 86	FY 87	FY 88	FY 89	FY 90	FY 91	FY 92	FY 93
Studies	Concept	Preliminary	Final	< - - - - -	Construction	- - - - - -	->	<- - - -	Operation	- - -
Approx Funding	1	600	2900	4800	5800	5400	4900	2000	2000	2000
Site	< - - Study and Tests - - >			Acquire Prep.	<- - Construction - ->					
Antennas/ Enclosure		Study		Spec. Contract	< - - - - Deliver - - - - > 1 2 3 4 5 6					
Receiver/LO	< - Set up Lab - >									
1		< - - - Develop - - - >		< - Construct 6 more - >						
2				< - - - - Develop - - - >		< - Construct 6 more - >				
3						< - - - Develop - - - >		< - Construct 6 more - >		
4								< - - - Develop ...		
IF distribution			Study	< Prototype >	Test	<- - - Finish - - ->				
Correlator		Study	<- - Prototype - - >		Test	<- - Construct - - >				
Software			Study	<- Develop ->	Test	<- - - Finish - - ->		< - Maintain/Upgrade...		

Figure 21. Possible time table and budget for constructing a submillimeter array. Details are given in Table 12 and Appendix B. Dollar amounts have been rounded to the nearest $100K. The construction is complete at the end of 1990 except for the receiver fabrication, which extends through 1993 at a cost of $750K.

B. Design Study

The most urgently needed studies are in the areas of (1) receiver and local oscillator development, (2) antenna design, (3) site selection, and (4) correlator design. Significant progress in each of these areas will require design money and the active participation and leadership of at least one expert in the appropriate field. The recruitment and hiring of an experienced, high-level person in each study area (with the exception of site selection) should proceed as quickly as possible. These new people will of course also be needed to develop the equipment throughout the construction and operational phases of the project.

The next most important step is to initiate site testing and studies. The sooner this is begun, the longer the time base of data that will be available to evaluate weather and phase stability. Such studies should be coordinated with other interested groups.

In the interim before the design money is appropriated, an in-house study group, in consultation with external experts, should continue to keep track of the latest developments in terms of technology, other submillimeter instruments, possible vendors, and possible candidates for recruitment. These steps will allow the actual design studies to begin quickly once funded.

C. Receiver Development

The array should be designed for operations between 1.3 mm (230 GHz) and 0.35 mm (860 GHz). Some important submillimeter astronomy has already been done at low angular resolution. However, although a number of receiver systems are operational, none is very good by microwave standards.

Furthermore, it is unclear which of the competing technologies (e.g., SIS, cooled Schottky diode) will ultimately prove to be the best. Because the array will probably consist of many elements, the investments in receivers will be substantial. Both the choice of a receiver system and its optimization will be crucial for the ultimate performance of the instrument. Receiver development will continue throughout the lifetime of the instrument.

It is desirable to gain as much lead time as possible on developing the receivers and the local oscillators. As the technology is so young, it is extremely unlikely that complete receivers with adequate sensitivity will be obtainable from commercial sources by 1990. Two approaches are possible: assemble a receiver group and develop the expertise internally, or collaborate with other groups. In-house development will be highly desirable because (1) the developed expertise will benefit other groups at the CfA, (2) timescale, goals, and priorities for the entire project can be set internally without external perturbations, and (3) maintenance of the submillimeter array at a remote site can be performed by the same people who actually developed the equipment.

Operating an array requiring six or more receivers for each of three observing wavelengths is a task that will almost surely require an active laboratory of about five people. Similarly, correlator design will require state-of-the-art development. A digital laboratory of comparable size to that for receivers is envisioned. It is possible that some of the personnel for the two laboratories can be shared. In any event, it is of the highest priority to proceed in these areas as quickly as possible.

D. Local Testing

Because of the complexity of designing and building a submillimeter wavelength interferometer, it would be highly desirable to build a working subsystem locally that would later be disassembled and placed at the site. A short baseline, two-element interferometer, operating at about 1-mm wavelength, seems an appropriate first step. Because the antennas are not immense structures it seems feasible to make them 'transportable.' Should the interferometer ultimately go to a site where construction is difficult (such as the top of Mauna Kea), it may even prove cost effective to design the entire system so that it can be built locally, disassembled, and moved to the site in pieces. We note that there may be a significant number of days in the wintertime when the atmospheric transmission is good enough in New England to permit observations at submillimeter wavelengths. When the temperature is $-20^{\circ}C$ ($-4^{\circ}F$), the relative humidity is 50 percent, and the scale height of water vapor is 2 km, the amount of precipitable water vapor is 1 mm (see equations (8)-(10)).

E. Comparison with Other Telescopes

It is useful to compare the proposed submillimeter telescope array with other existing or planned world-class instruments. The most important feature is the fact that the proposed angular resolution of about one arcsecond is directly comparable to the premier instruments at centimeter wavelength (VLA), millimeter wavelength (Various millimeter arrays: Berkeley, Caltech, IRAM, Nobeyama), near-infrared (LDR, SIRTF), optical (ST, NNTT), and ultraviolet (IUE). Another important feature is the fact that the proposed instrument will have sufficient collecting area and sensitivity to examine the same types of phenomena studied at other

wavelengths -- low energy phenomena at longer wavelengths and high energy phenomena at the shorter wavelengths. These points are extremely important, for it is the complete sampling of the electromagnetic spectrum at the same high angular resolution that is expected to reveal the underlying physics. The final and perhaps most important feature of this instrument is the fact that we will be exploring an entirely new regime in the frequency-angular size space. Certainly the timely results from the recent IRAS mission have suggested innumerable candidates, especially galaxies, for study in the submillimeter range. However, it is the serendipitous results, which are found in every new spectral and spatial window, that may be the most exciting.

F. Visitor Program

The proposed array will be a powerful tool for investigating a wide range of astronomical phenomena. The instrument can be used to fullest advantage only if it is available to a broad community of scientists. Both the injection of new ideas and the cross-fertilization with other groups will ensure the best science and the competitive spirit. We suggest that a visitor program be established whereby a substantial portion of the time on the instrument (25 - 50 percent) is made available to scientists outside of the CfA. To facilitate a visitor program, operations should be made 'user-friendly.' Data reduction packages should be exportable or compatible with the facilities at the home institution of each visitor. Short-term visits to the CfA should be encouraged to increase the level of interaction between outside users and CfA staff members.

VI. CONCLUSION

A. Science

A submillimeter array of the type considered here will make basic contributions to a wide range of astronomical disciplines, including studies of the solar system, star formation, astrochemistry, evolved stars, structure of galaxies, and energetics of quasars and active galactic nuclei. In addition, such an array will likely make unexpected discoveries, since its wavelength coverage would be equalled by only a few telescopes of very recent vintage, and since its angular resolution, ~ 1 arcsecond, would be finer by at least an order of magnitude than that of other submillimeter wavelength telescopes.

The submillimeter wavelengths are well matched to emission from the cool (10 to 50K) dust and molecules found in all molecular clouds in the Milky Way and other galaxies. High-resolution studies of such clouds, and of the stars forming in them, will probably be an important application of the array.

The scientific potential of a one-arcsecond-resolution submillimeter array is high, and such an instrument is both unique and desirable. Numerous technical questions must be studied in greater detail before definitive recommendations can be made concerning site, antennas, configuration, receivers, costs, and other issues. The next section summarizes our current technical conclusions and questions.

B. Technological Questions

An excellent site is required for ground-based observations in the submillimeter band. Existing data suggest that on about 80 days a year on Mauna Kea and 40 days a year on Mt. Graham there will be less than 1 mm of precipitable water vapor in the atmosphere. At 1 mm of H_2O, the zenith transmission in the bands at 1.3, 0.87, 0.65, 0.43, and 0.35 mm is about 0.9, 0.8, 0.5, 0.25, and 0.25, respectively. The transmission should be greater than 0.6 in the two longest wavelength bands at least half the time at both sites. Hence, if the array is designed with wavelength agility, it can be used productively at least half the time. The atmosphere is essentially nondispersive in the submillimeter windows, and phase fluctuations should scale inversely with wavelength. Experience with the VLA and the Hat Creek interferometer suggests that with 1 mm of precipitable water the rms phase fluctuations will be about 1 radian on a baseline of ~ 250,000 λ. Hence, high-quality maps should be obtainable with a resolution of ~ 0.6 arcseconds. The actual 'seeing' limit will be about 0.15 arcseconds. The above calculations assume that fluctuations in the water vapor distribution are the principal cause of phase noise. The amount of phase noise due to 'dry' air turbulence is not known accurately but is probably less than that due to water-vapor fluctuations.

The best way to test potential sites is with an interferometer operating at ~ 1 cm wavelength and observing either masers or artificial sources. This type of site evaluation is highly desirable, and a detailed study should be made of its feasibility. In addition we suggest that a careful evaluation be made of the submillimeter sky brightness data being taken on Mauna Kea and the 1.3-cm sky brightness data to be taken on Mt. Graham along with optical seeing data. If additional sites are to be

tested, we suggest that measurements with a 1.3-cm water-vapor radiometer be made.

We recommend that the telescope array be two-dimensional with about six 6-m-diameter antennas. The size of the antennas is controlled primarily by three factors: (1) field of view, (2) ease of calibration, and (3) maximization of total collecting area for fixed cost. A consideration of the relative cost of antennas and receivers suggests that the antenna diameter should be between 4 and 10 m. Field of view and calibration requirements push the size in opposite directions toward smaller and larger antennas, respectively. We recommend 6-m-diameter antennas as a compromise wherein ~ 30 calibrator sources could be detected in 15 minutes on each baseline and the field of view would be 36 arcsec at 0.87 mm.

A six-element two-dimensional array will be sensitive to a range of scale sizes of about a factor of ten. With 15 baselines, a good image at fixed resolution can be formed in one configuration for sources at all observable declinations. Moveable antennas and at least 12 antenna pads are needed to change resolution or to study the structure of sources over a larger range in scale sizes.

The fabrication of the antennas should pose no fundamental problems. We should be able to use the carbon fiber technology being developed by the UA/MPI group and their contractor, Dornier System GmbH, Friedrichshafen, Germany. The necessity for, and the type of, antenna enclosure (astrodome, radome, roll-off shed, flexible shelter, or central garage) needs further study.

The receiver technology is currently adequate at wavelengths longer than 0.87 mm (345 GHz) where 900K cooled Schottky mixer receivers can be built. This limit is also the current one at which multiplier type local oscillators can provide adequate power for this class of receiver. The areas of receiver and local oscillator development are ones where a major development effort is required. Because many groups are working in this wavelength region, the technology can be expected to advance rapidly. We recommend that each antenna be equipped with receivers covering three of the submillimeter windows (initially 1.3, 0.9, and 0.5 mm).

A reasonable limit to the system bandwidth is 1 to 2 GHz, dictated by the bandwidth of the IF amplifiers. Wider bandwidth and greater sensitivity could be achieved by installing parallel receivers and processing for orthogonal polarizations. Spectral analysis of bandwidths of the order of 1 GHz can best be achieved by a combination of filters and digital correlators. Current technology is adequate for this application.

The cost of the proposed array is about $25M ($15.6M, construction; $5.4M, salaries; and $4M, contingency funds). The operating staff will be about 35 and the annual operating budget about $2M.

ACKNOWLEDGMENTS

The committee is grateful to the following people who made formal presentations during the course of the study:

K.Y. Lo, California Institute of Technology
P.F. Goldsmith, University of Massachusetts
A.E.E. Rogers, Haystack Observatory
P.R. Schwartz, Naval Research Laboratory
G. Sollner, M.I.T. Lincoln Laboratory
R. Stachnik, Center for Astrophysics
S. Weinreb, National Radio Astronomy Observatory

Helpful comments were received on drafts of this report from the following staff members of the Center for Astrophysics:

A.G.W. Cameron
N.P. Carleton
A. Dalgarno
G.B. Field
A.E. Lilley
P. Nisenson
R.W. Noyes
H. Penfield
H.E. Radford
I.I. Shapiro
H.D. Tananbaum
W.A. Traub

We also acknowledge extensive discussions with the following members of the astronomical community outside of the CfA:

A.H. Barrett, Massachusetts Institute of Technology
J.W. Findlay, National Radio Astronomy Observatory
I. de Pater, University of California, Berkeley
D. Downes, Institut de Radio Astronomie Millimetrique
R. Genzel, University of California, Berkeley
D.N.B. Hall, Institute for Astronomy, University of Hawaii
R. Hildebrand, University of Chicago
R. Hills, Cambridge University
W.F. Hoffmann, University of Arizona
D.T. Jaffe, University of California, Berkeley
A.R. Kerr, Goddard Institute for Space Studies
C.J. Lada, University of Arizona
K. Mattila, University of Helsinki
F.N. Owen, National Radio Astronomy Observatory
T. Phillips, California Institute of Technology
P.F. Schloerb, University of Massachusetts
R.A. Sramek, National Radio Astronomy Observatory
P.A. Strittmatter, University of Arizona
P. Thaddeus, Goddard Institute for Space Studies and Columbia University
A.R. Thompson, National Radio Astronomy Observatory
B.L. Ulich, University of Arizona
W.J. Welch, University of California, Berkeley
W.J. Wilson, Jet Propulsion Laboratory

We thank Carolann Barrett for her careful work and unending patience in producing the many drafts of this report.

APPENDIX A

RELATIONSHIP BETWEEN PHASE FLUCTUATIONS AND 'SEEING'

If the phase fluctuations are assumed to vary linearly with wavelength, a frequency independent value for the 'seeing' can be derived. Let

$$\sigma_\phi = \alpha\omega d = \frac{2\pi\alpha c d}{\lambda} = 2\pi\alpha c u, \qquad \text{(A1)}$$

where

σ_ϕ = rms phase noise,

α = empirical constant,

ω = angular frequency = $2\pi\nu$,

d = baseline length,

λ = wavelength,

c = speed of light,

u = baseline in wavelengths = d/λ.

Since each measured point is corrupted by a random phase variable ϕ, the observed visibility V' will be related to the true visibility by the equation

$$V' = Ve^{i\phi}. \qquad \text{(A2)}$$

The expectation of the visibility, when ϕ is a Gaussian random variable, will be

$$\langle V' \rangle = V\langle e^{i\phi} \rangle = Ve^{-\sigma_\phi^2/2} \qquad \text{(A3)}$$

or

$$\langle V' \rangle = Ve^{-2\pi^2\alpha^2c^2u^2}.$$

Multiplication of the visibility by the weighting function W(u) corresponds to convolving the image with the Fourier transform of W(u), denoted W(θ). Hence, defining

$$W(u) = e^{-2\pi^2\alpha^2c^2u^2} \tag{A4}$$

implies that

$$W(\theta) \propto \exp\left[-\frac{\theta^2}{2\alpha^2c^2}\right]. \tag{A5}$$

The full width at half maximum of W(θ) is θ_s, given by

$$\theta_s = \sqrt{8\ \ln 2}\ \alpha c. \tag{A6}$$

Since

$$\alpha c = \frac{\sigma_\phi c}{\omega d} = \frac{\sigma_\phi \lambda}{2\pi d} = \frac{\sigma_d}{d}, \tag{A7}$$

where $\sigma_d = \frac{\sigma_\phi \lambda}{2\pi}$ is the rms uncertainty in path length, we obtain

$$\theta_s = 2.35\left[\frac{\sigma_d}{d}\right] \text{ (radians)}. \tag{A8}$$

Since σ_d/d is constant for the assumed model, θ_s is independent of wavelength (as is also obvious from equation (A6)).

APPENDIX B

CONSTRUCTION AND OPERATING BUDGET

We have prepared a detailed illustrative budget for the construction of the array. The construction budget is shown in Table B-1, and the personnel roster is shown in Table B-2. The construction schedule assumes that design funding starts in 1985, which is optimistic. A delay in the starting date would delay the completion date by a corresponding amount. The budget for the construction phase of the project as summarized in Table 12 includes all costs up to the end of 1990 plus $750K for receiver construction beyond 1990. Note that in Table 12 all the design costs are lumped together, as are the maintenance costs. The maintenance costs are based on the total capital investment after the first year. That is, no maintenance has been budgeted for the first year on any item of equipment. The operating budget as summarized in Table 15 is that for 1993. The $250K allocated in that year for the final receiver fabrication would be continued in succeeding years as a fund for new equipment. The personnel costs listed in Table B-2 include salaries and benefits appropriate for Smithsonian federal employees.

Some items of the construction budget should properly be called a preoperations budget. Such items as maintenance ($300K) and salaries for telescope operators and cooks/cleaners ($100K) employed before FY1991 are in this category.

Table B-1

Detailed Budget (in Thousands of 1984 Dollars)

	FY 85	FY 86	FY 87	FY 88	FY 89	FY 90	FY 91	FY 92	FY 93
SITE PLAN									
Site visits	10	20	20						
Site testing	150	150							
Site Preparation			50	450					
Vehicles				30					
Antenna Transporter					70				
Local Office Bldg.			150						
Control/Lab Bldg.				500					
Site Dormatory/Cafeteria					150				
Antenna Pads/Electrical				300	300				
Maintenance (1% of capital)				5	20	20	20	20	20
Total	160	170	220	1285	540	20	20	20	20
ANTENNAS/ENCLOSURES									
Pre Design Study	50								
Detailed Spec.		500							
Antenna Testing			500						
Purchase			1800	1600	1600	1600			
Maintenance (1% of capital)				15	30	45	60	60	60
Total	50	500	2300	1615	1630	1645	60	60	60
RECEIVERS/LO's									
Lab set up	100	400							
1'st receiver									
develop first		100	100						
build 6 more				250	250				
2'nd receiver									
develop first			100	100					
build 6 more						250	250		
3'rd receiver									
develop first					100	100			
build 6 more								250	250
Maintenance (1% of capital)				5	5	10	15	15	20
Total	100	500	200	355	355	360	265	265	270
IF DISTRIBUTION									
Design			100						
Construct				200	200				
Maintenance (1% of capital)					5	5	5	5	5
Total			100	200	205	5	5	5	5
CORRELATOR									
Study	50								
Lab set up		100	50						
Prototype		100	100						
Construct				200	300	300			
Maintenance (1% of capital)				5	5	10	10	10	10
Total	50	200	150	205	305	310	10	10	10
COMPUTER									
Study		50							
Correlator control			100						
Telescope control				100					
Off-line Analysis 1 (site)					250				
Off-line Analysis 2 (CfA)						250			
Maintenance (15% contract)				15	30	65	105	105	105
Total		50	100	115	280	315	105	105	105
CONSTRUCTION CONTINGENCY									
(20% of construction budget)		800	800	800	800	800			
Total		800	800	800	800	800			
OPERATIONS									
Travel				20	40	60	60	60	60
Utilities/phones/misc				40	80	100	140	140	140
Total				60	120	160	200	200	200
TOTAL EXPENSES (non personnel)	360	2220	3870	4635	4235	3615	665	665	670

Table B-2

Personnel Budget (Salaries and Benefits)

	FY 85	FY 86	FY 87	FY 88	FY 89	FY 90	FY 91	FY 92	FY 93
SAO...									
Project Scientist	65	65	70	70	75	75	80	80	85
Secretary	20	20	20	20	20	20	20	20	20
Project Manager		60	60	65	65	70	70	75	75
Contract Specialist		40	40	40	45	45	45	50	50
Purchasing Agent		20	20	20	20	20	20		
Shipping Clerk		15	15	15					
Receiver Leader	65	65	70	70	75	75	80	80	85
Receiver Tech	20	20	20	20	20	20	20	20	20
Receiver Tech		20	20	20	20	20	20	20	20
Digital Leader	65	65	70	70	75	75	80	80	85
Digital Tech		20	20	20	20	20	20	20	20
Software Leader		65	65	70	70	75	75	80	80
Programmer			40	40	40	40	40	40	40
Visiting Engineer			60	60	60	60	60		
Post Doc			30	30	30	30	30	30	30
ARRAY SITE...									
Site Manager				40	40	40	45	45	45
Site Secretary				15	15	20	20	20	20
Shipping clerk				15	15	15	15	15	15
Receiver Engineer		50	50	55	55	60	60	65	65
Receiver Tech						20	20	20	20
Digital Engineer		50	50	55	55	60	60	65	65
Digital Tech		20	20	20	20	20	20	20	20
Senior Systems/Prog		40	40	40	45	45	45	50	50
Programmer				40	40	40	40	40	40
Mechanical Engineer		40	40	40	45	45	45	50	50
Mechanical Tech			20	20	20	20	20	20	20
Mechanical Tech				20	20	20	20		
Electrical Engineer		40	40	40	45	45	45	50	50
Electrical Tech			20	20	20	20	20	20	20
Electrical Tech				20	20	20	20	20	20
General Technician				20	20	20	20	20	20
General Labor				15	15	15	15	15	15
General Labor				15	15	15	15		
Cook/Cleaning					15	15	15	15	15
Cook/Cleaning					15	15	15	15	15
Chief Operator						40	40	40	45
Telescope operator							20	20	20
Telescope operator							20	20	20
Telescope operator								20	20
Telescope operator								20	20
TOTAL EXPENSES (all personnel)	235	715	900	1120	1170	1255	1315	1280	1300

Notes:

1) all site employees hired before 1988 would start duties at SAO and move to the site when appropriate.
2) Approximately half of the employes do not have scheduled (non-inflationary) pay raises as an attempt to compensate for some job turnover.

REFERENCES

Angel, J.R.P., and Stockman, H.S. 1980 'Optical and Infrared Polarization of Active Extragalactic Objects,' Ann. Rev. Astron. Astrophys., 18, 321-361.

Archer, J.W. 1984 'Low Noise Heterodyne Receivers for Near Millimeter-Wave Radio Astronomy,' Proc. I.E.E.E., in press.

Aumann, H.H. et al. 1984 'Discovery of a Shell Around Alpha Lyrae,' Ap. J. (Letters), in press.

Balick, B., and Heckman, T.M. 1982 'Extranuclear Clues to the Origin and Evolution of Activity in Galaxies,' Ann. Rev. Astron. Astrophys., 20, 431-468.

Bally, J., Snell, R.L., and Predmore, R. 1983 'Radio Images of the Bipolar H II Region S106,' Ap. J., 272, 154-162.

Barrett, A.H. et al. 1983 'Report of Subcommittee on Millimeter- and Submillimeter-Wavelength Astronomy,' National Science Foundation Astronomy Advisory Committee.

Bean, B.R., Cahoon, B.A., Samson, C.A., and Thayer, G.D. 1966 'A World Atlas of Atmospheric Radio Refractivity,' ESSA Monograph 1 (Washington, D.C.: U.S. Government Printing Office).

Bean, B.R., and Dutton, E.J. 1966 Radio Meteorology (Washington, D.C.: U.S. Government Printing Office).

Beers, T.C., Geller, M.J., and Huchra, J.P. 1982 'Galaxy Clusters with Multiple Components. I. The Dynamics of Abell 98,' Ap. J., 257, 23-32.

Bieging, J.H., Morgan, J., Welch, W.J., Vogel, S.N., and Wright, M.C.H. 1984 'Interferometric Measurements of Atmospheric Phase Noise at 89 GHz,' Radio Science, in press.

Birch, J.R., Nicol, E.A., and Street, R.L.T. 1983 'New Near-Millimeter Wavelength Radome Material,' Applied Optics, 22, 2947-2949.

Birkinshaw, M., and Gull, S.F. 1983 'A Test for Transverse Motions of Clusters of Galaxies, Nature, 315-317.

Birkinshaw, M., and Gull, S.F. 1984 'Measurements of the Gas Contents of Clusters of Galaxies by Observations of the Background Radiation at 10.7 GHz-III,' M.N.R.A.S., 206, 359-375.

Blumenthal, G.R., and Gould, R.J. 1970 'Bremsstrahlung, Synchrotron Radiation and Compton Scattering of High Energy Electrons Transversing Dilute Gases,' Rev. Mod. Phys., 42, 237-270.

Bracewell, R.N. 1965 The Fourier Transform and its Applications (New York: McGraw-Hill).

Clancy, R.T., and Muhleman, D.O. 1983 'A Measurement of the $^{12}CO/^{13}CO$ Ratio in the Mesosphere of Venus,' Ap. J., 273, 829-836.

Clark, B.G. 1982 'Large Field Mapping,' in Synthesis Mapping, Proceedings of the NRAO-VLA Workshop held at Socorro, New Mexico, June 21-25, 1982, A.R. Thompson and L.R. D'Addario, eds. (Charlottesville: NRAO), chapter 10.

Claussen, M.J., Berge, G.L., Heiligman, G.M., Leighton, R.B., Lo, K.-Y., Masson, C.R., Moffett, A.T., Phillips, T.G., Sargent, A.I., Scott, S.L., Seilestad, G.A., Wannier, P.G., and Woody, D.P. 1983 'High Spatial Resolution Observations of ^{12}CO in Molecular Cloud Cores,' Bull. A.A.S., 15, 639.

Cohen, J. 1983 'HL Tauri and its Circumstellar Disk,' Ap. J. (Letters), 270, L69-71.

Cohen, M., Bieging, J.H., and Schwartz, P.R. 1982 'VLA Observations of Mass Loss from T Tauri Stars,' Ap. J., 253, 707-715.

Cohen, R.S., Cong, H., Dame, T.M., and Thaddeus, P. 1980 'Molecular Clouds and Galactic Spiral Structure,' Ap. J. (Letters), 239, L53.

Cornwell, T.J. 1983 'The Role of Antenna Size in Self Calibration,' VLBA Memo 187.

de Pater, I., Brown, R.A., and Dickel, J.R. 1984 'VLA Observations of the Galilean Satellites,' Icarus, 57, 93-101.

Elias, J.H. et al. 1978 '1 Millimeter Continuum Observations of Extragalactic Objects,' Ap. J., 220, 25-41.

Ennis, D.J., Neugebauer, G., and Werner, M. 1982 '1 Millimeter Continuum Observations of Quasars,' Ap. J., 262, 460-477.

Erickson, N., Davis, J.H., Evans, N.J., Loren, R.B., Muncy, L., Peters, W.L., Scholks, M., and Vanden Bout, P.A. 1980 'New Detections of Spectral Lines in the Frequency Range 260-285 GHz,' in Interstellar Molecules, B.H. Andrew, ed. (Dordrecht: D. Reidel), p. 25.

Erickson, N.R., Goldsmith, P.R., Snell, R.L., Berson, R.L., Huguenin, G.R., Ulich, B.L., and Lada, C.J. 1982 'Detection of Bipolar CO Outflow in Orion,' Ap. J. (Letters), 261, L103-107.

Field, G.B. et al. 1982 Astronomy and Astrophysics for the 1980's (Washington, D.C.: National Academic Press).

Gehrz, R.D., Black, D.C., and Solomon, P.C. 1984 'The Formation of Stellar Systems from Interstellar Molecular Clouds,' Science, 224, 823-830.

Gillett, F. 1984 Talk presented at Protostars and Planets. II., Tucson, January 6, 1984.

Hess, S.L. 1959 Introduction to Theoretical Meteorology (New York: Holt, Rinehart and Winston).

Ho, P.T.P., Martin, R.N., and Fur, K. 1982 'Temperatures and Sizescales of Giant Cloud Complexes in the Spiral Galaxy 1C342,' Astron. Astrophys., 113, 155-164.

Hollenbach, D. et al. 1982 Large Deployable Reflector Science and Technology Workshop, Volume II -- Scientific Rationale and Technology Requirements, NASA Conference Publication 2275.

Hummer, D.G., and Rybicki, G.B. 1968 'Redshifted Line Profiles from Differentially Expanding Atmospheres,' Ap. J. (Letters), 153, L107-110.

Keene, J., Davidson, J.A., Harper, D.A., Hildebrand, R.H., Jaffe, D.T., Loewenstein, R.F., Low, F.J., and Pernic, R. 1983 'Far-Infrared Detection of Low-Luminosity Star Formation in the Bok Globule B335,' Ap. J. (Letters), 274, L43-47.

Kellermann, K.I., and Pauliny-Toth, I.I. 1981 'Compact Radio Sources,' Ann. Rev. Astron. Astrophys., 19, 373-410.

Koepf, G.A., Buhl, D., Chin, G., Peck, D.D., Fetterman, H.R., Clifton, B.J., and Tannenwald., P.E. 1982 'CO (J=6-5) Distribution in Orion and Detection in Other Galactic Sources,' Ap. J., 260, 584-589.

Kwan, J., and Scoville, N. 1976 'The Nature of the Broad Molecular Line Emission at the Kleinmann-Low Nebula,' Ap. J., 210, L39-43.

Landau, R., Jones, T.W., Epstein, E.E., Neugebauer, G., Soifer, B.T., Werner, M.W., Puschell, J.J., and Balonek, T.J. 1983 'Extragalactic One Millimeter Sources: Simultaneous Observations at Centimeter, Millimeter, and Visual Wavelengths,' Ap. J., 268, 68-75.

Larson, R.B. 1972 'The Evolution of Spherical Protostars with Masses 0.25 $M_\odot$ to 10 $M_\odot$,' M.N.R.A.S., 157, 121.

Liebe, H.J. 1981 'Modeling Attenuation and Phase of Radio Waves in Air at Frequencies below 1000 GHz,' Radio Science, 16, 1183-1199.

Lin, C.C., and Shu, F.H. 1964 'On the Spiral Structure of Disk Galaxies,' Ap. J., 140, 646.

Lindblad, B. 1963 Stockholm Obs. Ann. 22, No. 5.

Lo, K.-Y. et al. 1984 'Aperture Synthesis Observations of CO Emission from the Nucleus of IC342,' Ap. J. (Letters), in press.

Longair, M.S. 1982 'The Scientific Significance of Submillimetre Astronomy,' in The Scientific Importance of Submillimetre Observations, T. De Graauw and T.D. Guyene, eds. (Paris: European Space Agency), p. 219.

Lovas, F.J., Snyder, L.E., and Johnson, D.R. 1979 'Recommended Rest Frequencies for Observed Interstellar Molecular Transitions,' Ap. J. (Suppl.), 41, 451.

Lovering, J.F., and Prescott, J.R.V. 1979 Last of Lands ... Antarctica (Melbourne: Melbourne Univ. Press), p. 8.

Meinel, A.B. 1979 'Multiple Mirror Telescopes of the Future,' in The MMT and the Future of Ground-Based Astronomy, T.C. Weeks, ed., SAO Special Report 385, pp. 9-22.

Moran, J.M. 1983 'Phased Arrays as VLBA Elements,' VLBA Memo 178.

Moran, J.M., Garay, G., Reid, M.J., Genzel, R., Wright, M.C.H., and Plambeck, R.L. 1983 'Detection of Radio Emission from the Becklin-Neugebauer Object,' Ap. J. (Letters), 271, L31-34.

Moran, J.M., and Rosen, B.R. 1981 'Estimation of the Propagation Delay through the Troposphere from Microwave Radiometer Data,' Radio Science, 16, 235-244.

Morris, M., and Rickard, L.J. 1982 'Molecular Clouds in Galaxies,' Ann. Rev. Astron. Astrophys., 20, 517, 546.

Morrison, D., and Cruikshank, D.P. 1974 'Physical Properties of the Natural Satellites,' Sp. Sci. Rev., 15, 641-739.

Morrison, D., Murphy, R.E., Cruikshank, D.P., Sinton, W.M., and Martin, T.Z. 1973 'Evaluation of Mauna Kea, Hawaii as an Observatory Site,' P.A.S.P, 85, 255-267.

Mundt, R., and Fried, J.W. 1983 'Jets from Young Stars,' Ap. J. (Letters), 274, L83-86.

Murcray, D.G., Murcray, F.J., Murcray, F.H., and Barker, D.B. 1981 'Atmospheric Composition Using Infrared Techniques,' Antarctic Journal of the United States, XVI, 199-200.

Neugebauer, G. et al. 1984 'IRAS Observations of Radio-Quiet and Radio-Loud Quasars,' Ap. J. (Letters), 278, L83-85.

Oda, F.S., Metz, M.C., Shigekuni, V., and Leong, T. 1983 Mauna Kea Science Reserve Complex Development Plan (Honolulu: Group 70).

Olnon, F.M. et al. 1984 'IRAS Observations of OH/IR Stars,' Ap. J. (Letters), in press.

Owen, F. 1982 'The Concept of a Millimeter Array' and 'Science with a Millimeter Array,' NRAO Millimeter Array Memos Nos. 1 and 2.

Owen, F., Spangler, S., and Cotton, W. 1980 'Simultaneous Radio Spectra of Sources with Strong Millimeter Components,' Ap. J., 85, 351-362.

Pearson, T.J., and Readhead, A.C.S. 1984 'Image Formation by Self Calibration in Radio Astronomy,' Ann. Rev. Astron. Astrophys., in press.

Phillips, T.G., and Woody, D.P. 1982 'Millimeter and Submillimeter Wave Receivers,' Ann. Rev. Astron. Astrophys., 20, 285-321.

Plambeck, R.L., Wright, M.C., Welch, W.J., Beiging, J.H., Baud, B., Ho, P.T.P., and Vogel, S.N. 1982 'Kinematics of Orion KL: Aperture Synthesis Maps of 86 GHz SO Emission,' Ap. J., 259, 617-624.

Predmore, R. et al. 1984 '3-mm VLBI Observations of 3C273B with Transcontinental Baselines,' Bull. A.A.S., in press.

Readhead, A.C.S., and Wilkinson, P.N. 1978 'The Mapping of Compact Radio Sources from VLBI Data,' Ap. J., 223, 25-36.

Readhead, A.C.S. et al. 1983 'Very Long Baseline at Wavelengths of 3.4 Millimeters,' Nature, 303, 504-506.

Rees, M.J. 1978a 'Relativistic Jets and Beams in Radio Galaxies,' Nature, 275, 516-517.

Rees, M.J. 1978b 'Accretion and the Quasar Phenomenon,' Physica Scripta, 17, 193-200.

Resch, G.M., Hogg, D.E., and Napier, P.J. 1984 'Correction to Interferometer Phases Using Water Vapor Interferometry,' Radio Science, 19, 411-422.

Roellig, T.L., Werner, M.W., Becklin, E.E., and Impey, C. 1984 'Submillimeter and Infrared Observations of Flat Spectrum Radio Sources,' Bull. A.A.S., 16, 520.

Rogers, A.E.E. et al. 1983 'Very-Long-Baseline Radio Interferometry: The Mark III System for Geodesy, Astrometry, and Aperture Synthesis,' Science, 219, 51-54.

Rogers, A.E.E., Moffet, A.T., Backer, D.C., and Moran, J.M. 1984 'Coherence Limits Imposed by Atmospheric Noise in VLBI Observations at 3 mm Wavelength,' Radio Science, in press.

Roosen, R.G., and Angione, R.J. 1977 'Variations in Atmospheric Water Vapor: Baseline Results from Smithsonian Observations,' P.A.S.P., 89, 814-822.

Roser, H.P. 1979 Ph.D. Thesis, U. Bonn.

Rowan-Robinson, M. et al. 1984 'The IRAS Mini-Survey,' Ap. J. (Letters), 278, L7-10.

Rubin, V.C., and Ford, W.K. 1981 'Radial Velocities and Line Strengths of Emission Lines Across the Nuclear Disk of M31,' Ap. J., 170, 25-52.

Rubin, V.C., Ford, W.K., and Kumar, C.K. 1973 'Stellar Motions Near the Nucleus of M31,' Ap. J., 181, 61-77.

Ruze, J. 1966 'Antenna Tolerance Theory -- A Review,' Proc. I.E.E.E., 54, 633-640.

Ryle, M. 1975 'Radio Telescopes of Large Resolving Power,' Science, 188, 1071-1079.

Sandage, A. 1961 The Hubble Atlas of Galaxies, Carnegie Institution of Washington.

Savage, B.D., and Mathis, J.S. 1979 'Observed Properties of Interstellar Dust,' Ann. Rev. Astron. Astrophys., 17, 73-111.

Scheuer, P.A.G., and Readhead, A.C.S. 1979 'Superluminally Expanding Radio Sources and Radio Quiet QSO's,' Nature, 277, 182-185.

Schwab, F.R., and Cotton, W.D. 1983 'Global Fringe Search Techniques for VLBI,' Ap. J., 88, 688-694.

Scoville, N.Z., and Hersh, K. 1979 'Collisional Growth of Giant Molecular Clouds,' Ap. J., 229, 578.

Shu, F.H. 1984 'Early Stellar Evolution,' talk presented at A.A.A.S. Symposium, 'How Stars Are Born.'

Snell, R.L., Loren, R.B., and Plambeck, R.L. 1980 'Observations of CO in L1551: Evidence for Stellar Wind Driven Shocks,' Ap. J. (Letters), 239, L17-22.

Snyder, L.E. 1982 'A Review of Radio Observations of Comets,' Icarus, 51, 1-24.

Soifer, B.T. et al. 1984 'Infrared Galaxies in the IRAS Minisurvey,' Ap. J. (Letters), 278, L71-74.

Sramek, R. 1983 'VLA Phase Stability at 22 GHz on Baselines of 100 m to 3 km,' VLA Test Memo 143 (also NRAO Millimeter Array Memo 8).

Stahler, S.W., Shu, F.H., and Taam, R.E. 1980 'The Evolution of Protostars. I. Global Formulation and Results,' Ap. J., 241, 637-654.

Sunyaev, R.A., and Zeldovich, Y.B. 1980 'Microwave Background Radiation as a Probe of the Contemporary Structure and History of the Universe,' Ann. Rev. Astron. Astrophys., 18, 537-560.

Thayer, G.D. 1974 'An Improved Equation for the Radio Refractive Index of Air,' Radio Science, 9, 803-807.

Townes, C.H. 1980 'Infrared Imaging and Interferometry' in Optical and Infrared Telescopes for the 1990's, A. Hewitt, ed. (Tucson: Kitt Peak National Observatory), pp. 797-824.

Ulich, B.L. 1983 'Weather Conditions on Mt. Lemmon and Mt. Graham,' SMT Technical Memorandum UA-83-8.

Ulich, B.L., Cogdell, J., and Davis, J.H. 1973 'Planetary Brightness Temperature Measurements at 8.6 mm and 3.1 mm Wavelengths,' Icarus, 19, 59-82.

Vogel, S.N., Wright, M.C.H., Plambeck, R.L., and Welch, W.J. 1984 'Interaction of the Outflow and Quiescent Gas in Orion: HCO^+ Aperture Synthesis Maps,' Ap. J., in press.

von Hoerner, A. 1975 'Radio Telescopes for Millimeter Wavelength,' Astron. Astrophys., 41, 301-306.

Warner, J.W. 1977 'Comparative Water Vapor Measurements for Infrared Sites,' P.A.S.P., 724-727.

Waters, J. 1976 'Absorption and Emission by Atmospheric Gases,' Methods of Experimental Physics, Volume 12B, M.L. Meeks, ed. (New York: Academic Press), pp. 142-176.

Weinreb, S. 1983 'Cost Equation of Millimeter Wave Array,' NRAO Millimeter Array Memo 6.

Westphal, J.A. 1974 Infrared Sky Noise Survey, Final Report NASA Grant NGR 05-002-185.

Whipple, F.L., and Huebner, W.F. 1976 'Physical Processes in Comets,' Ann. Rev. Astron. Astrophys., 14, 143-172.

Wilson, W.J. 1983 'Submillimeter Wave Receivers -- A Status Report,' IEEE Trans. Microwave Theory and Techniques MTT-31, 873-878.

Wilson, W.J., Klein, M.J., Kahar, R.K., Gulkis, S., Olsen, E.T., and Ho, P.T.P. 1981 'Venus. I. Carbon Monoxide Distribution and Molecular-Line Searches,' Icarus, 45, 624-637.

Winnewisser, G., Aliev, M.R., and Yamada, K. 1982 'Interstellar Hydrides,' in The Scientific Importance of Submillimeter Observations, T. deGraauw and T.D. Guyenne, eds. (Paris: European Space Agency), p. 23.

Wynn-Williams, C.G. 1982 'The Search for Infrared Protostars,' Ann. Rev. Astron. Astrophys., 20, 587-618.